Guidelines on the Evaluation of Vector Network Analysers (VNA)

EURAMET Calibration Guide No. 12

Version 3.0 (03/2018)

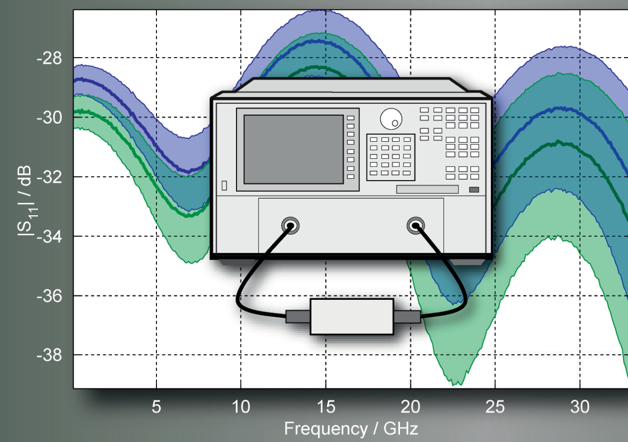

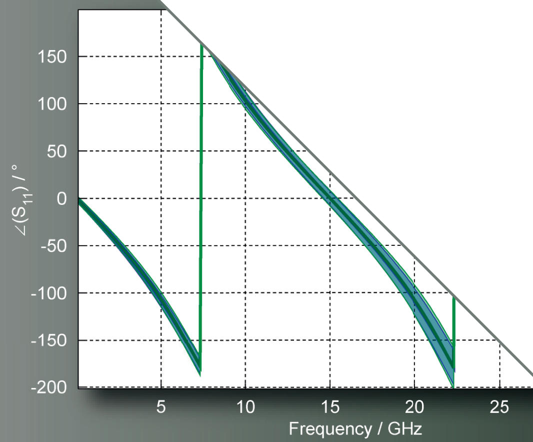

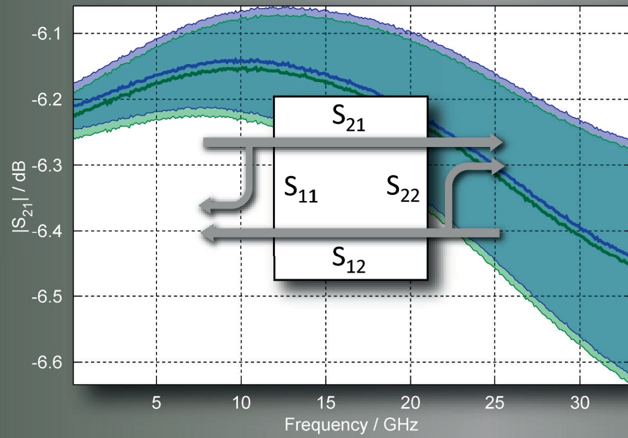

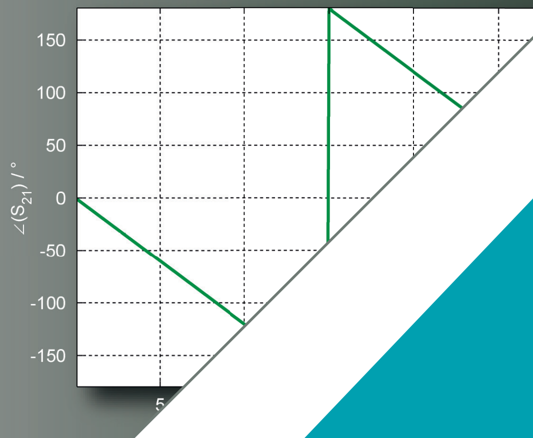

Electricity and Magnetism

Authorship and Imprint

This document was developed by the EURAMET e.V., Technical Committee for Electricity and Magnetism.
Authors: Markus Zeier (METAS, Switzerland), Djamel Allal (LNE, France), Rolf Judaschke (PTB, Germany).

Acknowledgement
The authors would like to thank for reviewing the guide: Thomas Reichel (Technical consultant), Blair Hall (MSL), Gary Bennett (National Instruments), Dave Blackham (Keysight Technologies), Andreas C. Böck (esz AG calibration & metrology), Andy Brush (TEGAM), Tekamul Buber (Maury Microwave), Albert Calvo (Rohde & Schwarz), Onur Cetiner (Keysight Technologies), Chris Eio (NPL), Andrea Ferrero (Keysight Technologies), Israel Garcia Ruiz (CENAM), Martin Grassl (Spinner), Tuomas Haitto (Millog Oy), Johannes Hoffmann (METAS), Matthias Hübler (Rohde & Schwarz), Ian Instone (Technical consultant), Harald Jäger (Rohde & Schwarz), Karsten Kuhlmann (PTB), Jian Liu (Keysight Technologies), Linoh Magalula (NMISA), Jon Martens (Anritsu), Guillermo Monasterios (INTI), Faisal Mubarak (VSL), Rusty Myers (Keysight Technologies), Reiner Oppelt (Rosenberger), Nick Ridler (NPL), Juerg Ruefenacht (METAS), Handan Sakarya (UME), Bart Schrijver (Keysight Technologies), Joachim Schubert (Rosenberger), Nosherwan Shoaib (INRIM, NUST), Hernando Silva (INTI), Pamela Silwana (NMISA), Laszlo Sleisz (NMHH), Daniel Stalder (METAS), Michael Wollensack (METAS), Ken Wong (Keysight Technologies), Sherko Zinal (PTB).

Version 3.0 March 2018
Version 2.0 March 2011
Version 1.0 July 2007

EURAMET e.V.
Bundesallee 100
38116 Braunschweig
Germany

E-mail: secretariat@euramet.org
Phone: +49 531 592 1960

Official language

The English language version of this document is the definitive version. The EURAMET Secretariat can give permission to translate this text into other languages, subject to certain conditions available on application. In case of any inconsistency between the terms of the translation and the terms of this document, this document shall prevail.

Copyright

The copyright of this document (EURAMET Calibration Guide No. 12, version 3.0 – English version) is held by © EURAMET e.V. 2007. The text may not be copied for sale and may not be reproduced other than in full. Extracts may be taken only with the permission of the EURAMET Secretariat.

ISBN 978-3-942992-51-0

Image on cover page by PTB.

Guidance publications

This document gives guidance on measurement practices in the specified fields of measurements. By applying the recommendations presented in this document, laboratories can produce calibration results that can be recognised and accepted throughout Europe. The approaches taken are not mandatory and are for the guidance of calibration laboratories. The document has been produced as a means of promoting a consistent approach to good measurement practice leading to and supporting laboratory accreditation.

The guide may be used by third parties, e.g. National Accreditation Bodies, peer reviewers, witnesses to measurements, etc., as a reference only. Should the guide be adopted as part of a requirement of any such party, this shall be for that application only and the EURAMET Secretariat should be informed of any such adoption.

On request EURAMET may involve third parties in stakeholder consultations when a review of the guide is planned. If you are interested, please contact the EURAMET Secretariat.

No representation is made nor warranty given that this document or the information contained in it will be suitable for any particular purpose. In no event shall EURAMET, the authors or anyone else involved in the creation of the document be liable for any damages whatsoever arising out of the use of the information contained herein. The parties using the guide shall indemnify EURAMET accordingly.

Further information

For further information about this document, please contact your national contact person in the EURAMET Technical Committee for Electricity and Magnetism (see https://www.euramet.org)

Version 3.0 (03/2018)

Guidelines on the Evaluation of Vector Network Analysers (VNA)

Purpose

This document has been produced to enhance the equivalence and mutual recognition of calibration results obtained by laboratories performing measurements with vector network analysers.

Contents

List of Figures 6

List of Tables 7

1 Introduction 9
1.1 Purpose of this guide . . . 9
1.2 Comparison with previous guideline . . . 9
1.3 Scope and Applicability . . . 10
1.4 Terminology . . . 10
1.4.1 VNA calibration . . . 10
1.4.2 Error model and measurement model . . . 11
1.4.3 Error coefficients and residual errors . . . 11

2 Traceability schemes and measurement standards 11
2.1 Traceability chain . . . 11
2.2 Measurement standards . . . 12

3 VNA calibration 13
3.1 Introduction . . . 13
3.2 Practical advice for VNA calibration . . . 14
3.3 Electronic calibration units . . . 14

4 Verification 15
4.1 Introduction . . . 15
4.2 Purpose of verification . . . 15
4.3 Verification Methods . . . 15
4.3.1 Coincidence tests . . . 15
4.3.2 Plausibility tests . . . 15
4.4 Verification procedure and practical advice . . . 16
4.5 Verification criteria . . . 17

5 Uncertainty contributions 18
5.1 Introduction . . . 18
5.2 Identification of influence quantities . . . 18
5.3 Characterization of uncertainty contributions . . . 19
5.3.1 Characterization of calibration standards . . . 19
5.3.2 Noise floor and trace noise . . . 20
5.3.3 VNA non-linearity . . . 20
5.3.4 VNA drift . . . 21
5.3.5 Isolation (cross-talk) . . . 22
5.3.6 Test port cable stability . . . 22
5.3.7 Connection repeatability . . . 22

6 Measurement model 23

7 Uncertainty evaluation **23**
7.1 Rigorous uncertainty evaluation 23
7.2 Ripple Method 24

8 Best measurement practice and practical advice **26**
8.1 Environmental conditions 26
8.2 VNA architecture, performance and settings 27
8.3 Use of mechanical calibration and verification standards 28
8.4 Use of electronic calibration units 29
8.5 Test port cables 29
8.5.1 Fixture and layout 29
8.5.2 Test port adapters 30
8.6 Connector care 31
8.7 Initial stability test 31
8.8 Repeatability 31

References **33**

Annexes **39**

A Glossary **39**

B Notation **43**

C S-parameter measurement uncertainties **44**
C.1 S-parameter data format 44
C.2 Representation of measurement uncertainties 44
C.2.1 Correlation 45
C.3 Evaluation of measurement uncertainty 45
C.4 Uncertainty propagation 46
C.5 Sample statistics and Type A uncertainty 47
C.5.1 Sample statistics of scalar quantities 47
C.5.2 Sample statistics of complex-valued quantities 47
C.5.3 Type A uncertainty 48
C.6 Expanded uncertainty 49

D VNA calibration **51**
D.1 One-port calibration techniques 51
D.2 Two-port calibration techniques 52
D.2.1 Introduction 52
D.2.2 Ten-term error model 52
D.2.3 Seven-term error model 55
D.3 Over-determined calibration 56

E VNA verification **57**
E.1 Verification standards 57
E.1.1 One-port verification standards 57
E.1.2 Two-port verification standards 58
E.2 Quantitative verification criteria 61
E.2.1 Scalar case 62
E.2.2 Multivariate case 62
E.2.3 Examples of quantitative verification 64

F VNA measurement models **67**
F.1 Introduction 67
F.2 One-port measurement model 67
F.3 Two-port measurement models 69
F.4 N-port measurement model 69
F.5 Measurement model based on residual error coefficients 69
F.6 Uncertainty contributions 71

G Characterization procedures of uncertainty contributions **73**
G.1 Noise floor and trace noise 73
G.2 VNA non-linearity 78
G.3 VNA drift 81
G.4 Test port cable stability 85
G.5 Connector repeatability 89

H Ripple Method **91**
H.1 Introduction 91
H.2 Uncertainties 91
H.3 Practical Preparation 91
H.4 Measurement model 92
H.4.1 One-port equation 92
H.4.2 Two-port equations 93
H.5 Uncertainty contributions 94
H.5.1 Directivity 94
H.5.2 Source match 97
H.5.3 Reflection tracking 98
H.5.4 Transmission tracking and load match 100
H.5.5 Isolation 100
H.5.6 Drift 100
H.5.7 Test port cables 101
H.5.8 Non-linearity 101
H.5.9 Repeatability 101

I Waveguide measurements **102**
I.1 Introduction 102
I.2 Equipment 102
I.2.1 VNA test ports 102

I.2.2 Calibration kits 102
I.2.3 Components 103
I.3 Calibration 104
I.3.1 SSL calibration 104
I.3.2 TRL calibration 104
I.4 Uncertainty Evaluation 105
I.4.1 Ripple Assessments 105
I.4.2 Other uncertainty components 105

J Examples **107**
J.1 One-port matched load 110
J.2 One-port mismatch 112
J.3 One-port short 114
J.4 Two-port Adapter 116
J.5 Two-port 20 dB attenuation device 122
J.6 Two-port 50 dB attenuation device 128

List of Figures

8.1	VNA test port cable setup	30
D.1	One-port error model	52
D.2	Four-receiver vs. three receiver VNA architecture	53
D.3	Ten-term forward VNA error model	54
D.4	Ten-term reverse VNA error model	54
D.5	Seven-term VNA error model	56
E.1	Schematic Beatty Line	59
E.2	Simulated Beatty line	60
E.3	T-checker	60
E.4	Quantitative verification criteria for a T-Checker	65
E.5	Quantitative verification criteria for a matched load	66
F.1	One-port VNA measurement model	68
F.2	Ten-term forward VNA measurement model	70
F.3	Seven-term VNA measurement model	70
F.4	Residual one-port VNA measurement model	71
F.5	Cable and Connector Model	72
G.1	Characterization of VNA noise floor	75
G.2	Characterization of VNA noise floor at low frequencies	75
G.3	Characterization of VNA trace noise magnitude	76
G.4	Characterization of VNA trace noise magnitude at low frequencies	76
G.5	Characterization of VNA trace noise phase	77
G.6	Characterization of VNA trace noise phase at low frequencies	77
G.7	Characterization of VNA non-linearity: full attenuation range	79
G.8	Characterization of VNA non-linearity: limited attenuation range	79
G.9	Characterization of VNA non-linearity: frequency dependence	80
G.10	Characterization of VNA drift related to reflection	83
G.11	Characterization of VNA drift related to transmission magnitude	84
G.12	Characterization of VNA drift related to transmission phase	84
G.13	Characterization of VNA test port cable: transmission magnitude stability	87
G.14	Characterization of VNA test port cable: transmission phase stability	87
G.15	Setup for characterization of VNA test port cable: start position	88
G.16	Setup for characterization of VNA test port cable: end position	88
G.17	Characterization of connector repeatability	90
H.1	Ripple pattern of residual directivity	95
H.2	Peak-to-peak magnitude of ripple pattern	95
H.3	Ripple pattern of residual source match	98
I.1	Directivity ripple in X-band waveguide	106
I.2	Source match ripple in X-band waveguide	106
J.1	Variations in ripple pattern of residual directivity	108
J.2	Example uncertainties of $\mathrm{Re}\left(\mathbf{S}_{11}\right)$ of a matched load	110
J.3	Example uncertainties of $\mathrm{Im}\left(\mathbf{S}_{11}\right)$ of a matched load	110
J.4	Example uncertainties of $\left\|\mathbf{S}_{11}\right\|$ of mismatch	112
J.5	Example uncertainties of $\arg\left(\mathbf{S}_{11}\right)$ of mismatch	112

J.6 Example uncertainties of $|\mathbf{S}_{11}|$ of short 114
J.7 Example uncertainties of $\arg(\mathbf{S}_{11})$ of short 114
J.8 Example uncertainties of $\mathrm{Re}(\mathbf{S}_{22})$ of an adapter 116
J.9 Example uncertainties of $\mathrm{Im}(\mathbf{S}_{22})$ of an adapter 116
J.10 Example uncertainties of $|\mathbf{S}_{12}|$ of an adapter 119
J.11 Example uncertainties of $\arg(\mathbf{S}_{12})$ of an adapter 119
J.12 Example uncertainties of $\mathrm{Re}(\mathbf{S}_{22})$ of a 20 dB attenuation device 122
J.13 Example uncertainties of $\mathrm{Im}(\mathbf{S}_{22})$ of an adapter 122
J.14 Example uncertainties of $|\mathbf{S}_{12}|$ of a 20 dB attenuation device 125
J.15 Example uncertainties of $\arg(\mathbf{S}_{12})$ of a 20 dB attenuation device 125
J.16 Example uncertainties of $\mathrm{Re}(\mathbf{S}_{22})$ of a 50 dB attenuation device 128
J.17 Example uncertainties of $\mathrm{Im}(\mathbf{S}_{22})$ of an adapter 128
J.18 Example uncertainties of $|\mathbf{S}_{12}|$ of a 50 dB attenuation device 131
J.19 Example uncertainties of $\arg(\mathbf{S}_{12})$ of a 50 dB attenuation device 131

List of Tables

8.1 Recommended minimal pin gaps of coaxial connections 32
D.1 Error coefficients of one-port error model 51
D.2 Error coefficients of ten-term error models 53
D.3 Error coefficients of seven-term error models 55
F.1 Influences in one-port measurement model 68
J.1 Uncertainty budget with rigorous method for $\mathrm{Re}(\mathbf{S}_{11})$ of matched load . . . 111
J.2 Uncertainty budget with rigorous method for $\mathrm{Im}(\mathbf{S}_{11})$ of matched load . . . 111
J.3 Uncertainty budget with Ripple Method for $\mathbf{S}_{11}$ of matched load 111
J.4 Uncertainty budget with rigorous method for $|\mathbf{S}_{11}|$ of mismatch 113
J.5 Uncertainty budget with rigorous method for $\arg(\mathbf{S}_{11})$ of mismatch 113
J.6 Uncertainty budget with Ripple Method for $\mathbf{S}_{11}$ of mismatch 113
J.7 Uncertainty budget with rigorous method for $|\mathbf{S}_{11}|$ of a short 115
J.8 Uncertainty budget with rigorous method for $\arg(\mathbf{S}_{11})$ of a short 115
J.9 Uncertainty budget with Ripple Method for $\mathbf{S}_{11}$ of a short 115
J.10 Uncertainty budget with rigorous method for $\mathrm{Re}(\mathbf{S}_{22})$ of an adapter 117
J.11 Uncertainty budget with rigorous method for $\mathrm{Im}(\mathbf{S}_{22})$ of an adapter 117
J.12 Uncertainty budget with Ripple method for $\mathbf{S}_{22}$ of an adapter 118
J.13 Uncertainty budget with rigorous method for $|\mathbf{S}_{12}|$ of an adapter 120
J.14 Uncertainty budget with rigorous method for $\arg(\mathbf{S}_{12})$ of an adapter 120
J.15 Uncertainty budget with Ripple method for $\mathbf{S}_{12}$ of an adapter 121
J.16 Uncertainty budget with rigorous method for $\mathrm{Re}(\mathbf{S}_{22})$ of a 20 dB attenuation device 123
J.17 Uncertainty budget with rigorous method for $\mathrm{Im}(\mathbf{S}_{22})$ of an adapter 123
J.18 Uncertainty budget with Ripple method for $\mathbf{S}_{22}$ of a 20 dB attenuation device 124
J.19 Uncertainty budget with rigorous method for $|\mathbf{S}_{12}|$ of a 20 dB attenuation device 126
J.20 Uncertainty budget with rigorous method for $\arg(\mathbf{S}_{12})$ of a 20 dB attenuation device 126
J.21 Uncertainty budget with Ripple method for $\mathbf{S}_{12}$ of a 20 dB attenuation device 127

J.22 Uncertainty budget with rigorous method for $\mathrm{Re}\left(\mathbf{S}_{22}\right)$ of a 50 dB attenuation device 129
J.23 Uncertainty budget with rigorous method for $\mathrm{Im}\left(\mathbf{S}_{22}\right)$ of an adapter 129
J.24 Uncertainty budget with Ripple method for $\mathbf{S}_{22}$ of a 50 dB attenuation device 130
J.25 Uncertainty budget with rigorous method for $|\mathbf{S}_{12}|$ of a 50 dB attenuation device 132
J.26 Uncertainty budget with rigorous method for $\arg\left(\mathbf{S}_{12}\right)$ of a 50 dB attenuation device 132
J.27 Uncertainty budget with Ripple method of $\mathbf{S}_{12}$ of a 50 dB attenuation device 133

1 Introduction

1.1 Purpose of this guide

1.1.1 This guide gives advice on how to measure reflection and transmission of guided electromagnetic waves (scattering parameters or S-parameters) with a vector network analyzer (VNA) in accordance with metrological principles. It is dedicated to advanced VNA users, i.e. the reader is expected to already have solid knowledge of VNA measurements. For introductory material to vector network analysis the reader is referred to [1, 2, 3, 4].

1.1.2 While this guide is primarily intended for accredited calibration laboratories it is as well useful for national metrology institutes and anybody else performing VNA measurements.

1.1.3 This guide explains how to establish SI (international system of units) traceability using reference standards (section 2). It gives advice on VNA calibration schemes (section 3) and verification (section 4). It has a particular focus on the evaluation of measurement uncertainties (sections 5, 6 and 7). Finally, advice on good measurement practice is given (section 8).

1.1.4 It was the intent to keep the main body of this guide reasonably short with a focus on practical aspects to make it useful for the practitioner. The appendices contain further details on many of the topics covered in the main body of the document. Examples are given to illustrate some of the concepts. A glossary is provided and references are cited for further reading.

1.2 Comparison with previous guideline

1.2.1 For many years, the previous versions of the guide (version 2.0 and earlier) have served as a valuable guideline in accredited calibration laboratories and in national metrology institutes. Advances in VNA metrology over the last years have prepared the foundation for a revision of the guide. The main improvements are summarized in the following.

1.2.2 The previous versions of the guide promoted SI traceability through beadless air-dielectric lines using the so-called Ripple Method. This method only partly relies on a measurement model and makes some questionable assumptions. It has a potential to either underestimate or overestimate the measurement uncertainty and is limited in applicability. At higher frequencies it becomes unpractical.

1.2.3 In 2011, Supplement 2 [5] of the ISO-GUM [6] has been published giving thorough advice on how to evaluate measurement uncertainties for multi-dimensional measurands, including complex-valued quantities. It is therefore the authoritative guideline for the determination of measurement uncertainties associated with S-parameters. In parallel, software capabilities have become available to support the sometimes elaborate calculation of the measurement uncertainty.

1.2.4 This guide therefore promotes the rigorous propagation of uncertainty contributions through a measurement model that covers the entire measurement process. The refined modeling puts the measured data of the device under test (DUT) in a mathematical relationship with the characterized values of the calibration standards and other influence quantities. Thus, it is possible to directly propagate uncertainties associated with the calibration standards and the influence quantities to the quantity of interest. This approach takes the multivariate nature (magnitude and phase or real and imaginary components) of the measured quantity fully into account and correlation is treated properly. Traceability to SI units is established through a set of characterized calibration standards and assumptions of ideality are not needed. This method is not limited in applicability and can principally be applied in all areas of VNA metrology. Furthermore, it fits to the purpose of supporting future trends in VNA metrology, such as higher frequencies, multiport, nonlinear, etc.

1.2.5 This guide gives advice on how to implement the rigorous propagation of uncertainty to achieve best accuracy in VNA measurements. Due to the widespread use of the Ripple Method, it is still included in the guide in an improved form, by clearly specifying its limits in terms of stated uncertainty and applicability.

1.2.6 Compared to previous versions, this guide provides additional advice on VNA measurement models, VNA calibration, VNA verification, and best measurement practice. Furthermore, it provides an introduction to measurement uncertainties associated with complex-valued quantities.

1.3 Scope and Applicability

This guide has a focus on linear VNA measurements in the coaxial line system up to 110 GHz. The discussion is limited to one-port and two-port VNA measurements, but the generalization to an arbitrary number of ports is principally straightforward. Many aspects can be adopted to other line types such as waveguide or on-wafer. A specific section on waveguide measurements can be found in appendix I.

1.4 Terminology

Some of the terms used in VNA metrology are rooted in history but are not coherent with contemporary terminology used in metrology. The subsequent clauses briefly address these issues.

1.4.1 VNA calibration

In this guide, the term “VNA calibration” is used to describe the determination of the VNA error coefficients by measuring a set of known reference standards. This terminology is not entirely in agreement with the definition of the term “calibration” in the International Vocabulary of Metrology (VIM) [7]. The term is nevertheless used here, because it is widely understood and there are associated terms as “calibration algorithm” or “calibration standard” which would need to be renamed as well. This would likely lead to confusion.

1.4.2 Error model and measurement model

This guide uses the terms "error model" for VNA calibration and VNA error correction and the term "measurement model" for the evaluation of VNA measurement uncertainties. This distinction is artificial. A VNA error model is nothing other than a VNA measurement model, reduced to the influencing quantities (error coefficients) that are determined and corrected during VNA calibration and VNA error correction. The full VNA measurement model contains all influence quantities, those which can be corrected (the error coefficients) and those which remain uncorrected, as e.g. noise or drift. It would be more coherent to withdraw the term error model and to just use measurement model. The distinction is nevertheless made, because the term error model is widely used and replacing it with measurement model might lead to confusion.

1.4.3 Error coefficients and residual errors

Error coefficients are determined during VNA calibration by measuring calibration standards. Errors in the characterization of these standards lead to errors in the determination of the error coefficients, something that is commonly referred to as residual errors. The terminology is not ideal, and it would be better to speak of model coefficients instead of error coefficients (see as well the remarks in 1.4.2). However, due to the wide spread use of these terms it was decided to keep them in this guide.

2 Traceability schemes and measurement standards

2.1 Traceability chain

2.1.1 S-parameters are dimensionless ratios of complex-valued wave quantities, which are defined and measured with respect to a reference impedance [8]. The traceability to SI units is defined through this reference impedance and with respect to a measurement reference plane.

2.1.2 The first fundamental step of the traceability chain of S-parameters is established with the characterization of calculable measurement standards [9, 10, 11, 12]. Known calculable coaxial standards are air-dielectric lines, offset shorts, flush shorts and offset opens. Calculable standards are parametrized and measured dimensionally. The mechanical model should cover the whole standard including the connector interface to achieve highest accuracy and to obtain a consistent definition of the measurement reference plane [13, 14]. Based on dimensional measurements and known material parameters the S-parameters of the calculable standards are determined with the help of analytical equations and numerical EM simulations in combination with electrical measurements. Calculable standards may be called primary standards. The process of establishing traceability by using primary standards is called a primary experiment. Primary experiments are elaborate and require measurement and modeling capabilities at a level that can usually only be provided by national metrology institutes.

2.1.3 A VNA being calibrated by using primary standards can be used to characterize other calibration standards to disseminate S-parameter traceability to lower levels in the

traceability chain. These standards are called transfer standards (or secondary standards) and don't need to be calculable. A good example for transfer standards are commercially available calibration kits, which contain open, short and matched load with both male and female connectors.

2.1.4 An accredited calibration laboratory can in principal perform a primary experiment as well, but due to the required expertise and effort it will normally obtain SI traceability for its VNA measurements through a set of standards that are calibrated by a national metrology institute.

2.1.5 VNA parameters, such as power level or frequency, need to be calibrated only if one of these parameters is important for the characterization of a DUT. An example is the measurement of a filter, which has a pronounced dependence of transmissivity with respect to frequency. A factory calibration or performance verification (a service typically offered by service centers of VNA manufacturers) is usually sufficient in these cases. How often such a factory calibration or performance verification should be performed can't be answered generally. It depends on the operating conditions of the VNA. Keeping a history of verification measurements is helpful in this matter, see 4.5.5.

2.2 Measurement standards

Practical advice on use and handling of measurement standards can be found in 8.3 and 8.4.

2.2.1 Two types of measurement standards can be distinguished in VNA measurements, calibration standards and verification standards. The name calibration and verification refers to the purpose the standards are used for. Calibration standards are used to calibrate a VNA and determine its error coefficients, as discussed in section 3. Depending on the calibration scheme, the choice of calibration standards may vary. Verification standards are used to verify that the calibration of the VNA was successful, as discussed in section 4.

2.2.2 Measurement standards are traditionally mechanical components, which need to be individually connected to the VNA test port. More recently, electronic calibration units (ECUs) have become available as a convenient alternative, see 3.3.

2.2.3 Traceability to SI units is established preferably through calibration standards. This requires a model of the measurement process and propagation of uncertainties through the measurement model, as discussed in 7.1. To establish traceability this way it is necessary to have SI traceably characterized calibration standards.

2.2.4 Alternatively, by treating the VNA partly as a black box it is possible to establish traceability through beadless air-dielectric lines, as discussed in 7.2. To establish SI traceability this way it is necessary to have SI traceably characterized air-dielectric lines. With the black box approach it is not necessary to have SI traceably characterized calibration standards.

2.2.5 Regardless of the method of uncertainty evaluation adopted, it is advisable to hold an SI traceably characterized set of verification standards. Advice for the selection of

verification standards is given in section 4.

2.2.6 Some of the calibration and verification standards might be of the same type but they must be physically different items. A single standard must not be used for calibration and verification simultaneously. The only exception is the re-measurement of the calibration standards after calibration to test the stability of the measurement system, as described in 4.3.2.

2.2.7 The memory of older VNAs is limited in size. To cope with this limitation, manufacturers of calibration standards used a polynomial representation [3, 15] to model the frequency response of the highly reflective calibration standards. In addition it is assumed that the matched load is ideal. The measurement accuracy is directly limited by the quality of the polynomial curve fit, representing the highly reflective standards, and how well the matched load approximates the reference impedance, e.g. 50 Ω. At higher frequencies, typically above 2 GHz, a sliding load is used instead of a fixed load since it provides superior matching performance.

2.2.8 Modern VNAs are able to make use of data-based standard definitions. The S-parameters of the standards and associated uncertainties are stored as data sets with reasonably high frequency resolution. Uncertainties associated with the characterization of the standards determine the measurement accuracy of the calibrated VNA. Measurement accuracy is not dependent on the fixed load being matched as perfectly as possible. Thus the use of a sliding load is dispensable. It is still necessary that the standards behave in a “normal” way, i.e. that the fixed load offers a reasonable matching and the highly reflective standards principally act as reflecting devices. For best measurement accuracy, it is essential that the S-parameters of the standards, at any frequency, do not cluster in a single location of the complex measurement plane.

3 VNA calibration

3.1 Introduction

3.1.1 VNA calibration is the process of determining the VNA systematic measurement errors, which are called error coefficients (sometimes also referred to as error terms or calibration coefficients). The process is based on a VNA error model. A VNA error model relates the values indicated by the VNA (raw S-parameters) to the S-parameters of the device connected to the test port of the VNA. Part of this mathematical relationship are the unknown error coefficients. During VNA calibration, a set of known calibration standards is measured and the error coefficients are determined. They can then be used to transform the raw S-parameters of a DUT measurement into corrected S-parameters, a step which is usually being referred to as VNA error correction.

3.1.2 VNA error models are based on the idea that the signal flow in a VNA can be modeled as a linear network. The VNA error model can be illustrated graphically by a signal flow graph. There are methods for reducing signal flow graphs into mathematical equations, as e.g. described in [16, 17]. These mathematical equations are used to perform VNA calibration and VNA error correction.

3.1.3 VNA calibration standards are characterized components. It has to be emphasized that the characterization is never perfect and that the error related to it will be propagated to the error coefficients and ultimately to the error-corrected S-parameters of the DUT. It is the purpose of uncertainty evaluation, as discussed in section 7, to estimate the effect of this influence and other influencing quantities, see section 5.

3.1.4 Since the development of computer-controlled VNAs, several calibration methods have been developed. The choice between them depends on the final application, the number and the type of the calibration standards and the desired accuracy. Some details on one-port and two-port calibration schemes can be found in appendix D.

3.2 Practical advice for VNA calibration

3.2.1 If stable short - open - load (SOL) standards are available and if their characterization is data-based, the SOL calibration scheme for one-port measurements is preferable. For two-port measurements, the short - open - load - thru (SOLT) calibration should be used, if the movement of the test port cable is relatively small and a flush thru connection is possible (insertable test port configuration). The use of a sliding load is not advised. See remarks in 2.2.7, 2.2.8 and 8.3.2.

3.2.2 A useful alternative to SOLT is the SOLR (short - open - load - reciprocal, also known as Unknown Thru) calibration [18]. It uses measurements of short, open and matched load at each port and the reciprocity condition in the transmission measurement of the DUT to determine the error coefficients. SOLR should be applied in situations where the measurement of a flush thru is not practical. This includes cases where the DUT is of extended size, i.e. a relatively large cable movement would be necessary between the measurement of the flush thru during calibration and the subsequent measurement of the DUT. It further includes measurements of non-insertable DUTs and DUTs that have different connector types and/or different impedance definitions at each port. It should be noted that applying the SOLR calibration usually requires a four-receiver architecture of the VNA. Compared to SOLT, SOLR calibration is more sensitive to the characterization of short and open calibration standards. For further details on VNA architecture, SOL, SOLT and SOLR refer to appendix D.

3.2.3 Using more calibration standards than needed results in an over-determined calibration algorithm. For details see D.3. This type of calibration is useful to enhance the accuracy of the calibration and to detect problems with single calibration standards. The software (VNA firmware or external program), however, has to to support this type of calibration.

3.3 Electronic calibration units

3.3.1 Electronic calibration units are an attractive alternative to mechanical standards to perform VNA calibrations more efficiently. Up to now, ECUs are manufacturer-specific, i.e. they can only be used with a VNA from the same manufacturer. Remote control of an ECU from an external software is limited. This can be problematic if it is desired to propagate the uncertainties associated with the characterization of the ECU states to the measurement result. If a laboratory intends to establish SI traceability through

an ECU it is recommended to contact the manufacturer and/or a national metrology institute for advice. Stability effects of ECUs related to temperature and aging are addressed in 8.4.

4 Verification

4.1 Introduction

According to the VIM [7], verification generally denotes provision of objective evidence that a given item fulfills specified requirements. In the present case of VNA measurements, the purpose of verification is to confirm that the VNA, test port cables, and calibration standards are working together correctly as a measurement system, i.e., that the stated measurement uncertainty is met. This section has a focus on practical advice related to verification. More details are provided in appendix E.

4.2 Purpose of verification

After a VNA calibration has been completed, it is necessary to investigate the validity and quality of the calibrated measurement setup. The measurement uncertainty is calculated from the influences discussed in section 5. Underestimation of these influences or any additional source of error, as e.g. faulty calibration caused by mixed-up, damaged or unstable calibration standards, use of the wrong calibration standard definitions, incorrect operation, non-linearity due to too excessive source power, VNA failure and a faulty setup (e.g. a loose connection) might not be covered by the calculated measurement uncertainty. It is the purpose of verification to discover such sources of error.

4.3 Verification Methods

Verification can be performed in various ways. Besides quantitative coincidence tests, see 4.3.1 and E.2, it is also possible to perform more qualitative plausibility tests, see 4.3.2, that might be helpful to analyze potential problems with the measurements.

4.3.1 Coincidence tests

Verification is generally performed by measuring characterised, stable, high-accuracy standards and performing a coincidence test using their reference data, e.g. from a calibration certificate. Different verification standards and their response to the residual errors of the VNA are discussed in E.1. Fail/pass criteria for coincidence tests are discussed in 4.5 and E.2.

4.3.2 Plausibility tests

Plausibility tests address the soundness of the VNA calibration in a more qualitative way by investigating frequency response and physical limits of standards, based on fundamental considerations.

4.3.2.1 An initial test after calibration can be performed by re-measuring the calibration standards. If the re-measurement does not precisely match the characterization data of the calibration standard, there is a stability or noise issue in the measurement system. Note that the re-measurement of calibration standards is not a verification of the calibration. It neither identifies faulty calibration, by using the wrong calibration standard definitions or mixed up standards, nor potential malfunction of the standards. A set of standards that is physically different from the calibration standards needs to be used for that purpose, see 2.2.6.

4.3.2.2 In the most common case of the reflection coefficient $\mathbf{S}_{11}$ of mechanical offset opens and offset shorts, the frequency response loci should produce approximately circular arcs on the Smith Chart edge approaching the reflection coefficient $\mathbf{S}_{11} = 1$ point (right-hand side) for the opens and $\mathbf{S}_{11} = -1$ (left-hand side) for the shorts for low (MHz) frequencies, respectively.

4.3.2.3 The measurement of a flush short is suitable to test how well the reference plane has been defined by VNA calibration. As a flush short is a passive device it is expected that the magnitude of the reflection coefficient will not exceed $|\mathbf{S}_{11}| = 1$. A perfect flush short would show no phase change with frequency. Due to imperfections in the fabrication process this is, however, never the case. In reality the phase should show a slow monotonous clockwise change starting at -180 deg. Any deviation from this behavior is an indication that the reference plane has not been properly defined during VNA calibration, see e.g. [13].

4.3.2.4 Applying different VNA calibration algorithms, preferably with different sets of calibration standards, should generally lead to equivalent results for the measurements of the DUTs, conditional to the associated measurement uncertainties. An effective and also quantitative test is the comparison of SOLT and SOLR calibration, as discussed in E.1.2.6.

4.3.2.5 After an SOLT calibration it is useful to measure a reciprocal two-port device with finite electrical length to verify the symmetry, i.e. $\mathbf{S}_{21} = \mathbf{S}_{12}$. Any significant deviation would indicate problems related to the calibration.

4.3.2.6 If the frequency range is divided up into bands, and different sets of calibration standards or different calibration methods are used, then measurement results should show fairly continuous transitions when crossing between frequency bands.

4.4 Verification procedure and practical advice

4.4.1 In a strict sense, complete verification includes all S-parameters to be tested at each measurement frequency point. Since in case of data-based calibrated verification standards, reference data are available only for a limited number of frequency points, and furthermore, since there is certain correlation between nearby frequency points, the existing frequency grid will sometimes not be in line with the demands of the DUT. However, if reference data for the verification standards are available it is recommended to choose this frequency grid for VNA calibration and DUT measurement too.

4.4.2 The uncertainty associated with the characterization of the verification artifacts should be smaller (or at least not larger) than the uncertainty associated with the measurements of the verification artifacts.

4.4.3 Verification and calibration standards that have been calibrated by the same laboratory can potentially be used to apply sharper verification criteria, see 4.5.6. It is therefore recommended but not necessary.

4.4.4 As a general rule it is advised to perform a coincidence test using at least one verification standard having a response similar to the DUT.

4.4.5 For a more general verification covering the entire region of the Smith Chart the verification should be performed as a two-step procedure. First, the one-port performance of all ports has to be checked by measuring calibrated one-port verification standards. This is followed by the two-port verification.

4.4.6 For the one-port verification it is recommended to measure two highly reflective standards with different phase (different offset lengths compared to calibration standards) and one matched load. The matched load might be replaced by a matched attenuation device with $\geq$30 dB of attenuation. To check the non-linearity of the measurements it is also recommended to measure a mismatch standard with a reflection coefficient of approximately 0.2 to 0.5.

4.4.7 For the two-port verification a transparent device (beaded air-dielectric line or adapter) and a set of matched attenuation devices should be measured. Most manufacturer verification kits contain a 20 dB and a 40 dB attenuation device. It is recommended to perform an additional measurement using a 3 dB attenuation device to have a better coverage of the Smith Chart and to detect problems related to non-linearity.

4.5 Verification criteria

4.5.1 Pass/fail criteria for verification measurements have to take into account that the measurement and the reference data of the verification device each have an associated uncertainty. A statement about the agreement between measurement and reference data is therefore always a probability statement. The acceptable probability level is usually determined by common sense and by convention.

4.5.2 Generally, the result of a linear VNA measurement is expressed as frequency-dependent, complex-valued S-parameters. In most cases, characterization data along with its associated uncertainties are given in magnitude and phase or alternatively, in real and imaginary part. The uncertainty (covariance) matrix might be known as well. Verification can be performed on a single scalar parameter, e.g. magnitude or phase or on the full two-dimensional complex-valued quantity. The former is justified if there is only interest in a single scalar component of the DUT's S-parameters.

4.5.3 Visual inspection of the frequency response of the data, i.e. the difference between measurement and characterization data with associated uncertainties, is highly recommended. It allows a judgement to be made about the quality of the verification

and helps to identify problems. In most cases visual inspection is sufficient to identify potential problems.

4.5.4 Quantitative evaluation of verification data requires mathematical analysis of the data and the associated uncertainties. Automation of data analysis might be useful if a large amount of data has to be evaluated. A method for quantitative evaluation of verification data is shown in E.2.

4.5.5 In either case, visual or quantitative evaluation, it is recommended to build a history of the measurements of the verification standards. This is helpful to detect gradual changes, e.g. if a calibration standard is drifting (long-term stability). The first measurement of the verification standard is taken as the reference. Subsequent measurements give an indication of the size of random effects affecting the measurement. Any deviation beyond that or a systematic trend indicates a problem.

4.5.6 If calibration standards and verification standards have been calibrated by the same laboratory, there is likely to be a strong positive correlation between standards of the same type, e.g. the matched load used for calibration and the matched load used for verification. Consequently this will lead to a similar correlation between measurement and reference data of the verification standard. This will further lead to a smaller uncertainty associated with the difference between measurement and reference data and therefore to a sharper pass/fail decision. However, this can only be exploited, if the correlation information between calibration and verification standards is available and if the evaluation of the uncertainty associated with the measurement of the verification standards considers this correlation information to the full extent. Obviously, quantitative evaluation according to the formalism in E.2 is needed to take correlation into account.

5 Uncertainty contributions

5.1 Introduction

This section identifies and discusses quantities influencing VNA measurements. There are a number of quantities with significant influence on the result of a VNA measurement. The measurement models discussed in section 6 refer to these quantities explicitly. Estimates of these quantities, and the uncertainties associated, are inputs to the measurement models to determine a value and uncertainty associated with the quantity of interest, usually the S-parameters of the DUT.

5.2 Identification of influence quantities

5.2.1 The accuracy of S-parameter measurements is affected by the following influence quantities:

- Characterization of calibration standards
- VNA noise floor and trace noise

- VNA non-linearity
- VNA drift
- Isolation (cross-talk)
- Test port cable stability
- Connection repeatability

In some specific cases other VNA parameters such as frequency or output power have to be considered in the uncertainty analysis too. However, this is rather unusual and therefore not considered here (see also 2.1.5).

5.2.2 All these influences are sources of measurement errors. It is therefore essential that they be part of any model that describes the measurement and that is being used to evaluate the uncertainty of the measurement. Any uncertainty evaluation that does not address all the components listed above has to be considered as incomplete.

5.3 Characterization of uncertainty contributions

Below, the influences listed in 5.2.1 are discussed. Some of them depend on the setting of the VNA, measurement setup, environmental and operating conditions, etc. The characterization procedures to determine uncertainty contributions based on these influences are not unique and strongly depend on the measurement model being used. Detailed step by step procedures are shown in appendix G and are specifically dedicated to the measurement models in appendix F.

5.3.1 Characterization of calibration standards

5.3.1.1 Characterized calibration standards are necessary if the uncertainty evaluation is performed with the rigorous method, according to 7.1. If the Ripple Method is applied, according to 7.2, it is also possible just to use manufacturer data, which is often provided along with the calibration kit.

5.3.1.2 The reference data of calibration standards with associated uncertainties are taken from a calibration certificate, unless the laboratory has its own realization of traceability to SI units. Normally, this is only the case for national metrology institutes.

5.3.1.3 Usually the dominant source of uncertainty in a VNA measurement are associated with characterisations of calibration standards. Accurate characterization of the calibration standards includes both body and connector [13]. For an accurate determination of the measurement uncertainty it is preferable that correlations between the uncertainty components of the calibration standards are taken into account. Neglecting correlations can lead to either underestimation or overestimation of the measurement uncertainty.

5.3.1.4 Older VNAs require the calibration standards to be characterized by polynomial coefficients (see 2.2.7 as well). A polynomial representation was used in the past due to the memory limitations of the VNA firmware. Modern VNAs allow characterization data to be stored in a data-based form, i.e. as a frequency dependent list of reference values. This is generally a more flexible and accurate way to store characterization data. The data-based characterization can also be used with older VNAs if an appropriate software, e.g. [19], is applied to perform calculations externally on a computer.

5.3.1.5 Calibration standards can drift or change unexpectedly over time. A slow drift due to aging is normal and it is therefore necessary to recalibrate the standards on a regular basis. The recalibration interval depends on the operating conditions and needs to be defined on a case to case basis. Unusual drift or change can be detected through verification, see section 4. Good care and best measurement practice, see section 8, are advised to minimize aging. Aprupt changes or drift in the calibration standards can also be detected by using more calibration standards than necessary and performing an over-determined calibration, see D.3.

5.3.2 Noise floor and trace noise

An example of a step by step characterization of noise floor and trace noise is given in G.1.

5.3.2.1 Noise denotes random signal fluctuations, which are characteristic of all electronic circuits. For VNA measurements two types of noise are distinguished. Noise floor denotes random fluctuations in the absence of a deterministic signal. Trace noise denotes random fluctuations of the measurement result. When trace noise is far above the noise floor, it is proportional to the measured value, i.e., it is a constant fraction of the result. In absolute notation, however, trace noise grows in proportion to an increasing measurement result. The noise content of a transmission coefficient can thus be characterized by a single dB value, as far as the contribution from the noise floor is negligible. Noise floor and trace noise are dependent on the setting of the VNA, for additional information see 8.2.5 and 8.2.6. Smaller IF bandwidth and averaging reduce the effect.

5.3.2.2 Noise contributions to the measurement uncertainty are in principle already included in the characterization of the connection repeatability, see 5.3.7. It is not possible to separate the two effects and one might be tempted to neglect an extra noise contribution to the measurement uncertainty. Neglecting an extra noise contribution is principally possible but care should be taken, because the noise contribution varies, depending on the VNA settings and also depending on the S-parameters of the DUT.

5.3.3 VNA non-linearity

An example of a step by step characterization of VNA non-linearity is given in G.2.

5.3.3.1 The VNA is being modeled as a linear network, i.e. there is a linear relation between the forward and backward propagating waves and their detection by the receivers. The term VNA non-linearity, sometimes also called dynamic accuracy, denotes deviations from this behavior. The effect is dependent on the setting of the source power level

of the VNA. The frequency dependence is generally weak, unless compression effects are present. Compression effects should be avoided by choosing appropriate settings of the VNA, see 8.2.

5.3.3.2 VNA non-linearity combines effects from different components: amplifiers, filters, ADC non-linearities, etc. Noise also results in an apparent non-linear behavior at low signal levels, but this effect is already addressed in 5.3.2. Refined modeling could assign individual uncertainties to each of the contributors. A review of existing methods to determine the non-linearity of receivers by means of step attenuation devices or power sensors as well as a method based on two phase-locked signal sources is given in [20].

5.3.3.3 Due to the lack of access to the individual components in a VNA it is usually more practical to characterize non-linearity at the level of receiver signal ratios, i.e. S-parameters. The step by step characterization in G.2 determines the non-linearity of receiver signal ratios with the help of a step attenuation device.

5.3.3.4 The characterization of step attenuation devices over a wide frequency range may be quite laborious. Alternatively, the procedure described in G.2 is only applied at low frequencies, whereas the non-linearity of the upper frequency range is checked with a characterized fixed attenuation device, e.g. 10 dB.

5.3.3.5 The characterization in G.2 aims at determining residual non-linearities with the measurement of passive devices, assuming that the source power level has already been reduced such that compression effects are avoided. Further information on how to ensure this is given in 8.2.

5.3.4 VNA drift

An example of a step by step characterization of VNA drift is given in G.3.

5.3.4.1 Drift in VNA measurements occurs due to temperature changes and resulting relaxation effects. These effects lead to changes in the electrical length of signal paths and to changes in the performance of couplers, receivers, and other components. Some of the dielectric materials used in test port cables are phase sensitive to temperature changes. At the measurement level this leads to changes in the error coefficients that have been determined during the calibration of the VNA. Drift is not just a phenomenon of the VNA itself, but strongly dependent on environmental factors, measurement setup and operating conditions. Furthermore, drift effects are dependent on the time elapsed after the calibration of the VNA.

5.3.4.2 Drift can be accounted for in different ways. With refined modeling it is in principle possible to assign drift parameters to individual components of the VNA, possibly taking temperature readings into account. In practice it might be more feasible to model drift at the level of the linear network, as shown for the measurement models in appendix F. Drift is assigned to each individual error coefficient. Procedures are described in G.3.

5.3.4.3 A simple and practical procedure to determine drift effects is to measure the calibration standards twice, at the beginning and at the end of a measurement session, and subsequently evaluate the differences between both data sets in terms of drift terms for the individual error coefficients.

5.3.5 Isolation (cross-talk)

5.3.5.1 Isolation is represented by error coefficients in VNA error models, e.g. $\mathbf{E}_{03}$ and $\mathbf{E}_{30}$ in figure D.5. It is generally of minor importance in coaxial measurements with modern VNAs. For older VNAs it is known that it affects measurements of large attenuation to the extent that a correction needs to be applied. Because the effect might as well depend on the setup and has a potential to drift it should be characterized with each measurement, as it is done for the other error coefficients.

5.3.5.2 The treatment of isolation, as done in appendices D and F, might be inadequate for measurements other than coaxial. E.g., for on-wafer measurements additional leakage and cross-talk paths need to be considered. This is not further discussed here. More information can be found in [21, 22].

5.3.5.3 The procedure of characterization follows the characterization of the noise floor, as described in G.1. The uncertainty associated with the isolation terms cannot be separated from the noise floor. It is therefore usually justified to assume that the uncertainty is already included in the noise floor.

5.3.5.4 If the characterization G.1 results in a mean of $\mathbf{S}_{21}$ or $\mathbf{S}_{12}$ that is significantly different from 0, e.g. if the difference is larger than the standard uncertainty associated with the repeated measurements of $\mathbf{S}_{21}$ or $\mathbf{S}_{12}$, the measurement of the DUT needs to be error corrected using the mean value of $\mathbf{S}_{21}$ or $\mathbf{S}_{12}$ as the error coefficient related to isolation.

5.3.6 Test port cable stability

An example of a step by step characterization of test port cable stability is given in G.4.

5.3.6.1 Test port cables are sensitive to temperature changes, movement and other mechanical influences. This section addresses the sometimes unavoidable movement of test port cables. Temperature effects of cables are summarized under drift effects, as discussed in 5.3.4. Other influences inducing mechanical stress should be avoided as far as possible, see 8.5.

5.3.6.2 Moving the test port cable(s) during calibration or DUT measurement will change the error coefficients of the VNA. Thus, cable movement and cable torsion should be avoided as much as possible. Related best practice is discussed in 8.5.1. For measurements that involve more than one VNA port, cable movement is inevitable. The effects of cable movement are strongly dependent on the quality of the test port cable. Even for cables of the same type differences in stability might be rather large. Furthermore, there is a dependency on the measurement setup and how the cables are connected to the VNA, see 8.5. Therefore it is recommended to individually characterize the cables in the specific measurement setup.

5.3.7 Connection repeatability

An example of a step by step characterization of connector repeatability is given in G.5.

5.3.7.1 Deviations from ideal connector geometry lead to mechanical stress and unwanted deformations when mating connectors. This causes changes in electrical behavior for

re-connections under different connector orientations. This effect is dependent on each individual combination of connector pairs. Nevertheless, it is possible to determine a typical repeatability for different connector families as described in example in G.5.

5.3.7.2 It is, however, still recommended to measure at least four re-connections under different azimutal positions for all components that are connected to the test port to verify the typical performance, see 8.8 for further discussion.

5.3.7.3 Furthermore, for a reliable characterization of repeatability it is necessary to use test port adapters with recessed pin depths, as described in 8.5.2, to avoid near-field coupling and potential resonant behavior [23].

6 Measurement model

6.1 A VNA measurement model is the basis for the evaluation of the measurement uncertainty. The measurement model is an analytical expression that relates inputs and influence quantities to the final output quantities, as discussed in more detail in C.3. In VNA metrology it relates the influence quantities discussed in 5.3 to the S-parameters of the DUT. Using methods of uncertainty propagation, as discussed in section 7, the uncertainties associated with the influence quantities can be propagated to evaluate the uncertainty associated with the final result.

6.2 A measurement model is not necessarily a single large equation. It is often more convenient and more natural to have a set of connected equations, each of which representing either a different part of the measurement process, e.g. VNA calibration and VNA error correction, or a refined model of one of the influences, e.g. a drift model taking time spans between measurements and/or temperature readings into account.

6.3 A measurement model of the VNA is closely related to the error model that is applied during VNA calibration. See appendix F for details.

7 Uncertainty evaluation

Two methods of uncertainty evaluation are presented below, the rigorous method with uncertainty propagation through a full measurement model and the Ripple Method. It should be pointed out that both methods deliver the same measurement result (i.e., the same estimates of S-parameters of the DUT), when the same standards and calibration scheme are used for VNA calibration. The different methods will, however, obtain different measurement uncertainties for the same result. For general remarks on S-parameter uncertainties refer to appendix C. The result of any uncertainty evaluation should be verified regardless of the applied method, see section 4 and appendix E.

7.1 Rigorous uncertainty evaluation

7.1.1 Rigorous uncertainty evaluation follows the methodology recommended by the ISO-GUM documents by using a full measurement model and taking the multivariate characteristics of the quantities fully into account. It is not limited in applicability and it is also

suited to be applied at higher frequencies. It requires, however, the use of specialized software to carry out the elaborate calculations.

7.1.2 Rigorous uncertainty evaluation is based on a measurement model, which covers the entire measurement process, i.e. the calibration of the VNA using calibration standards and subsequent error correction of a measurement of the DUT. Details on the measurement model are provided in section 6 and appendix F. An essential part is the characterization of the basic influence quantities. Following the instructions in 5.3 measurement uncertainties are assigned to the basic influence quantities. These uncertainties are propagated through the measurement model by linear or numerical (e.g. using the Monte Carlo Method in [5]) uncertainty propagation.

7.1.3 Based on the discussion in C.4 it might be more economical to use linear uncertainty propagation instead of numerical methods. However, the equations of linear uncertainty propagation, taking correlations fully into account, are elaborate, see [24]. It is beyond the scope of this guide to write these equations down, because the evaluation by hand or in a spreadsheet is not feasible. Instead software support is needed.

7.1.4 Suitable software solutions, which are able to handle the uncertainty propagation of complex-valued quantities, are available [25, 26, 27]. These tools provide general frameworks to realize custom-built implementations of rigorous S-parameter uncertainty evaluation. For software solutions that are specifically targeting S-parameter measurements see [28, 19, 29, 30]. These solutions already contain the VNA measurement models and support different calibration algorithms, i.e. programming is not necessary. Questions related to validation of a software are not addressed in this guide, because they can't be generally answered and have to be evaluated case by case.

7.1.5 Depending on the implementation of rigorous uncertainty propagation it not only provides the correlation between the two components of a complex-valued S-parameter, but also the correlation information between the individual S-parameters and possibly even the cross-frequency correlations. This is valuable if the measured S-parameters are used to calculate derived quantities.

7.1.6 It is a disadvantage of the rigorous method that the equations of the measurement model can't be easily printed in this guide and the user needs to rely on external software. All other elements that are needed to implement the method are available in this guide.

7.1.7 The traceability to SI units is established through the calibration standards. It is therefore necessary to have an SI traceably characterized calibration kit to implement the rigorous method. See the remarks in section 2 as well.

7.2 Ripple Method

7.2.1 The Ripple Method has a long history of usage. It was developed as a pragmatic and adequate approach to measurement uncertainty evaluation when data processing

technologies, computational power and software solutions were not as advanced. The method has already been described in the previous editions of this guide.

7.2.2 The Ripple Method starts with the calibrated VNA. It uses measurements with a beadless air-dielectric line to determine the residuals of the error coefficients. These residuals are used to assign measurement uncertainties to the error coefficients. These uncertainties are propagated through a reduced measurement model, the so-called residual model (F.5), to assign a measurement uncertainty to the DUT measurement.

7.2.3 The Ripple Method has shortcomings and disadvantages, some of which are inherent to the method (at least if the method is applied in its simplest form) and others that are related to the implementation in the previous versions of this guide.
The method requires the handling of beadless air-dielectric lines, which becomes more tedious with increasing frequencies. The air-dielectric lines are assumed to be ideal, neglecting the reflection at the connector interfaces and any losses [31]. The method is unable to determine the residual error of the tracking term. Furthermore, it is limited to the magnitudes of the residuals and the measurand. It does not determine an uncertainty associated with the phase. The method is unable to take correlation effects into account. Uncertainty information is limited to discrete frequencies, the spacing of which is determined by the length of the air-dielectric line. Abrupt changes with frequency in the residual error coefficients can be problematic. The residual measurement model assumes that the VNA is measuring error corrected S-parameters, hence influences of raw error coefficients are neglected.
The implementation of the Ripple Method in the previous versions of the guide lacked a measurement model considering all the influences listed in section 5. Important contributions to the measurement uncertainty, such as e.g. cable movements in two-port measurements, have been dealt with improperly. See as well [32] for an evaluation of the equations used in the previous versions of the guide with respect to form and content.

7.2.4 The Ripple Method is retained in this guide for backward compatibility, acknowledging the fact that many laboratories are still applying this method. The method is presented here in a modified form to eliminate some of the shortcomings mentioned in 7.2.3. Details of the implementation are described in appendix H.

7.2.5 Due to the reflections at the connector of the air-dielectric line it is possible to obtain large variations of the ripple amplitude depending on the position of the center conductor. Together with the inability to take correlation effects into account this can potentially lead to a significant overestimation or underestimation of the measurement uncertainty. The treatment in appendix H has therefore built in some safeguards to avoid underestimation. As a consequence the uncertainties that are obtained by the Ripple Method are in some cases significantly larger when compared to rigorous uncertainty propagation, as can be seen in the examples in appendix J.

7.2.6 It should be pointed out that the worst case measures that are taken in appendix H aim solely to protect from unrealistic small measurement uncertainties. If other measures are taken, as e.g. those mentioned in 7.2.8, it is possible to adjust the evaluation accordingly and relax some of the worst case restrictions. This needs to be decided on a

case by case basis.

7.2.7 An advantage of the Ripple Method is that everything needed to apply the method is documented in this guide and it is not necessary to rely on external specialized software to implement it. The equations in appendix H are sufficiently simple to be implemented in a spreadsheet.

7.2.8 It has been demonstrated that it is possible to increase the quality of the Ripple Method with considerable additional effort. Many of the shortcomings mentioned in 7.2.3 can be resolved this way. The enhanced method requires a characterized air-dielectric line with a positionally controlled center conductor and advanced methods of data processing. Due to the complexity of the method it is not considered in this guide. Though it should be pointed out that in this improved form the Ripple Method can be a valid alternative to evaluate the measurement uncertainty of S-parameter measurements. For details see [33, 34, 35, 36, 37, 38].

8 Best measurement practice and practical advice

Measurement models are only approximations of reality. Influences that are not included in the model will lead to degraded results and erroneous measurement uncertainties. VNA measurements are demanding and susceptible to mistakes. Good measurement practice is therefore an inevitable requirement for performing high quality measurements with associated uncertainties that are reliable.

8.1 Environmental conditions

8.1.1 The standard laboratory temperature for electrical measurements is 23 °C. Deviations from the standard temperature might change the characteristics of the calibration standards and introduce an additional error during VNA calibration. This effect depends on design details of the calibration standards. User guides of calibration kits often specify environmental requirements. As a rule of thumb deviations up to ± 1 °C from standard temperature are of no concern for the characteristics of typical VNA calibration standards.

8.1.2 Changes in the temperature during and after calibration might lead to drift in the error coefficients of the VNA and will directly affect measurements of the DUT. This is generally more significant than the effect of absolute deviation from standard laboratory temperature on the calibration standards. Drift occurring after calibration can be specified for specific environmental conditions, see 5.3.4, and needs to be considered in the evaluation of the measurement uncertainty. A measurement setup including test port cables is more sensitive to temperature effects. On the other hand a test port cable decouples the measurement devices from the VNA test port. Heat flow from the VNA test port might otherwise lead to heating of the components and change their electrical characteristics. For reasonably stable environmental conditions it is therefore recommended to use a test port cable.

8.1.3 Special care should be taken to avoid local heating through unnecessary touching of components and connectors. The effect can be minimized through the use of gloves or finger cots. Adequate waiting time between manipulation and measurement should be considered for cool off.

8.1.4 After an extended period of shutdown VNAs should be allowed to reach thermal equilibrium before resuming operation. If the VNA has been exposed to extreme temperatures, i.e. during a transport in winter time, stabilization might take several hours or even days.

8.1.5 Humidity has low impact on VNA measurements as long as extreme values are avoided. A relative humidity of $(40 \pm 20)\%$ is recommended. High humidity might cause unwanted effects due to condensation. Very low humidity increases the chance of damaging the VNA due to electrostatic discharge.

8.1.6 Operating the VNA in a rack cabinet with appropriate ventilation and proper management of the power supply is recommended. It results in more stable temperature conditions.

8.2 VNA architecture, performance and settings

8.2.1 The four-receiver architecture of VNAs is advantageous for accurate measurements, because it allows to directly measure the VNAs switch terms. Furthermore, calibration algorithms other than SOL and SOLT can be applied. For more details see D.2

8.2.2 Not all VNA errors caused by hardware imperfections are corrected during calibration. An example is non-linearity. Constructional specifics of a VNA might influence its drift behavior. VNAs with good drift stability are less sensitive to environmental changes and help to increase the accuracy of the measurements.

8.2.3 The error coefficients source match and load match, see D.2.2, are corrected through calibration. However, it is better if the VNA has a good raw match performance, because both, source match and load match, have a tendency to magnify the measurement errors that arise when characterising highly reflective calibration standards. Depending on the calibration scheme, this enhancing effect can be more or less pronounced.

8.2.4 Compression effects can affect both reflection and transmission measurements. The source power of the VNA should be chosen so that compression effects are avoided. This can be checked using an uncalibrated fixed attenuation device (3 dB or 10 dB), which is measured repeatedly with the error corrected VNA, starting at a high source power and then gradually decreasing it. Stabilization of the measured attenuation value over the whole frequency range indicates the maximum permissible source power for compression-free operation. For reflection measurements the same procedure can be carried out with a mismatch standard.

8.2.5 The impact of noise on measurement can be lowered by reducing the IFBW (intermediate frequency bandwidth) and/or applying averaging. Both approaches will increase the measurement time, though IFBW does so to a lesser extent. The impact of drift

scales with the measurement time. Therefore, as a rule, averaging should only be applied if further reduction of the IFBW does not result in an improvement. There are two basic types of averaging available, point by point averaging (multiple measurements at each frequency point) and trace averaging (multiple measurements of the whole trace). Contemporary VNAs usually support both types. The two methods differ in how drift becomes noticeable in the measurement results. There is no general preference between point and trace averaging and the choice depends on application and measurement conditions.

8.2.6 Noise can be reduced through smoothing as well. This functionality should be used with care, however. Pronounced features in the frequency dependence, e.g. in a measurement of a filter, might be altered. Smoothing has the potential to introduce additional measurement error if used negligently.

8.3 Use of mechanical calibration and verification standards

8.3.1 Mechanical calibration standards are usually taken from a commercial calibration kit. It is not advised to mix open and short standards, respectively, originating from different calibration kits, unless they are matched in their electrical lengths.

8.3.2 Many calibration kits contain sliding loads to replace the fixed load at higher frequencies. A sliding load increases the accuracy of the measurement if the physically imperfect fixed load is assumed to be ideal, i.e. without reflection. The assumption of an ideal load is usually made in combination with the polynomial representation of open and short. A sliding load is not needed if the definition of the fixed load is data-based. See comments in 2.2.7 and 2.2.8.

8.3.3 A key quality characteristic of mechanical standards is stability, which has a direct impact on the accuracy of measurement. A high connection repeatability with low sensitivity to connector orientation is essential (see 5.3.7 and 8.8), as is long term stability (see 5.3.1.5).

8.3.4 Quality criteria for mechanical calibration standards that can be assessed visually are: concentricity of center conductor, integrity of contact fingers of female interfaces and surface finish of the electrical contact areas. The electrical stability of the standards is directly impacted by these factors.

8.3.5 Some mechanical calibration and verification standards or test port adapters are available in two different designs of the female connector interface, slotted and slotless. Slotted interfaces are more sensitive to variations of the male pin diameter compared to an optimized slotless design. Slotless designs, on the other hand, might have a larger reflection coefficient. From a metrological point of view the latter is of less concern. A slotless design is therefore preferable, because it generally provides better repeatability. See the notes in 8.5.2 as well.

8.3.6 Calibration standards can change their characteristics because of heat flow caused by mating with a warm test port or by touching, see 8.1. Both should be avoided as much as possible. Typical indicators of this problem are phase changes of highly reflective

components or changes in the magnitude of the reflection coefficient of matched components at low frequencies.

8.4 Use of electronic calibration units

8.4.1 The impedance states of ECUs are susceptible to environmental temperature changes. Therefore in most cases ECUs have an internal heater to keep the impedance standards at a constant temperature. This temperature is usually several degrees above the standard laboratory temperature. Thus, heat flow occurs from the ECU, as soon as the ECU is connected to the VNA test port or the test port cable. The achievable measurement accuracy is therefore limited, because the heat flow changes the error coefficients of the VNA [39].

8.4.2 The impedance states of an ECU are subject to aging and hence the recalibration intervals have to be chosen accordingly. Long-term stability tests under controlled laboratory conditions are indicating that ECU states are stable on the time scale of months and years. However, this is very much dependent on the design of the ECU and on the operating conditions. It is therefore impossible to generally quantify the recalibration interval. It is advised to start with short recalibration intervals to build an evidence-based history of the ECU and then adjust the interval accordingly.

8.5 Test port cables

Apart from non-linearity and noise effects, the stability of test port cables is often the most important uncertainty contributor for transmission coefficient measurements. Using high performance test port cables is generally beneficial in terms of measurement uncertainties. An appropriate fixture and layout, see 8.5.1, helps to minimize cable effects. The SOLR calibration scheme, see D.2.3, is an alternative to SOLT that can avoid excessive cable movement. The procedure to evaluate the stability of cables is described in G.4. Appropriate test port adapters, see 8.5.2, act as test port protectors and avoid near field resonance effects.

8.5.1 Fixture and layout

8.5.1.1 An appropriate fixture that supports and defines the layout of the test port cables is a necessary accessory for accurate VNA measurements. A simple cable fixture can be realized with a plain and solid surface in front of the VNA (e.g. a commercially available breadboard) using foam pads and clamps. An example is shown in figure 8.1. The fixture should keep the test port cable fixed during one-port measurements. For two-port measurements one cable remains fixed and the other one should be arranged so that unnecessary cable movements are avoided. If possible, the test port cables should be maintained in a horizontal plane defined by the test port connectors of the VNA. Cable twisting, extreme curvature and stress on the connection should be avoided.

8.5.1.2 High performance test port cables often have a natural bend due to the production process. Maintaining the natural bending helps to reduce measurement error due to cable movement. Even then it is still possible that small angular changes in the connection of the test port cable to the VNA can lead to differences in phase stability. This can

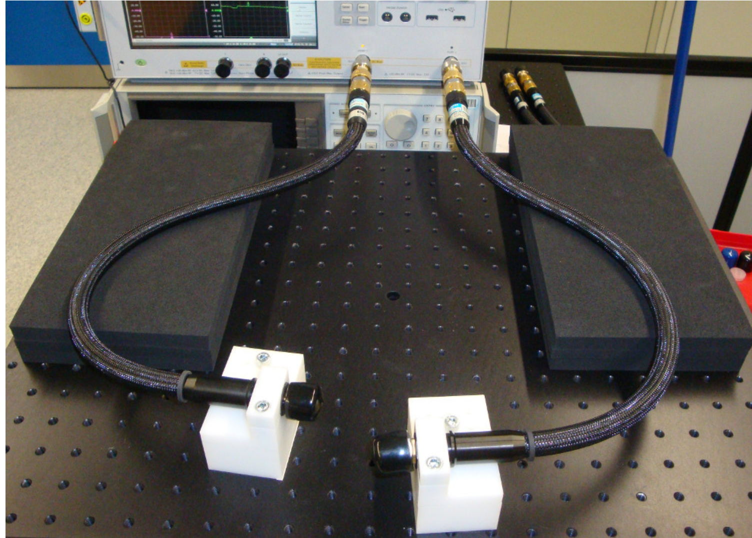

Figure 8.1: Recommended setup of VNA test port cables. A breadboard serves as work space. The cables are supported by foam pads to avoid sagging from the VNA test ports. Clamps are used to keep the cables fixed during measurements.

be examined and optimized by connecting a short at the reference plane (end of the test port cable) and observing how phase variations depend on cable movement while changing slowly the angular orientation of the connection between test port cable and VNA.

8.5.1.3 For reasons given in 8.5.2 it is recommended to use an adapter in combination with the test port cable. The most stable cable-adapter combination is achieved by using ruggedized connectors at the cable-adapter interface. The ruggedized connector can be found on many VNA test ports. It has a large threaded body that helps to stabilize the connection.

8.5.1.4 The selection of the correct VNA calibration scheme can help to reduce measurement error due to cable movement as well, as discussed in 3.2.

8.5.2 Test port adapters

8.5.2.1 It is recommended to use test port adapters for several reasons. If any damage occurs to the connector only the adapter has to be changed or repaired, rather than the entire test port cable or VNA test port. Using a metrology grade adapter with geometries close to the nominal values and good concentricity of the center conductor will minimize mechanical stress and improve electrical repeatability. Finally, an optimal pin depth with respect to the reference plane, see 8.5.2.2, can be established on the test port side.

8.5.2.2 In the past, the objective was always to have a connection at the measurement reference plane as flush as possible, i.e. the pin gap at the center conductor was kept as small as possible. It has been shown [23] that this causes coupling effects, resulting in an undefined reference plane, and possibly even resonance effects and repeatability

issues. It is therefore recommended [40] to keep the size of the pin gap not smaller than the values given in table 8.1 for typical connector geometries. As the DUT can have a pin recession down to zero it is advised to use test port adapters that have a recessed pin depth not smaller than the values given in table 8.1.

8.5.2.3 The simple stability test described in 8.7 is a good method to identify any stability problems related to the test port adapters, i.e. a loose connection between test port cable and adapter.

8.6 Connector care

8.6.1 The appropriate handling of connectors is an important aspect of good measurement practice. A large amount of literature on the topic is available and only the most important aspects are summarized below. Further reading is recommended, see e.g. [41, 42]. Manufacturers of precision connectors provide additional information on good handling practice.

8.6.2 Metrology grade connectors are precision components that require special care. Overtorquing, rotating the body of the component during connection and rough abrasive handling should be avoided. Cleaning, visual inspections, and pin depth measurements should be carried out regularly. Dirty connectors often show degraded repeatability. This especially holds for small connectors. It is not only the area of the contact zones that is sensitive to contamination (resulting in magnitude and phase changes). Even a contaminated thread of the connecting nut might affect the impact of the torque force and degrade the repeatability. Protruding center pins and defects might cause damage when mated with other components. Mechanical stress on the connection should be avoided, see 8.5.1, because it will degrade the electrical performance of the measurement or even lead to damage.

8.7 Initial stability test

8.7.1 To test the basic stability of the VNA measurement setup before calibration, the following simple procedures can be performed. Connect a short to each test port and knock on the housing of the test port adapter, perform small movements of the cable end and reconnect the short under different connector orientations to reveal instabilities near the measurement reference plane. An unusual spread in the raw uncorrected data in each of the above test measurements might be an indication of one or more of the following problems: unstable cable-connector interface, structural issues with the test port adapter or instabilities directly at the measurement reference plane, represented by the connector interface.

8.8 Repeatability

8.8.1 It is recommended to repeat each measurement for at least four different connector orientations. The purpose of this practice is partly to verify the specific repeatability of a certain connector type, but also to see if any component has a stability issue. It is not uncommon that ill-behaving components show two or more different electrical

Table 8.1: Recommended minimal size of pin gaps for coaxial connections at the measurement reference plane to avoid resonance effects. The values are listed in metric and imperial units.

Connector type	Minimal pin gap	
	$/10^{-6}$ m	$/10^{-4}$ in
1.0 mm	5	2
1.85 mm	5	2
2.4 mm	15	6
2.92 mm	10	4
3.5 mm	15	6
Type-N (50 Ω)	12	5

states imposed by the varying mechanical stress during the measurements at different connector orientations.

8.8.2 It is important to completely disconnect the center conductor before changing the connector orientation. This prevents rotational stress on the female contact fingers and the male pin. Rotational stress might bend the contact fingers, resulting in a change of contact point, or damage the surface plating. The operator must exercise care. Bad alignment of the connectors, excessive pushing or pulling during mating and disconnecting will provide extra stress on the center conductor, impacting structures or circuits attached to it, as e.g. soldering joints or resistive elements.

References

[1] V. Teppati, A. Ferrero, and M. Sayed, editors. *Modern RF and Microwave Measurement Techniques*. Cambridge University Press, 2013. ISBN 978-1-107-03641-3.

[2] J. Dunsmore. *Handbook of Microwave Component Measurements: with Advanced VNA Techniques*. John Wiley & Sons, Ltd, 2012. ISBN 978-1-119-97955-5.

[3] M. Hiebel. *Fundamentals of Vector Network Analysis*. Rohde & Schwarz, 2007. ISBN 978-3-939837.

[4] Keysight Technologies. Network Analyzer Basics. Electronic document. Back to Basics Series, available at www.keysight.com.

[5] BIPM, IEC, IFCC, ILAC, ISO, IUPAC, IUPAP and OIML. *Evaluation of measurement data - Supplement 2 to the "Guide to the expression of uncertainty in measurement" - Extension to any number of output quantities*, 2011. JCGM 102:2011; available at http://www.bipm.org/en/publications/guides/.

[6] BIPM, IEC, IFCC, ILAC, ISO, IUPAC, IUPAP and OIML. *Evaluation of Measurement Data - Guide to the expression of uncertainty in measurement*, 2008. JCGM 100:2008; available at www.bipm.org/en/publications/guides/gum.html.

[7] BIPM, IEC, IFCC, ILAC, ISO, IUPAC, IUPAP and OIML. *International Vocabulary of Metrology - Basic and General Concepts and Associated Terms (VIM 3rd edition)*, 2012. JCGM 200:2012; available at http://www.bipm.org/en/publications/guides/.

[8] R. B. Marks and D. F. Williams. A General Waveguide Circuit Theory. *J. Res. Natl. Stand. Technol.*, 97(5):533 – 562, 1992.

[9] M. Zeier, J. Hoffmann, P. Hürlimann, J. Rüfenacht, D. Stalder, and M. Wollensack. Establishing traceability for the measurement of scattering parameters in coaxial line systems. *Metrologia*, 55:S23 – S36, 2018.

[10] J. Hoffmann, J. Ruefenacht, M. Wollensack, and M. Zeier. Comparison of 1.85mm Line Reflect Line and Offset Short Calibration. In *ARFTG Conference Digest*, number 76, pages 1 – 7, 2010.

[11] N. M. Ridler and A. G. Morgan. New primary reference standard for vector network analyser calibration at millimetre wavelengths in coaxial line. *Meas. Science and Technol.*, 19:065103, 2008.

[12] K. Wong. Characterization of calibration standards by physical measurements. In *ARFTG Conference Digest*, number 39, pages 53–62, 1992.

[13] K. Wong and J. Hoffmann. Improve VNA Measurement Accuracy by Including Connector Effects in the Models of Calibration Standards. In *ARFTG Conference Digest*, number 82, pages 1–7, 2013.

[14] J. Hoffmann, M. Wollensack, J. Ruefenacht, and M. Zeier. Extended S-parameters for imperfect test ports. *Metrologia*, 52:121 – 129, 2015.

[15] Keysight Technologies. Specifying Calibration Standards and Kits for Keysight Vector Network Analyzers - Application Note. Electronic document. Available at http://literature.cdn.keysight.com/litweb/pdf/5989-4840EN.pdf.

[16] P. I. Somlo and J. D. Hunter. *Microwave Impedance Measurements - IEE electrical measurement series; 2*. Peter Peregrinus Ltd, London, UK, 1985.

[17] D. M. Pozar. *Microwave Engineering*. John Wiley & Sons, Inc., 4th edition, 2011. ISBN 978-0-470-63155-3.

[18] A. Ferrero and U. Pisani. Two-port network analyzer calibration using an unknown thru. *IEEE Microwave & Guided Wave Letters*, 2(12):505 – 507, 1992.

[19] METAS VNA Tools, available at www.metas.ch/vnatools.

[20] K. Wong. Receiver Linearity Measurement Using Two CW Signals. In *ARFTG Conference Digest*, number 78, pages 1–5, 2011.

[21] J. V. Butler, D. K. Rytting, M. F. Iskander, R. D. Pollard, and M. Vanden Bossche. 16-term error model and calibration procedure for on-wafer network analysis measurements. *IEEE Trans. Microwave Theory & Tech.*, 39(12):2211 – 2217, 1991.

[22] A. Ferrero and F. Sanpietro. A Simplified Algorithm for Leaky Network Analyzer Calibration. *IEEE Microwave & Guided Wave Letters*, 5(4):119 – 121, 1995.

[23] J. Hoffmann, P. Leuchtmann, and R. Vahldieck. Pin Gap Investigations for the 1.85 mm Coaxial Connector. In *Proceedings of the 37th European Microwave Conference*, number 76, pages 388 – 391, 2007.

[24] M. Garelli and A. Ferrero. A Unified Theory for S-Parameter Uncertainty Evaluation. *IEEE Trans. Microwave Theory & Tech.*, 60(12):3844 – 3855, 2012.

[25] B. D. Hall. Computing uncertainty with uncertain numbers. *Metrologia*, 43:L56 – L61, 2006.

[26] M. Zeier, J. Hoffmann, and M. Wollensack. Metas.UncLib - a measurement uncertainty calculator for advanced problems. *Metrologia*, 49:809 – 815, 2012.

[27] B. D. Hall. Object-oriented software for evaluating measurement uncertainty. *Meas. Sci. Technol.*, 24:055004, 2013.

[28] M. Zeier, J. Hoffmann, J. Ruefenacht, and M. Wollensack. Contemporary evaluation of measurement uncertainties in vector network analysis. *tm - Technisches Messen*, 84(5):348 – 358, 2017.

[29] NIST Microwave Uncertainty Framework, available at www.nist.gov/ctl/rf-technology/related-software.cfm.

[30] Dynamic uncertainty for S-parameters, Option 015, Keysight Technologies, available through www.keysight.com.

[31] J. Hoffmann, P. Leuchtmann, J. Ruefenacht, and K. Wong. S-parameters of Slotted and Slotless Coaxial Connectors. In *ARFTG Conference Digest*, number 74, pages 1 – 5, 2009.

[32] B. D. Hall. VNA error models: Comments on EURAMET/cg-12/v.01, 2010. ANAMET Report 051.

[33] F. Mubarak and G. Rietveld. Uncertainty Evaluation of Calibrated Vector Network Analyzers. *IEEE Trans. Microwave Theory & Tech.*, PP(99):1 – 13, 2017.

[34] R. Judaschke, G. Wuebbeler, and C. Elster. Second-Order Error Correction of a Calibrated Two-Port Vector Network Analyzer. In *ARFTG Conference Digest*, number 73, pages 1–3, 2009.

[35] G. Wuebbeler, C. Elester, T. Reichel, and R. Judaschke. Determination of the Complex Residual Error Parameters of a Calibrated One-Port Vector Network Analyzer. *IEEE Trans. Instr. & Meas.*, 58(9):3238 – 3244, 2009.

[36] G. Wuebbeler, C. Elester, T. Reichel, and R. Judaschke. Determination of Complex Residual Error Parameters of a Calibrated Vector Network Analyzer. In *ARFTG Conference Digest*, number 69, 2007.

[37] J. Stenarson and K. Yhland. Residual error models for the SOLT and SOLR VNA calibration algorithms. In *ARFTG Conference Digest*, number 69, pages 133 – 139, 2007.

[38] J. Stenarson and K. Yhland. A new assessment method for the residual errors in SOLT and SOLR calibrated VNAs. In *ARFTG Conference Digest*, number 69, pages 140 – 145, 2007.

[39] M. Zeier, J. Hoffmann, P. Huerlimann, J. Ruefenacht, M. Wollensack, R. Judaschke, and K. Kuhlmann. Stability tests of electronic calibration units. In *CPEM Conference Digest*, pages 16 – 17, 2014.

[40] J. Hoffmann and P. Huerlimann. Key parameters of coaxial connector models - mechanical design features and electrical properties. electronic document, 2015. available at www.metas.ch/hf/docs.

[41] A. D. Skinner. ANAMET connector guide. available at http://www.npl.co.uk/anamet-connector-guide, 2007. 3rd edition.

[42] J. Hoffmann and J. Ruefeneacht. How to make good coaxial connections. electronic document, 2013. available at www.metas.ch/hf/docs.

[43] R. W. Beatty. A $\lambda_g/4$ waveguide standard of voltage standing-wave ratio. *Electronics Letters*, 9(2):24 – 26, 1973.

[44] BIPM, IEC, IFCC, ILAC, ISO, IUPAC, IUPAP and OIML. *Evaluation of measurement data - Supplement 1 to the "Guide to the expression of uncertainty in measurement" - Propagation of distributions using a Monte Carlo method*, 2008. JCGM 101:2008; available at http://www.bipm.org/en/publications/guides/.

[45] C. A. Hoer and G. F. Engen. Calibrating a Dual Six-Port or Four-Port for Measuring Two-Ports with Any Connectors. In *IEEE MTT-S International Microwave Symposium Digest*, pages 665 – 668, 1986.

[46] A. Ferrero and U. Pisani. QSOLT: a new fast calibration algorithm for two port S-parameter measurements. In *ARFTG Conference Digest*, number 38, pages 15 – 24, 1991.

[47] O. Ostwald. T-Check accuracy test for vector network analyzers utilizing a Tee-junction. Electronic document, June 1998. Rohde & Schwarz Application Note 1EZ43_0E, Available at https://www.rohde-schwarz.com.

[48] G. F. Engen and C. A. Hoer. Thru-reflect-line: An improved technique for calibrating the dual six-port automatic network analyzer. *IEEE Trans. Microwave Theory & Tech.*, 27(12):987 – 993, 1979.

[49] N. M. Ridler and M. J. Salter. An approach to the treatment of uncertainty in complex S-parameter measurements. *Metrologia*, 39:295 – 302, 2002.

[50] B. D. Hall. Evaluating the measurement uncertainty of complex quantities: a selective review. *Metrologia*, 53:S25 – S31, 2016.

[51] R. Willink and B. D. Hall. A classical method for uncertainty analysis with multidimensional data. *Metrologia*, 39:361 – 369, 2002.

[52] R. Willink and B. D. Hall. An extension to GUM methodology: degrees-of-freedom calculations for correlated multidimensional estimates. eprint, arXiv:1311.0343 [physics.data-an], 2013.

[53] B. D. Hall. Expanded uncertainty regions for complex quantities. *Metrologia*, 50:490 – 498, 2013.

[54] B. D. Hall. Expanded uncertainty regions for complex quantities in polar coordinates. *Metrologia*, 52:486 – 495, 2015.

[55] R. B. Marks. Formulations of the basic vector network analyzer error model including switch-terms. In *ARFTG Conference Digest*, number 50, pages 115 – 126, 1997.

[56] D. Blackham. Application of weighted least squares to OSL vector error correction. In *ARFTG Conference Digest*, number 61, pages 11–21, 2003.

[57] M. J. Salter, N. M. Ridler, and P. M. Harris. Over-determined calibration schemes for RF network analysers employing generalised distance regression. In *ARFTG Conference Digest*, number 62, pages 127 – 142, 2003.

[58] J. Hoffmann, P. Leuchtmann, J. Ruefenacht, and R. Vahldieck. A stable bayesian vector network analyzer calibration algorithm. *IEEE Trans. Microwave Theory & Tech.*, 57(4):869 – 880, 2009.

[59] M. Wollensack, J. Hoffmann, J. Ruefenacht, and M. Zeier. VNA Tools II: S-parameter uncertainty calculation. In *ARFTG Conference Digest*, number 79, pages 1 – 5, 2012.

[60] K. V. Mardia, J. T. Kent, and J. M. Bibby. *Multivariate Analysis*. Academic Press, 2003.

[61] F. Mubarak, M. Zeier, J. Hoffmann, N. M. Ridler, M. J. Salter, and K. Kuhlmann. Verification concepts in S-parameter measurements. In *CPEM Conference Digest*, 2016.

[62] A. Lewandowski. *Multi-frequency approach to vector-network-analyzer scattering-parameter measurements*. PhD thesis, Warsaw University of Technology, 2010.

[63] F. Mubarak, G. Rietveld, D. Hoogenboom, and M. Spirito. Characterizing Cable Flexure Effects in S-parameter Measurements. In *ARFTG Conference Digest*, number 82, 2013.

[64] K. Yhland and J Stenarson. A simplified treatment of uncertainties in complex quantities. In *CPEM Conference Digest*, pages 652 – 653, 2004.

[65] IEEE. *IEEE 287-2007 Standard for Precision Coaxial Connectors (DC to 110 GHz)*, 2007.

[66] T. Reichel, R. H. Judaschke, and F. Rausche. Effect of Uncorrected Test Port Match of a Vector Network Analyzer on the Transmission Coefficient Gained after SOLT Calibration. accepted by CPEM conference, 2018.

[67] N. M. Ridler and C. Graham. Some typical values for the residual error terms of a calibrated vector automatic network analyser (ANA). In *Proc BEMC Conference*, pages 45/1 – 45/4, 1999. Brighton, UK.

[68] J. Hoffmann. Errors in the Ripple Technique due to Pin Gap. electronic document, 2016. available at www.metas.ch/hf/docs.

[69] B. D. Hall. On the expression of measurement uncertainty for complex quantities with unknown phase. *Metrologia*, 48:324 – 332, 2011.

[70] T. Reichel. Derivation of the Uncertainty assigned to the Residual Reflection Tracking Parameter with SOL(T) calibrations. electronic document, 2018. available at www.metas.ch/hf/docs.

[71] A. R. Kerr. Mismatch caused by waveguide tolerances, corner radii, and flange misalignment. Technical report, National Radio Astronomy Observatory, Charlottesville, VA, USA, 2009. Electronics Division Technical Note No 215, available at http://www.gb.nrao.edu/electronics/edtn/edtn215.pdf.

[72] D. J. Bannister, E. J. Griffin, and T. E. Hodgetts. On the dimensional tolerances of rectangular waveguide for reflectometry at millimetric wavelengths. Technical report, National Physical Laboratory, Teddington, UK, 1989. NPL Report DES 95.

[73] N. M. Ridler and M. J. Salter. Cross-connected Waveguide Lines as Standards for Millimeter- and Submillimeter-wave Vector Network Analyzers. In *ARFTG Conference Digest*, number 81, 2013.

[74] T. Schrader, K. Kuhlmann, R. Dickhoff, J. Dittmer, and M Hiebel. Verification of scattering parameter measurements in waveguides up to 325 GHz including highly-reflective devices. *Adv. Radio Sci.*, 9:9 – 17, 2011.

[75] N. M. Ridler. Choosing line lengths for calibrating waveguide vector network analysers at millimetre and sub-millimetre wavelengths. Technical report, National Physical Laboratory, Teddington, UK, 2009. NPL Report TQE 5.

A Glossary

ADC	Analog to digital converter.
Air-dielectric line	Air-dielectric coaxial transmission line.
Beaded air-dielectric line	An air-dielectric line with a fixed center conductor that is kept in place by one or more dielectric beads.
Beadless air-dielectric line	An air-dielectric line consisting of two separate parts, the center conductor and the outer conductor. The center conductor is kept in place by the counterparts when the air-dielectric line is mounted.
Beatty Line	A mismatched air-dielectric line with a central section deviant from 50 Ω (e.g. 25 Ω) and 50 Ω sections at both ends [43].
Cartesian coordinates	Also called rectangular coordinates. The two-dimensional Cartesian coordinate system consists of a horizontal and a vertical axis, conventionally denoted as x-axis and y-axis.
Directivity	VNA error coefficient.
DUT	Device under test.
ECU	Electronic calibration unit.
Fixed load	Alternative expression for matched load. Usually used to differentiate from a sliding load.
Flush short	A short without a section of transmission line and with a reflection coefficient close to -1.
Flush thru	Direct connection of two test ports, corresponding to the flush mating of two reference planes, with nominal reflection coefficients of 0 and transmission coefficient of 1.
IFBW	Intermediate frequency bandwidth. A VNA setting that affects the noise floor of the VNA.
ISO-GUM	Guide to the Expression of Uncertainty in Measurement, consisting of a main document [6] and supplementary documents, e.g. [44, 5]. Authoritative guidance for the evaluation of measurement uncertainties.
Isolation	VNA error coefficient.
Load match	VNA error coefficient.
LRL calibration	VNA two port calibration (Line-Reflect-Line) based on measurements of highly reflective standards (open or short) and air-dielectric lines [45].

Matched load	Impedance matched one-port device with a reflection coefficient close to 0.
Mismatch	Impedance mismatched one-port device. Typical commercially available mismatch standards have reflection coefficients between 0.1 and 0.5.
Offset open	An open with a section of transmission line with finite electrical length in front of it. Often just referred to as open.
Offset short	A short with a section of transmission line with finite electrical length in front of the shorting plane. Often just referred to as short.
Open	One port device with a reflection coefficient close to 1 at DC.
OSM calibration	See SOL calibration.
PDF	Probability density function. Function that describes the relative likelihood of a random variable to take on a given value.
Primary experiment	The process of the SI traceable characterization of primary measurement standards.
Primary standard	Measurement standard that can be characterized through a primary experiment. Typical primary standards are air-dielectric lines, offset shorts, flush shorts and offset opens.
Reflection tracking	VNA error coefficient.
Rigorous Method	Uncertainty evaluation of VNA measurements based on rigorous modeling of the entire VNA measurement process.
Ripple Method	Uncertainty evaluation of VNA measurements based on the determination of residual VNA error coefficients. The residual error coefficients are determined through the analysis of measured ripple patterns.
S-parameters	Scattering parameters.
Short	One port device with a reflection coefficient close to -1 at DC. Two types of shorts are typically distinguished: offset short and flush short.
Signal flow graph	Graphical representation of a linear network, consisting of branches and nodes.

Sliding load	One-port device consisting of an air-dielectric line terminated with a matched load. The load is an integral part of the air-dielectric line and can be moved in the longitudinal direction within the air-dielectric line, thus changing the phase relation of the reflected signal.
SOL calibration	VNA one port calibration based on short, open and (matched) load standards. Sometimes also called OSM or OSL calibration.
SOLR calibration	Short-Open-Load-Reciprocal VNA two port calibration [18]. Also known as Unknown Thru calibration.
SOLT calibration	VNA two port calibration based on short, open, (matched) load standards and the measurement of a flush thru connection. Sometimes also called OSMT calibration.
Source match	VNA error coefficient.
QSOLT calibration	Quick SOLT. VNA two port calibration method based on the transfer of the calibration from one port to the other [46].
SSS calibration	VNA one port calibration based on offset shorts.
SSST calibration	VNA two port calibration based on offset shorts and a flush thru measurement.
T-checker	Two-port verification device based on a T-junction, one port of which is terminated by a load impedance [47].
TOSM calibration	See SOLT calibration.
Transmission tracking	VNA error coefficient.
TRL calibration	VNA two port calibration based on measurements of flush thru connection, reflects (open or short) and air-dielectric lines [48].
Unknown Thru calibration	see SOLR calibration.
VNA	Vector network analyzer.
VNA calibration	Determination of VNA error coefficients and VNA switch terms by the measurement of a set of VNA calibration standards.
VNA calibration standards	Characterized measurement standards, which are used during VNA calibration to determine error coefficients and switch terms.
VNA error model	Model of the systematic errors in a VNA measurement. It can be represented graphically as a signal flow graph of a linear network.

VNA error coefficients	Coefficients in the VNA error model, which are determined during VNA calibration.
VNA isolation	VNA error coefficient describing cross-talk effects.
VNA switch term	VNA error coefficient describing the effect when the source is switched to the other port.
VNA measurement model	VNA error model extended with influences that are affecting the measurement. Represents the basis for the evaluation of the measurement uncertainty.

B Notation

The quantities in VNA measurements are typically complex-valued. They are written in bold face, such as $\mathbf{S}_{11}$. Real and imaginary component are represented by $\mathrm{Re}[\mathbf{S}_{11}]$ and $\mathrm{Im}[\mathbf{S}_{11}]$, respectively. Magnitude and phase are represented by $|\mathbf{S}_{11}|$ and $\arg(\mathbf{S}_{11})$, respectively. Vectors and matrices are written in bold face whereas scalar values are printed in plain face.

When properly dealing with measurement quantities and uncertainties one has to distinguish between the quantity itself and an estimate of the quantity. Quantities are denoted by plain characters, e.g. $\mathbf{S}_{11}$, whereas estimates are accented with a hat, e.g. $\hat{\mathbf{S}}_{11}$.

Quantity estimates (and measured values) are never exactly equal to the quantities themselves; there is always some measurement error involved. For that reason, an uncertainty is associated with each estimate of a quantity. In the scalar case uncertainties are denoted by a plain faced $\mathrm{u}(\cdot)$, e.g. $\mathrm{u}(\mathrm{Re}[\hat{\mathbf{S}}_{11}])$ and in the complex-valued or vector case by a bold faced $\mathbf{u}(\cdot)$, e.g. $\mathbf{u}(\hat{\mathbf{S}}_{11})$. In the latter case the uncertainty is represented by a matrix, as shown in appendix C.

C S-parameter measurement uncertainties

A basic framework for the evaluation of measurement uncertainty of S-parameters has been described in [49]. This was already largely in agreement with the treatment of multidimensional (or multivariate) quantities promoted in Supplement 2 [5] of the ISO-GUM [6], which was published more than a decade later.

The purpose of this section is to provide a brief introduction to S-parameter measurement uncertainties and point out some aspects that are relevant in practical measurements. This is by no means comprehensive and further information should be obtained from literature. Recommended reading is [5] for the general treatment of multivariate measurement uncertainties and [50], which is more specifically related to complex-valued quantities.

C.1 S-parameter data format

S-parameters are complex-valued quantities and can be represented either by polar coordinates (magnitude and phase) or Cartesian coordinates (real and imaginary components). Polar coordinates are directly related to some of the physical phenomena occurring during a measurement and are therefore sometimes preferred for the interpretation and understanding of results. It has been demonstrated, however, that polar coordinates might cause problems when used in statistical analysis or for uncertainty evaluation [49]. It is therefore recommended to perform any calculations in Cartesian coordinates. For the interpretation the data can be transformed to polar coordinates. Especially for the reflection coefficient of highly reflective devices the visualization in polar coordinates is usually more meaningful, whereas well matched devices are preferably studied in Cartesian coordinates.

The following sections will therefore use Cartesian coordinates only, though the formalism is in principle also applicable to polar coordinates if the necessary precautions are taken.

C.2 Representation of measurement uncertainties

A quantity of interest (the measurand) cannot be determined exactly because of measurement error. Therefore, the measured value can only be regarded as an estimate of the measurand, the unknown error being covered with the stated uncertainty.

Uncertainty associated with the measurement of a quantity of interest is characterized by a probability density function (PDF). For an S-parameter, or any other complex-valued quantity, a two-dimensional PDF is used. The type of distribution and a scale factor for the extent of the distribution will be chosen to represent the uncertainty of measurement. For a real-valued quantity, the so-called "standard uncertainty" is the standard deviation (square root of the variance) of the PDF. In the case of complex quantities (and indeed for other multidimensional quantities), the variances and covariances of the chosen PDF play a similar role.

This is formally shown for a single complex-valued quantity x (e.g. one of the S-parameters). The variable $\hat{\mathrm{x}}$ denotes the estimate of that quantity. The measurement uncertainty associated with $\hat{\mathrm{x}}$ depends on the real and imaginary components and is

conveniently represented by a symmetric uncertainty matrix, which is sometimes also called covariance matrix:

$$\mathbf{u}(\hat{\mathbf{x}}) = \begin{pmatrix} u_{11} & u_{12} \\ u_{21} & u_{22} \end{pmatrix}, \tag{C.1}$$

where

$$\begin{aligned} u_{11} &= (\mathrm{u}(\mathrm{Re}\,[\hat{\mathbf{x}}]))^2 \\ u_{22} &= (\mathrm{u}(\mathrm{Im}\,[\hat{\mathbf{x}}]))^2 \\ u_{12} = u_{21} &= r\,(\mathrm{Re}\,[\hat{\mathbf{x}}]\,, \mathrm{Im}\,[\hat{\mathbf{x}}])\,\mathrm{u}(\mathrm{Re}\,[\hat{\mathbf{x}}])\,\mathrm{u}(\mathrm{Im}\,[\hat{\mathbf{x}}])\,, \end{aligned} \tag{C.2}$$

with $\mathrm{u}(\mathrm{Re}\,[\hat{\mathbf{x}}])$ and $\mathrm{u}(\mathrm{Im}[\hat{\mathbf{x}}])$ the standard uncertainties associated with the real and imaginary components and $r(\mathrm{Re}[\hat{\mathbf{x}}], \mathrm{Im}[\hat{\mathbf{x}}])$ the correlation coefficient between the real and imaginary component estimates.

C.2.1 Correlation

Correlation in measured values is caused by common influences. A few examples: the use of the same reference standard for the characterization of calculable calibration standards will cause correlations between the mechanical measurements of calculable standards. If these standards are used to characterize transfer standards, i.e. an SOL kit, short, open and matched load will be correlated. The measurements of a short standard during a VNA one-port calibration will influence the determination of the reflection tracking and the source match resulting in correlation between them. The multiplication of measured values for two complex-valued quantities (i.e. two reflection coefficients) in Cartesian coordinates will lead to correlation between the real and imaginary components of the product, even if the initial measurements were uncorrelated (i.e. the quantity estimates are not correlated).

Correlation in VNA measurements is unavoidable, and it can either increase or decrease the measurement uncertainty. The best way to take correlation effects into account is through refined modeling of the measurement process. Common influence quantities are part of the measurement model. Rigorous uncertainty propagation based on such a measurement model, see 7.1, will take correlation properly into account. For random effects it is possible to evaluate correlation in a statistical way by using the formalism in C.5.

C.3 Evaluation of measurement uncertainty

Uncertainty analysis requires a mathematical model, the so-called measurement model, which relates the quantity of interest $\mathbf{y}$, e.g. the S-parameter of a DUT, to input quantities $\mathbf{x}_1$, $\mathbf{x}_2$, ... that influence the outcome of the measurements, e.g. the characterization of VNA calibration standards or VNA device parameters as noise, non-linearity and drift:

$$\mathbf{y} = \mathbf{f}\,(\mathbf{x}_1, \mathbf{x}_2, ...)\,. \tag{C.3}$$

The terms that appear in a measurement model (C.3) refer to actual quantities. But as pointed out in C.2 there are only estimates available. An estimate of the quantity

of interest is obtained by evaluating the measurement model with the estimates of the input quantities.

The measurement uncertainty associated with the estimate (measured value) of the quantity of interest $\mathbf{y}$ is evaluated in three steps.

1. Determination of the estimates $\hat{\mathbf{x}}_1$, $\hat{\mathbf{x}}_2$, ... and associated uncertainties $\mathbf{u}(\hat{\mathbf{x}}_1)$, $\mathbf{u}(\hat{\mathbf{x}}_2)$, ... of the input quantities $\mathbf{x}_1$, $\mathbf{x}_2$, ...: characterization of input quantities by statistical analysis, systematic studies, previous evaluations, device specifications, etc. The ISO-GUM [6] distinguishes between Type A (statistical analysis), see remarks in C.5, and Type B (by any other means) evaluations.

2. Calculation of uncertainty of the quantity of interest: propagation of the estimates $\hat{\mathbf{x}}_1$, $\hat{\mathbf{x}}_2$, ... and uncertainties $\mathbf{u}(\hat{\mathbf{x}}_1)$, $\mathbf{u}(\hat{\mathbf{x}}_2)$, ... of the input quantities $\mathbf{x}_1$, $\mathbf{x}_2$, ... through the measurement model (C.3) to obtain an estimate $\hat{\mathbf{y}}$ of the quantity of interest $\mathbf{y}$, with an associated uncertainty $\mathbf{u}(\hat{\mathbf{y}})$. See remarks in C.4.

3. Scaling of $\mathbf{u}(\hat{\mathbf{y}})$ by a coverage factor k to obtain an expanded uncertainty with a desired coverage probability. This is typically 95%. See remarks in C.6.

C.4 Uncertainty propagation

To propagate the uncertainties associated with estimates of the input quantities $\mathbf{x}_1$, $\mathbf{x}_2$, ... to the quantity of interest $\mathbf{y}$ through the measurement model (C.3) two established techniques are available. Both techniques have the capability to take into account correlations between the estimates of the input quantities.

1. Linear uncertainty propagation: this method is described in GUM Supplement 2 [5] and is a generalization of the scalar case described in [6]. Variances and covariances of the input quantities are propagated through a linearized measurement model. The uncertainty in the measured value of the quantity of interest is assumed to be characterized by a multivariate Gaussian PDF. The variance-covariance of this PDF is found by propagating variance-covariance information associated with the input quantity estimates through the measurement model. The result can be obtained through an analytical calculation.

2. Monte Carlo method: this method is described in GUM Supplement 2 [5] and generalizes the scalar method in GUM Supplement 1 [44]. Here the distributions are propagated through the measurement model by making repeated draws from the PDFs of the input quantities. The result is a PDF of the quantity of interest. Numerical methods with the generation of pseudo-random numbers are usually needed to obtain the result.

Linear uncertainty propagation makes some simplifying assumptions to allow for an analytical calculation. In the large majority of the cases the results are nevertheless accurate enough. For complex-valued quantities there are some cases known where linear uncertainty propagation can fail, e.g. when transforming values near zero between Cartesian and polar coordinates. The computational effort is, however, generally significantly larger for the Monte Carlo method compared to linear uncertainty propagation. This is a criterion for VNA measurements, which often consist of sweeps over

several hundred frequency points. In linear uncertainty propagation, sensitivity coefficients (derivatives) are calculated. With this information it is easy to provide an uncertainty budget. An uncertainty budget is valuable to understand the significance of the different influence factors affecting the measurement. The compilation of an uncertainty budget with the Monte Carlo method increases the already large computational effort significantly. For these reasons it is often preferable to use linear uncertainty propagation for VNA measurements. The Monte Carlo method can still be used for comparison purposes.

C.5 Sample statistics and Type A uncertainty

C.5.1 Sample statistics of scalar quantities

When a scalar quantity x is estimated from a sample of n observations $x_m(1)$, $x_m(2)$, ..., $x_m(n)$ the sample mean is

$$\mathrm{m}(x) = \frac{1}{n}\sum_{i=1}^{n} x_m\,(i)\,. \tag{C.4}$$

The sample variance of the n observations is

$$\mathrm{v}(x) = \frac{1}{n-1}\sum_{i=1}^{n} \left(x_m\,(i) - \mathrm{m}(x)\right)^2 . \tag{C.5}$$

The sample variance of the mean of the n observations is

$$\mathrm{v}(\mathrm{m}(x)) = \frac{\mathrm{v}(x)}{n}. \tag{C.6}$$

Closely related to the variance is the standard deviation of the n observations

$$\mathrm{s}(x) = \sqrt{\mathrm{v}(x)} \tag{C.7}$$

and the standard deviation of the mean

$$\mathrm{s}(\mathrm{m}(x)) = \sqrt{\mathrm{v}(\mathrm{m}(x))} = \frac{\mathrm{s}(x)}{\sqrt{n}}. \tag{C.8}$$

C.5.2 Sample statistics of complex-valued quantities

The scalar formalism can be generalized for a complex-valued quantity, as e.g. an S-parameter. If the complex-valued quantity $\mathbf{x} = \mathrm{Re}[\mathbf{x}] + \mathrm{j}\,\mathrm{Im}[\mathbf{x}]$, with the imaginary unit j, is estimated from a sample of n observations $\mathbf{x}_m(1)$, $\mathbf{x}_m(2)$, ..., $\mathbf{x}_m(n)$ the sample mean is

$$\mathbf{m}(\mathbf{x}) = \mathrm{m}(\mathrm{Re}\,[\mathbf{x}]) + \mathrm{j}\mathrm{m}(\mathrm{Im}\,[\mathbf{x}]) \tag{C.9}$$

with the scalar mean $\mathrm{m}(\cdot)$ according to equation (C.4). The covariance matrix of the n observations is

$$\mathbf{v}(\mathbf{x}) = \begin{pmatrix} v_{11} & v_{12} \\ v_{21} & v_{22} \end{pmatrix}, \tag{C.10}$$

where

$$
\begin{aligned}
v_{11} =& \mathrm{v}(\mathrm{Re}\,[\mathbf{x}]) \\
v_{22} =& \mathrm{v}(\mathrm{Im}\,[\mathbf{x}]) \\
v_{12} = v_{21} =& \frac{1}{n-1} \sum_{i=1}^{n} \left(\mathrm{Re}\,[\mathbf{x}_m\,(i)] - \mathrm{m}(\mathrm{Re}\,[\mathbf{x}])\right) \left(\mathrm{Im}\,[\mathbf{x}_m\,(i)] - \mathrm{m}(\mathrm{Im}\,[\mathbf{x}])\right),
\end{aligned}
$$

with the scalar variance $\mathrm{v}(\cdot)$ and the scalar mean $\mathrm{m}(\cdot)$ according to equations (C.5) and (C.4), respectively. The covariance matrix of the mean is accordingly

$$\mathbf{v}(\mathbf{m}(\mathbf{x})) = \frac{1}{n}\mathbf{v}(\mathbf{x})\,. \tag{C.11}$$

The formalism for complex-valued quantities is defined in direct analogy to the scalar case with the notable addition of the correlation information, which is contained in v_{21} in equation (C.10). The same principle formalism holds for vectors of length N, resulting in a mean vector of length N for scalar quantities (2N for complex-valued quantities) and covariance matrix of size $N \times N$ for scalar quantities ($2N \times 2N$ for complex-valued quantities).

C.5.3 Type A uncertainty

The statistical analysis in C.5.1 and C.5.2 can be used to assig measurement uncertainties based on repeated measurements of a quantity. In the ISO-GUM [6] this is referred to as Type A evaluation of a measurement uncertainty. The discussion below is limited to uncertainties used in linear uncertainty propagation. For the use with the Monte Carlo method information can be found in [44, 5].

C.5.3.1 Large sample size

If the length n of the sample of observations is large the results in C.5.1 and C.5.2 can be directly used. For a scalar quantity x the mean according to equation (C.4) is the best estimate $\hat{x}$ with an uncertainty $\mathrm{u}(\hat{x})$

$$\mathrm{u}(\hat{x}) = \mathrm{s}(\mathrm{m}(x))\,, \tag{C.12}$$

with the standard deviation of the mean $\mathrm{s}(\mathrm{m}(x))$ according to equation (C.8).

For a complex-valued quantity $\mathbf{x}$ the mean according to equation (C.9) is the best estimate $\hat{\mathbf{x}}$ with an uncertainty matrix $\mathbf{u}(\hat{\mathbf{x}})$

$$\mathbf{u}(\hat{\mathbf{x}}) = \mathbf{v}(\mathbf{m}(\mathbf{x})) \tag{C.13}$$

with the covariance matrix of the mean $\mathbf{v}(\mathbf{m}(\mathbf{x}))$ according to equation (C.11).

C.5.3.2 Small sample size

If the length n of the sample of observations is small, applying equations (C.12) and (C.13) would underestimate the measurement uncertainty. The ISO-GUM documents are currently not consistent in the way they deal with such a situation.

The ISO-GUM [6] recommends to use uncertainties according to equations (C.12) and (C.13) together with degrees of freedom, which are defined as $n-1$, with n the size of the measurement sample. This information is later used to derive expanded combined uncertainties, see C.6.

GUM Supplement 2 [5] recommends to increase the uncertainty, which is derived from the statistical analysis, by a factor $[(n-1)/(n-N-2)]^{1/2}$, with n the size of the measurement sample and N the dimension of the quantity. For scalar quantities ($N=1$) this leads to

$$\mathrm{u}(\hat{x}) = \sqrt{\frac{n-1}{n-3}}\mathrm{s}(\mathrm{m}(x))\,, \tag{C.14}$$

and for complex-valued quantities ($N=2$) to

$$\mathbf{u}(\hat{\mathbf{x}}) = \frac{n-1}{n-4}\mathbf{v}(\mathbf{m}(\mathbf{x}))\,. \tag{C.15}$$

These uncertainties are directly used in the subsequent measurement uncertainty propagation and there is no need to use degrees of freedom to derive expanded combined uncertainties, see C.6. However, to apply equations (C.14) and (C.15) at least four (scalar quantity) or five (complex-valued quantity) measurement repetitions are necessary. If say one cares about correlation between all four S-parameter of a two-port measurement ($N=8$), then at least 11 measurement repetitions would be needed.

C.5.3.3 Other considerations

Assigning measurement uncertainties based on a Type A analysis as described in C.5.3.1 or C.5.3.2 assumes that the quantity has a time invariant and unique true value. If the value of the quantity is drifting over time or if the value changes discretely, e.g. a coaxial connection showing two or more states under different connector orientations, blindly applying the Type A formalism would lead to an underestimation of the measurement uncertainty.

A large number of measurement repetitions is not always feasible. The effort needs to be considered with respect to the contribution of the Type A uncertainty to the overall measurement uncertainty. If the contribution is small a reduced number of repetitions is sufficient. If effects described in the previous paragraph can't be excluded and a large number of measurement repetitions to study the effects is not feasible, it is recommended to take a more conservative approach and e.g. take the half-width between maximum and minimum value of the sample of observations as the measurement uncertainty. Personal judgement is advised in such cases.

C.6 Expanded uncertainty

In the final step of any evaluation of measurement uncertainty the standard uncertainty of the quantity of interest is often multiplied by a coverage factor k to obtain an expanded uncertainty, which has a desired coverage probability, typically 95%. The exact meaning of this coverage depends on the interpretation of probability. Up to now the ISO-GUM documents are not consistent in that respect. This is related to the inconsistency mentioned previously in C.5.3.2. The discussion below is limited to uncertainties

obtained with linear uncertainty propagation, i.e. it is assumed that the PDF associated with the measured value of the quantity of interest has a Gaussian shape. Expanded uncertainties based on the Monte Carlo method are described in [44, 5].

C.6.1 Method according to GUM Supplement 2 [5]: if the Type A uncertainties are calculated with the equations (C.14) and (C.15), the coverage factors for the combined uncertainty are $k = 1.96$ for 95% coverage in the scalar case and $k = 2.45$ for 95% coverage in the two-dimensional case. The latter can be applied to a complex-valued quantity and corresponds to an elliptical region in the complex plane.

C.6.2 If the Type A uncertainties are calculated according to equations (C.12) and (C.13) and propagated to the combined uncertainty, it is necessary to calculate effective degrees of freedom by applying the Welch-Satterthwaite formula. The coverage factor is then dependent on the effective degrees of freedom. This is described in the ISO-GUM [6] for the case of uncorrelated scalar quantities. A generalization of the procedure to multivariate and complex-valued quantities is described with an example in [50]. Further details are given in [51, 52].

C.6.3 The discrepancies between the two methods described in C.6.1 and C.6.2 become apparent when Type A uncertainties based on a small sample sizes (as discussed in C.5.3.2) make a significant contribution to the overall uncertainty. Otherwise the two approaches converge to the same coverage factors. The method in C.6.1 is easier to apply, but there are indications [52] that it provides overly conservative coverage regions compared to the method in C.6.2.

C.6.4 The expanded uncertainty of a complex-valued quantity corresponds to a region in the complex plane. It is common to use an elliptical region, because this corresponds to the contour of a two-dimensional Gaussian PDF. Alternative shapes are discussed in [53, 54].

D VNA calibration

In this section, further details are given for commonly used VNA calibration schemes. The discussion is limited to methods that are relevant (not exclusively) for coaxial measurements. It is not the intent to give a complete overview on all existing VNA calibration algorithms.

D.1 One-port calibration techniques

For one-port DUT measurements, the one-port error model, illustrated as a signal flow graph in figure D.1, is used. It contains the three error coefficients in table D.1 relating the reflection coefficient indicated by the VNA, $\mathbf{S}_{11}^{m}$, to the true reflection coefficient $\mathbf{S}_{11}$ of the device being measured. $\mathbf{S}_{11}^{m}$ is sometimes also referred to as a raw S-parameter. Evaluation of the signal flow graph leads to

$$\mathbf{S}_{11}^{m} = \mathbf{E}_{00} + \frac{\mathbf{E}_{01}\mathbf{S}_{11}}{1 - \mathbf{E}_{11}\mathbf{S}_{11}}. \tag{D.1}$$

Three known reflection standards are necessary to determine estimates of the error coefficients. Measuring the three standards successively gives three independent equations, according to equation (D.1), with the three error coefficients as the unknown variables. The three equations can be linearized through parameter substitution and solved by classical linear algebra techniques. Solving equation (D.1) for $\mathbf{S}_{11}$ leads to

$$\mathbf{S}_{11} = \frac{\mathbf{S}_{11}^{m} - \mathbf{E}_{00}}{\mathbf{E}_{11}\left(\mathbf{S}_{11}^{m} - \mathbf{E}_{00}\right) + \mathbf{E}_{01}}, \tag{D.2}$$

which is used to perform the error correction on the DUT measurement. The previously determined estimates of the error coefficients are substituted into equation (D.2) together with $\mathbf{S}_{11}^{m}$ for the DUT to obtain an estimate of the S-parameter, $\hat{\mathbf{S}}_{11}$, for the DUT. $\hat{\mathbf{S}}_{11}$ is sometimes also referred to as the error corrected S-parameter.

The most common one-port calibration method for coaxial measurements is based on a short, an open and a matched load as calibration standards. Common acronyms are SOL (short - open - load) or OSM (open - short - match).

An alternative to SOL is to use a set of shorts with different offset lengths. However, this technique is band-limited and more than three offset shorts are necessary to cover larger frequency ranges. The acronym for this technique is SSS. It is based on calculable standards and can therefore be used for primary experiments, see the note on

Table D.1: List of error coefficients of one-port error model.

Symbol	Error coefficient
$\mathbf{E}_{00}$	Directivity
$\mathbf{E}_{01}$	Reflection tracking
$\mathbf{E}_{11}$	Source match

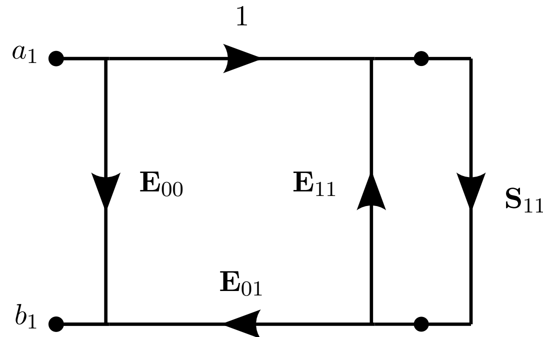

Figure D.1: Signal flow graph representing a one port VNA error model with the error coefficients listed in table D.1, which relate indicated reflection coefficient $\mathrm{S}_{11}^{m} = b_1/a_1$ with true reflection coefficient S_{11}.

SSST in D.2.2. An advantage of SSS is that shorts are typically more robust and stable than other types of standards. A disadvantage is the bandwidth limitation. It is possible to overcome the bandwidth limitation at low frequencies by using additional open and matched load standards.

D.2 Two-port calibration techniques

D.2.1 Introduction

For two-port DUT measurements, two different error models are commonly used, the seven-term error model and the ten-term error model. These two models are traditionally related to two different VNA architectures, the four-receiver VNA or dual reflectometer VNA, where each reflectometer has its own reference channel, and the three-receiver VNA with a single reference channel. These architectures are shown in figure D.2. For further details see e.g. [1, 3]. The two error models and the different two port calibration algorithms are related to each other. In [55, 1] it is discussed under which conditions a transformation from one model to the other can be performed.

D.2.2 Ten-term error model

The ten-term error model has been developed for three-receiver VNAs but is also applicable to four-receiver VNAs. This model assumes that each port has two different states:

- In the first state, the test port is connected to the source and two receivers measure the incoming and outgoing waves. This corresponds to the configuration of one-port measurements and is characterized by the three error coefficients, directivity, source match and reflection tracking, which can be determined with a set of three one-port standards, as discussed in D.1.
- In the second state, the port is connected to the switch termination, and incoming waves are measured by only one receiver. This state is modeled with two error

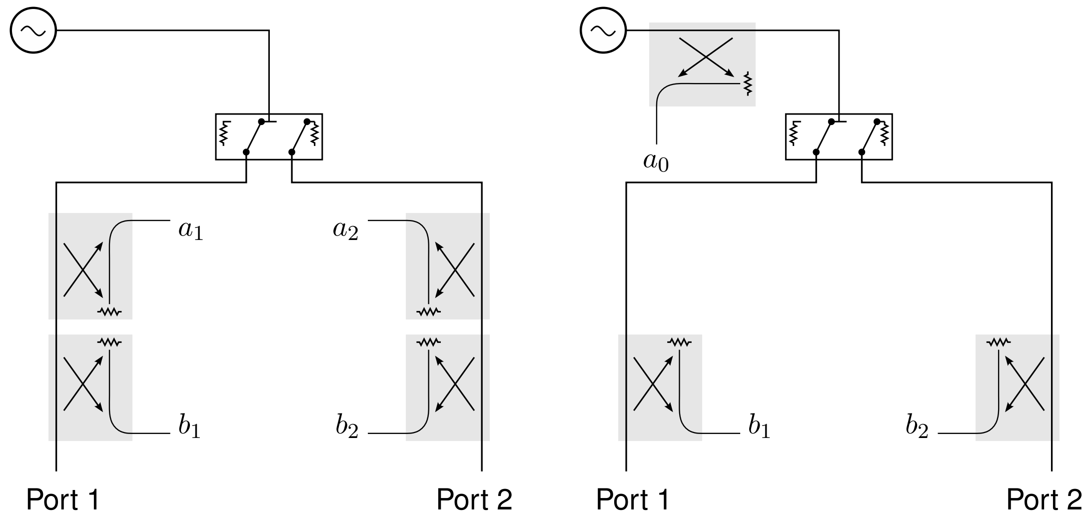

Figure D.2: Four-receiver (left) vs. three-receiver (right) VNA architecture. a_i and b_i denote the wave quantities measured by the reference and test receivers, respectively.

coefficients, the load match and the transmission tracking, which can be determined by the measurement of a two-port standard. With a four-receiver VNA, the corresponding reference channel is not used.

Figure D.2 (right side) shows port 1 in the first state and port 2 in the second state. Changing the switch will put port 2 into the first state and port 1 into the second state. This results in two error models. The forward model (figure D.3), relates indicated and true forward S-parameters, $\mathbf{S}_{11}^m$, $\mathbf{S}_{21}^m$ and $\mathbf{S}_{11}$, $\mathbf{S}_{21}$, respectively. The reverse model (figure D.4), relates indicated and true reverse S-parameters, $\mathbf{S}_{22}^m$, $\mathbf{S}_{12}^m$ and $\mathbf{S}_{22}$, $\mathbf{S}_{12}$, respectively. The error coefficients are listed in table D.2. The ten-term error model is also referred to as twelve-term error model, if isolation terms are also taken into account.

Table D.2: List of error coefficients of forward and reverse ten-term error model.

Symbol		Error coefficient
forward	reverse	
$\mathbf{E}_{00}^F$	$\mathbf{E}_{33}^R$	Directivity
$\mathbf{E}_{01}^F$	$\mathbf{E}_{32}^R$	Reflection tracking
$\mathbf{E}_{11}^F$	$\mathbf{E}_{22}^R$	Source match
$\mathbf{E}_{22}^F$	$\mathbf{E}_{11}^R$	Load match
$\mathbf{E}_{32}^F$	$\mathbf{E}_{01}^R$	Transmission tracking
$\mathbf{E}_{30}^F$	$\mathbf{E}_{03}^R$	Isolation

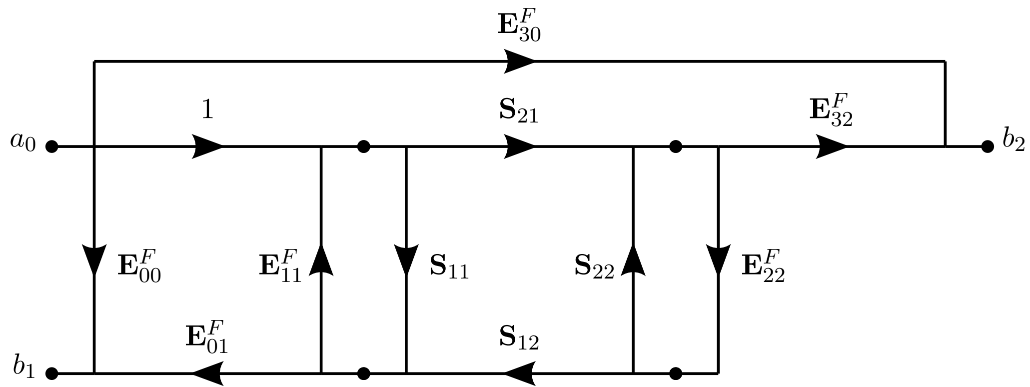

Figure D.3: Signal flow graph representing the ten-term forward VNA error model (including the isolation term) for two port measurements with the error coefficients listed in table D.2. The model relates indicated forward S-parameters, $\mathrm{S}_{11}^m = b_1/a_0$ and $\mathrm{S}_{21}^m = b_2/a_0$, with true S-parameters, S_{11} and S_{21}.

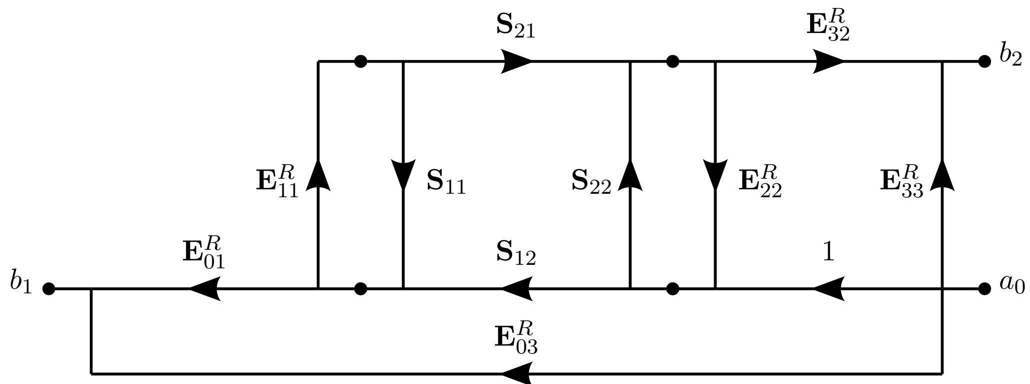

Figure D.4: Signal flow graph representing the ten-term reverse VNA error model (including the isolation term) for two-port measurements with the error coefficients listed in table D.2. The model relates indicated reverse S-parameters, $\mathrm{S}_{22}^m = b_2/a_0$ and $\mathrm{S}_{12}^m = b_1/a_0$, with true S-parameters, S_{22} and S_{12}.

The determination of the error coefficients of the ten-term error model is based on an SOL calibration at each port with an additional measurement of a flush thru. The flush thru is realized by directly connecting the two test ports. It is defined as a perfect connection of both reference planes with zero length in-between. Common acronyms for this calibration method are SOLT and TOSM.

NOTE — In principle, a characterized transmission line or adapter can be used instead of the flush thru standard in the SOLT calibration. However, this generally degrades the accuracy.

As described for the one-port case, the two-port offset short calibration is an alternative as well. The acronym is SSST. SSST is based on calculable standards and can therefore be applied for primary experiments. It is an alternative to the LRL (line - reflect - line) calibration at higher frequencies when the handling of air-dielectric lines becomes more difficult, see D.2.3.

D.2.3 Seven-term error model

The signal flow graph of the seven-term error model is shown in figure D.5. It includes seven (nine, if the isolation terms are taken into account) unknown error coefficients and two switch terms listed in table D.3. This error model is sometimes called the eight-term error model, ignoring the fact that one of the tracking terms is set to 1 due to normalization.

Several calibration techniques based on the seven-term error model have been developed, using any sufficient combination of one-port and two-port standards. The most popular calibration methods are short-open-load-reciprocal (SOLR), also known as Unknown Thru [18], thru-reflect-line (TRL) [48], line-reflect-line (LRL) [45] and QSOLT [46].

For the determination of the switch terms, and thus for the use of VNA calibrations that are based on the seven-term error model, it is in principle necessary that the VNA has a four-receiver architecture. There is however a way to overcome this limitation. With the help of an additional SOLT calibration it is possible to determine the switch terms computationally. The theory is based on [55]. In some VNAs proprietary implementations of this method are available in the firmware.

Table D.3: List of error coefficients of seven-term error model.

Symbol		Error coefficient
port 1	port 2	
$\mathbf{E}_{00}$	$\mathbf{E}_{33}$	Directivity
$\mathbf{E}_{01}$	$\mathbf{E}_{32}\ \mathbf{E}_{23}$	Reflection tracking
$\mathbf{E}_{11}$	$\mathbf{E}_{22}$	Source match
$\mathbf{E}_{30}$	$\mathbf{E}_{03}$	Isolation
$\mathbf{W}_{00}$	$\mathbf{W}_{33}$	Switch term

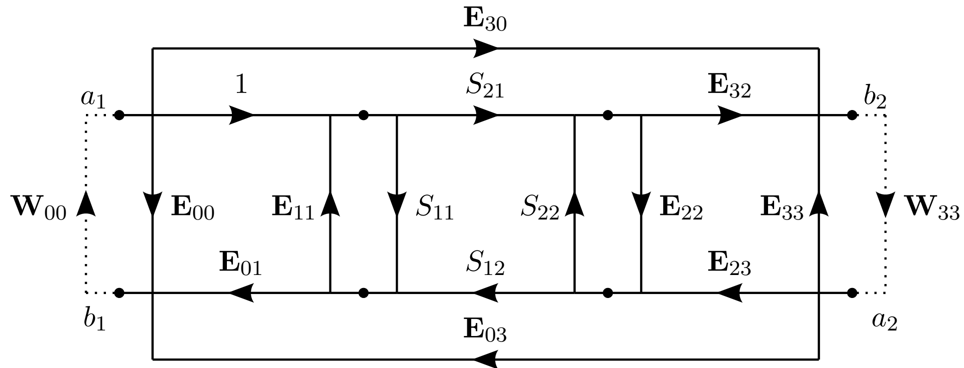

Figure D.5: Signal flow graph representing the seven-term VNA error model (including isolation terms) for two port measurements with the error coefficients and the switch terms listed in table D.3. The model relates indicated S-parameters, $S^m_{11} = b_1/a_1$, $S^m_{21} = b_2/a_1$, $S^m_{22} = b_2/a_2$ and $S^m_{12} = b_1/a_2$, with true S-parameters, S_{11}, S_{21}, S_{22} and S_{12}.

D.3 Over-determined calibration

More recently, optimization calibration algorithms have been proposed, where more calibration standards than needed are measured. In any of the previously mentioned calibration algorithms it is possible to measure more than the minimum number of calibration standards required to determine the error coefficients. This results in an over-determined system of equations which can be solved by an optimization algorithm, e.g. a least squares routine. Different implementations are known [56, 57, 58, 59] and some commercial VNA firmware supports over-determined calibration as well, e.g. in combination with electronic calibration units or with offset short calibration kits.

Using more than the necessary number of standards potentially increases the accuracy of the calibration and reduces the measurement uncertainty. It provides an excellent diagnostic tool to detect problems (drift or change) of single calibration standards. For this purpose it is necessary to calculate the residuals of the optimization, i.e. the difference between the reference data and the corrected measurements of the calibration standards. If one of the standards shows a significant larger difference than the others, further investigations are advised.

E VNA verification

This section provides additional information related to VNA verification. A discussion of different verification standards and their relation to VNA error coefficients is given in E.1. Quantitative pass/fail criteria for verification measurements are discussed in E.2.

E.1 Verification standards

Depending on the type and characteristics of the device under test, different verification artifacts can be used to verify the calibration of a VNA. The overall Smith chart region, for both one- and two-port measurements, cannot be completely covered by one single verification standard over the entire frequency range. For a full coverage of the Smith chart several different verification standards are needed, as described below. Proximity to the DUT response increases the significance of a single verification measurement.

E.1.1 One-port verification standards

To achieve confidence in reflection measurements, calibrated matched, mismatched, and highly reflective one-port artifacts (with both male and female interfaces) can be measured. A sensitivity analysis can be based on the residual measurement model, which is introduced in F.5. Ignoring all influence terms except the residual error coefficients and linearizing with respect to them [32] leads for the one-port case to

$$\mathbf{S}_{11}^{c} = \delta\mathbf{E}_{00} + (1 + \delta\mathbf{E}_{01})\,\mathbf{S}_{11} + \delta\mathbf{E}_{11}\,\mathbf{S}_{11}^{2}. \tag{E.1}$$

This equation relates the error corrected reflection coefficient $\mathbf{S}_{11}^{c}$ to the true reflection coefficient $\mathbf{S}_{11}$ of the DUT via the residual one-port error coefficients, $\delta\mathbf{E}_{00}$ (directivity), $\delta\mathbf{E}_{11}$ (source match) and $\delta\mathbf{E}_{01}$ (reflection tracking). Since the sensitivity of $\mathbf{S}_{11}^{c}$ to the individual residual error coefficients depends on the reflectivity of the DUT, $\mathbf{S}_{11}$, equation (E.1) might serve as a guideline to choose verification standards appropriately to identify potential sources of erroneous calibration.

E.1.1.1 Matched load standard

With a matched load the central part of the Smith chart is being tested ($|\mathbf{S}_{11}| \simeq 0$). According to equation (E.1) the measurement of a matched load is directly and exclusively sensitive to the residual directivity. A load measurement helps to identify problems related to misuse or defective behavior of a fixed load (or sliding load) during VNA calibration.

E.1.1.2 Highly reflective standard

Following equation (E.1), the measurement of highly reflective standards ($|\mathbf{S}_{11}| \simeq 1$) are sensitive to all residual error coefficients and help to identify problems related to misuse or defects of highly reflective standards used during VNA calibration.

A flush short is particularly useful to test how well the reference plane has been defined during the VNA calibration, as pointed out in 4.3.2.

E.1.1.3 Mismatch standard

Mismatch standards with e.g. $0.2 < |\mathbf{S}_{11}| < 0.5$ are suitable to cover the intermediate regions of the Smith chart. Problems related to non-linearity, e.g. a receiver operated in compression mode, can be detected with such a verification measurement.

E.1.2 Two-port verification standards

In analogy to the one-port case equations can be derived to express the sensitivities of $\mathbf{S}_{11}^c$ and $\mathbf{S}_{21}^c$ with respect to the 2-port residual error coefficients [32]. This is based on a linearization of the two-port residual measurement model and leads to

$$\mathbf{S}_{11}^c = \delta\mathbf{E}_{00}^F + \left(1 + \delta\mathbf{E}_{01}^F\right)\mathbf{S}_{11} + \delta\mathbf{E}_{11}^F\,\mathbf{S}_{11}^2 + \delta\mathbf{E}_{22}^F\,\mathbf{S}_{21}\mathbf{S}_{12} \quad \text{(E.2)}$$

$$\mathbf{S}_{21}^c = \delta\mathbf{E}_{11}^F\,\mathbf{S}_{11}\mathbf{S}_{21} + \delta\mathbf{E}_{22}^F\,\mathbf{S}_{22}\mathbf{S}_{21} + \left(1 + \delta\mathbf{E}_{32}^F\right)\,\mathbf{S}_{21}. \quad \text{(E.3)}$$

These equations relate the error corrected S-parameters, $\mathbf{S}_{11}^c$ and $\mathbf{S}_{21}^c$, to the true S-parameters $\mathbf{S}_{11}$ and $\mathbf{S}_{21}$ of the DUT via the residual error coefficients, $\delta\mathbf{E}_{00}^F$ (directivity), $\delta\mathbf{E}_{11}^F$ (source match), $\delta\mathbf{E}_{01}^F$ (reflection tracking), $\delta\mathbf{E}_{22}^F$ (load match) and $\delta\mathbf{E}_{32}^F$ (transmission tracking). Analogous equations exist for the reverse residual error model

E.1.2.1 Beadless air-dielectric line

Ideal beadless air-dielectric lines theoretically provide the best possible impedance reference, since they can be both fabricated and mechanically characterized with high precision. In reality, beadless air-dielectric lines are not ideal. They are not lossless, their connectors cause reflections and the fact that the position of the center conductor is not fixed impairs reproducibility, see [23]. These effects become more pronounced at higher frequencies. To use beadless air-dielectric lines as accurate verification devices they need to be characterized and the position of the center conductor needs to be controlled [10]. Their handling, especially for the higher frequency connector systems, demands a skilled operator. Despite these limitations, beadless air-dielectric lines are used to estimate residual source match and residual directivity with the Ripple Method, as described in 7.2.

E.1.2.2 Beaded air-dielectric line or adapter

Characterized beaded air-dielectric lines or adapters are a good alternative to beadless air-dielectric lines. They offer excellent reproducibility and are easier to handle. As weakly reflecting nearly transparent devices ($|\mathbf{S}_{11}|, |\mathbf{S}_{22}| \simeq 0$ and $|\mathbf{S}_{21}|, |\mathbf{S}_{12}| \simeq 1$) they are sensitive to residual load match, directivity and transmission tracking, as seen from equations (E.2) and (E.3), respectively.

E.1.2.3 Matched attenuation device

Measurements of matched attenuation devices with small to medium attenuation values, e.g. 3 dB to 20 dB, are useful to test the non-linearity of VNA receivers with two-port measurements. For large attenuation values on the other hand, the sensitivity of the reflection coefficients with respect to the residual errors approaches the behavior of a one-port matched load, see E.1.1.1. Matched attenuation devices typically show good stability because the center conductor is supported by two beads. Such a design

is more robust and therefore less affected by deviations in concentricity of the coaxial structure in the mating counterpart. A matched attenuation device with a value of 30 dB or higher might therefore be used as an alternative for a matched load.

NOTE — Differences in $\mathbf{S}_{21}$ and $\mathbf{S}_{12}$ are theoretically possible for attenuation devices made with electrically anisotropic materials. However, in practice most attenuation devices are reciprocal and if differences in $\mathbf{S}_{21}$ and $\mathbf{S}_{12}$ are observed they will be related to drift or to problems with the VNA calibration.

E.1.2.4 Mismatched air-dielectric line (Beatty Line)

Transmission accuracy can be checked using a mismatched verification standard as well. The impedance-stepped air-dielectric line invented by Beatty [43] includes a 25 Ω line section, see figure E.1, which performs a quarter-wavelength transformation at all odd integer multiples of the frequency f_0 with $f_0 = c/(4L)$ where c denotes the velocity of light and L the length of the 25 Ω section. Figure E.2 shows the simulated S-parameter magnitudes of a typical Type-N Beatty standard. At even integer multiples of the frequency f_0 the low impedance section acts as a half-wave transformer, virtually connecting the two ports of the VNA by a low-reflect, low-loss line. At these frequencies (e.g. 2.14 GHz) the Beatty line should have low reflection, typically $|\mathbf{S}_{11}| < 0.01$ ($<$-40 dB), and exhibit low transmission loss, typically $|\mathbf{S}_{21}| > 0.99$ ($>$-0.1 dB). At odd integer multiples of f_0, quarter-wavelength transformation leads to a transformation of the 50 Ω input impedance of the VNA to 12.5 Ω, $|\mathbf{S}_{11}| \simeq 0.6$ (-4.44 dB), and hence a decreased transmission coefficient, $|\mathbf{S}_{21}| \simeq 0.8$ (-1.94 dB). A Beatty line combines the behavior of a transparent device (adapter or beaded air-dielectric line) with a one-port mismatch standard and an attenuation device.

Beadless Beatty Lines suffer from the same issues as beadless air-dielectric lines (E.1.2.1). For quantitative verification only characterized beaded Beatty Lines should be used.

E.1.2.5 T-checker

An quick and easy test of VNA calibration validity utilizes a common T-junction, one port of which is terminated by a load impedance, $\mathbf{Z}$ [47] as shown in figure E.3. The

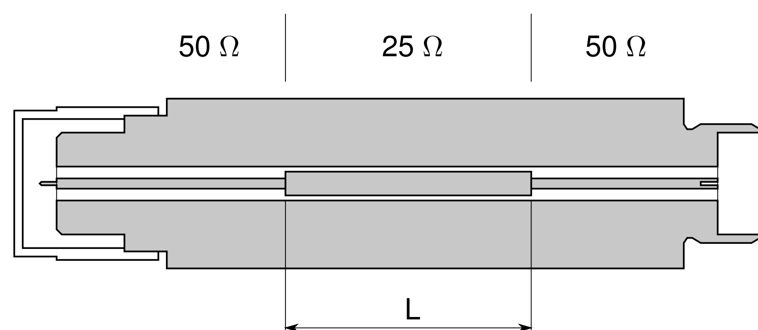

Figure E.1: Schematic of a mismatched air-dielectric line (Beatty Line).

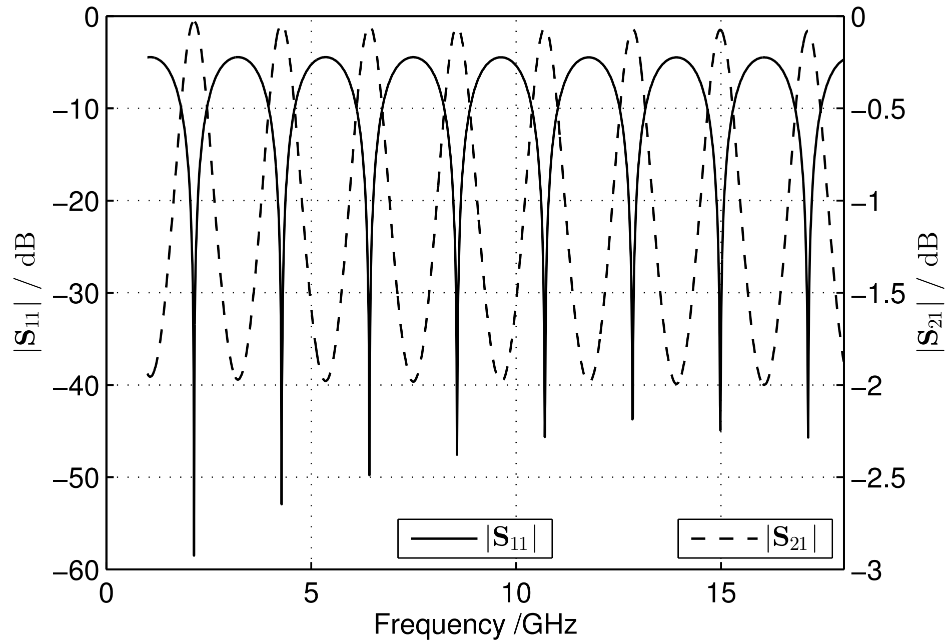

Figure E.2: Simulated S-parameter magnitudes of an ideal Type-N Beatty line with a 25 Ω section length of 70 mm.

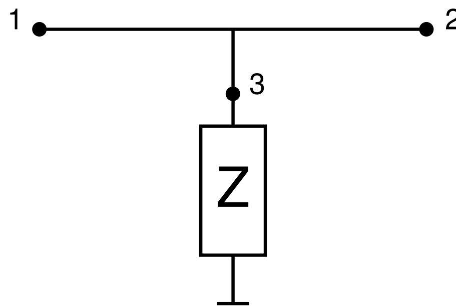

Figure E.3: Equivalent circuit of a T-checker.

so-called T-check parameter c_T is expressed as

$$c_\mathrm{T} = \frac{|\mathbf{S}_{11}\mathbf{S}_{21}^{*} + \mathbf{S}_{12}\mathbf{S}_{22}^{*}|}{\sqrt{\left(1 - |\mathbf{S}_{11}|^2 - |\mathbf{S}_{12}|^2\right)\left(1 - |\mathbf{S}_{21}|^2 - |\mathbf{S}_{22}|^2\right)}} \quad \text{(E.4)}$$

with * denoting the conjugate transpose. The S-parameters in the equation refer to measurements at the ports labelled 1 and 2 in figure E.3. If the T-junction is lossless, c_T is unity, independent of the load impedance $\mathbf{Z}$, which can be chosen arbitrarily.

If the lossless condition is fulfilled, which might be approximately the case at low frequencies ($<$ 6 GHz), deviation of c_T from unity indicates measurement inaccuracies of the VNA under investigation. As a rule of thumb, deviations in the range 1 $\pm$ 0.1 can be regarded as minor. Since the T-check is sensitive to both one- and two-port error coefficients, it enables an overall verification; however, it might not help to identify inaccuracies of individual error coefficients.

For a truly quantitative statement based on $c_\mathrm{T} = 1$ the losslessness of the T-junction needs to be demonstrated and uncertainties associated with the experimental and theoretical parameter c_T need to be determined. Unless this is done the T-checker provides merely a qualitative verification test.

A characterized T-checker can be used for quantitative verification as can any other stable two-port device. Reflection and transmission coefficients of commercially available T-checker devices are typically in the order of 0.2 to 0.4 and -2 dB to -5 dB, respectively.

E.1.2.6 Flush thru

After an SOLR calibration it is most useful to measure a flush thru by directly connecting the two reference planes, provided that the DUT is insertable. Ideally, this measurement should by definition result in $\mathbf{S}_{11} = \mathbf{S}_{22} = 0$ and $\mathbf{S}_{21} = \mathbf{S}_{12} = 1$, allowing for measurement uncertainties. In order not to undermine the SOLR advantage of minimizing cable movements this measurement should be done at the end after all calibration standards and the DUT have been measured. If the VNA firmware or the software permit an error correction of an earlier measurement it can also be done at the beginning before all other measurements start.

After an SOLT calibration followed by a two-port measurement of a passive, reciprocal DUT the following test can be carried out: the measurement data of the DUT can be used to perform an SOLR calibration. The SOLR error correction can then be applied to the raw measurement of the flush thru, which has already been measured during the SOLT calibration. The result should again provide the ideal values, allowing for measurement uncertainties.

The verification measurement of a flush thru is a highly quantitative test that helps to identify problems related to the characterization data for the highly reflective standards that were used during VNA calibration.

E.2 Quantitative verification criteria

As pointed out in 4.5, the visual comparison between reference and measurement data of a verification standard is often a good starting point to recognize problems. The

quantitative methods shown below, in E.2.1 for the scalar case and E.2.2 for the multidimensional case, should be regarded as supplements that can be implemented in software. They may be used to automate any type of conformity assessment of the measurement data. If correlation information between measurement and reference data of the verification standards is available, see remarks in 4.5.6, the quantitative evaluation will support a sharper pass/fail decision.

E.2.1 Scalar case

A suitable quantitative verification criteria for a scalar parameter is based on the normalized difference ϵ, also referred to as normalized error (E_n), between measurement and reference data. The pass condition is $\epsilon \leq 1$ for all frequency points. ϵ is expressed as

$$\epsilon = \frac{|\hat{d}|}{k\,\mathrm{u}\left(\hat{d}\right)}. \tag{E.5}$$

The quantity d is the frequency dependent difference between measurement and reference of a scalar quantity related to the verification standard. The scalar quantity is e.g. the magnitude of $\mathbf{S}_{11}$. An estimate of d is in this case

$$\hat{d} = \left|\hat{\mathbf{S}}_{11}^{c}\right| - \left|\hat{\mathbf{S}}_{11}^{r}\right|, \tag{E.6}$$

with the error corrected measurement and the reference data denoted by the superscripts c and r, respectively.

$\mathrm{u}(\hat{d})$ is the standard uncertainty associated with $\hat{d}$. It is calculated from the individual uncertainties associated with $|\hat{\mathbf{S}}_{11}^{c}|$ and $|\hat{\mathbf{S}}_{11}^{r}|$ and, if available, from the associated correlation coefficient $r(|\hat{\mathbf{S}}_{11}^{c}|, |\hat{\mathbf{S}}_{11}^{r}|)$:

$$\mathrm{u}\left(\hat{d}\right) = \sqrt{\left(\mathrm{u}\left(\left|\hat{\mathbf{S}}_{11}^{c}\right|\right)\right)^2 + \left(\mathrm{u}\left(\left|\hat{\mathbf{S}}_{11}^{r}\right|\right)\right)^2 - 2r\left(\left|\hat{\mathbf{S}}_{11}^{c}\right|, \left|\hat{\mathbf{S}}_{11}^{r}\right|\right)\mathrm{u}\left(\left|\hat{\mathbf{S}}_{11}^{c}\right|\right)\mathrm{u}\left(\left|\hat{\mathbf{S}}_{11}^{r}\right|\right)}. \tag{E.7}$$

k is the coverage factor used to expand the uncertainty in the denominator of equation (E.5). The value of k determines the normalization factor and determines the statistical significance of the pass criteria. Larger k represent more relaxed conditions. A value that is often used is $k = 1.96$. It expands the uncertainty associated with $\hat{d}$ to a 95% coverage interval. $k = 1$ corresponds to a 68% coverage interval. This verification procedure assumes that the underlying PDF associated with $\hat{d}$ is Gaussian.

Equations (E.6) and (E.7) are shown for the magnitude of $\mathbf{S}_{11}$. Analog expressions can be used for the phase of $\mathbf{S}_{11}$ or any other scalar component of an S-parameter. In case of the phase of the S-parameter it is advised to use the unwrapped phase to avoid problems related to the cyclicality of the phase.

E.2.2 Multivariate case

The multidimensional verification procedure uses multivariate statistics. It is beyond the scope of this guide to provide an introduction to this topic and the reader is referred to text books on the subject, e.g. [60], and to [5].

A straightforward generalization of the scalar criterion (E.5) is expressed by the matrix equation

$$\epsilon = \frac{1}{k}\sqrt{\hat{\mathbf{d}}\left(\mathbf{u}\left(\hat{\mathbf{d}}\right)\right)^{-1}\hat{\mathbf{d}}'} \tag{E.8}$$

with the prime denoting the transposed. For a visual interpretation of this expression refer to [61]. In the scalar case limit (E.8) equals (E.5). The pass criterion is as well $\epsilon \leq 1$.

$\mathbf{d}$ is a row vector, which contains the components of the difference between measurement and reference data, e.g.

$$\hat{\mathbf{d}} = \left(\mathrm{Re}\left[\hat{\mathbf{S}}^c_{11} - \hat{\mathbf{S}}^r_{11}\right]\ \mathrm{Im}\left[\hat{\mathbf{S}}^c_{11} - \hat{\mathbf{S}}^r_{11}\right]\right), \tag{E.9}$$

with superscripts c and r denoting error corrected measurement and reference, respectively.

$\mathbf{u}(\hat{\mathbf{d}})$ is the uncertainty (covariance) matrix associated with $\hat{\mathbf{d}}$. It is expressed as

$$\mathbf{u}\left(\hat{\mathbf{d}}\right) = \mathbf{u}\left(\hat{\mathbf{S}}^c_{11}\right) + \mathbf{u}\left(\hat{\mathbf{S}}^r_{11}\right) - \mathbf{u}\left(\hat{\mathbf{S}}^c_{11}, \hat{\mathbf{S}}^r_{11}\right) - \mathbf{u}\left(\hat{\mathbf{S}}^r_{11}, \hat{\mathbf{S}}^c_{11}\right) \tag{E.10}$$

with $\mathbf{u}(\hat{\mathbf{S}}^c_{11})$ and $\mathbf{u}(\hat{\mathbf{S}}^r_{11})$ according to equations (C.1) and (C.2) and

$$\mathbf{u}\left(\hat{\mathbf{S}}^c_{11}, \hat{\mathbf{S}}^r_{11}\right) = \begin{pmatrix} u\left(\mathrm{Re}\left[\hat{\mathbf{S}}^c_{11}\right], \mathrm{Re}\left[\hat{\mathbf{S}}^r_{11}\right]\right) & u\left(\mathrm{Re}\left[\hat{\mathbf{S}}^c_{11}\right], \mathrm{Im}\left[\hat{\mathbf{S}}^r_{11}\right]\right) \\ u\left(\mathrm{Im}\left[\hat{\mathbf{S}}^c_{11}\right], \mathrm{Re}\left[\hat{\mathbf{S}}^r_{11}\right]\right) & u\left(\mathrm{Im}\left[\hat{\mathbf{S}}^c_{11}\right], \mathrm{Im}\left[\hat{\mathbf{S}}^r_{11}\right]\right) \end{pmatrix} \tag{E.11}$$

$$\mathbf{u}\left(\hat{\mathbf{S}}^r_{11}, \hat{\mathbf{S}}^c_{11}\right) = \begin{pmatrix} u\left(\mathrm{Re}\left[\hat{\mathbf{S}}^r_{11}\right], \mathrm{Re}\left[\hat{\mathbf{S}}^c_{11}\right]\right) & u\left(\mathrm{Re}\left[\hat{\mathbf{S}}^r_{11}\right], \mathrm{Im}\left[\hat{\mathbf{S}}^c_{11}\right]\right) \\ u\left(\mathrm{Im}\left[\hat{\mathbf{S}}^r_{11}\right], \mathrm{Re}\left[\hat{\mathbf{S}}^c_{11}\right]\right) & u\left(\mathrm{Im}\left[\hat{\mathbf{S}}^r_{11}\right], \mathrm{Im}\left[\hat{\mathbf{S}}^c_{11}\right]\right) \end{pmatrix}. \tag{E.12}$$

The elements in the matrices represent covariances, which are generally expressed as $u(\hat{a}_1, \hat{a}_2) = r(\hat{a}_1, \hat{a}_2)\,\mathrm{u}(\hat{a}_1)\ \mathrm{u}(\hat{a}_2)$ with $r(\hat{a}_1, \hat{a}_2)$ denoting the correlation coefficient and $\mathrm{u}(\hat{a}_1)$ and $\mathrm{u}(\hat{a}_2)$ denoting standard uncertainties associated with estimates of a_1 and a_2, respectively. (E.11) and (E.12) are zero unless there is correlation between $\hat{\mathbf{S}}^c_{11}$ and $\hat{\mathbf{S}}^r_{11}$.

The coverage factor k plays the same role as in the scalar case, but for 95% coverage probability in the two-dimensional case the value $k = 2.45$ should be used, see [5]. For $k = 1$ the coverage probability is 39%. Again, this assumes that the probability density function associated with the measurement uncertainty of $\hat{\mathbf{d}}$ is a bivariate Gaussian one.

Equations (E.9), (E.10), (E.11) and (E.12) are valid for $\mathbf{S}_{11}$. Analog expressions can be used for the other S-parameters. Instead of using real and imaginary components the same formalism can be applied for magnitude and phase, but this should only be done in cases where the phase is well defined, see remarks in C.1.

The same formalism can be applied to dimensions larger than two, by e.g. using all four S-parameters that have been measured for a two-port device. This corresponds to an eight-dimensional evaluation and the factor k needs to be adjusted accordingly.

E.2.3 Examples of quantitative verification

Applications of the methods presented in E.2.1 and E.2.2 are shown as examples in figures E.4 and E.5.

Figure E.4 shows the result of a verification measurement of a T-checker, see E.1.2.5. Reference data (solid red lines) are compared with measurement data (dashed blue lines) for the magnitude, $|\mathbf{S}_{11}|$, and phase, $\arg(\mathbf{S}_{11})$, of the reflection coefficient. The three lines in each case indicate the data (center line) bounded by the interval of the standard uncertainty. The phase is normalized to the reference data for better visual comparison.

$\epsilon(|\mathbf{S}_{11}|)$ and $\epsilon(\arg(\mathbf{S}_{11}))$ are scalar normalized differences according to equation (E.5) for the magnitude and phase of $\mathbf{S}_{11}$, respectively. The solid line is for $k = 1$ and the dashed line is for $k = 1.96$. The solid horizontal line indicates the threshold value of $\epsilon = 1$. The graph at the bottom ($\epsilon(\mathbf{S}_{11})$) applies the multidimensional criterion (E.8) to the vector $\mathbf{S}_{11} = (|\mathbf{S}_{11}| \;\; \arg(\mathbf{S}_{11}))$ with $k = 1$ (solid line) and $k = 2.45$ (dashed line).

Figure E.5 shows the same analysis as figure E.4 but for a matched load. Instead of magnitude and phase the real and imaginary components, $\mathrm{Re}[\mathbf{S}_{11}]$ and $\mathrm{Im}[\mathbf{S}_{11}]$, are evaluated. In both cases, the measurement data are normalized to the reference data.

The multivariate criterion requires a condition to be met in each scalar component in order to pass, i.e. a “bad” result in one component can’t be compensated for with a “very good” result in another component. A failure in a single component is sufficient to create a multivariate fail condition. The multivariate criterion is therefore a suitable check for overall acceptance. In case of rejection it might be useful to apply the scalar criterion to each scalar component to identify the problem.

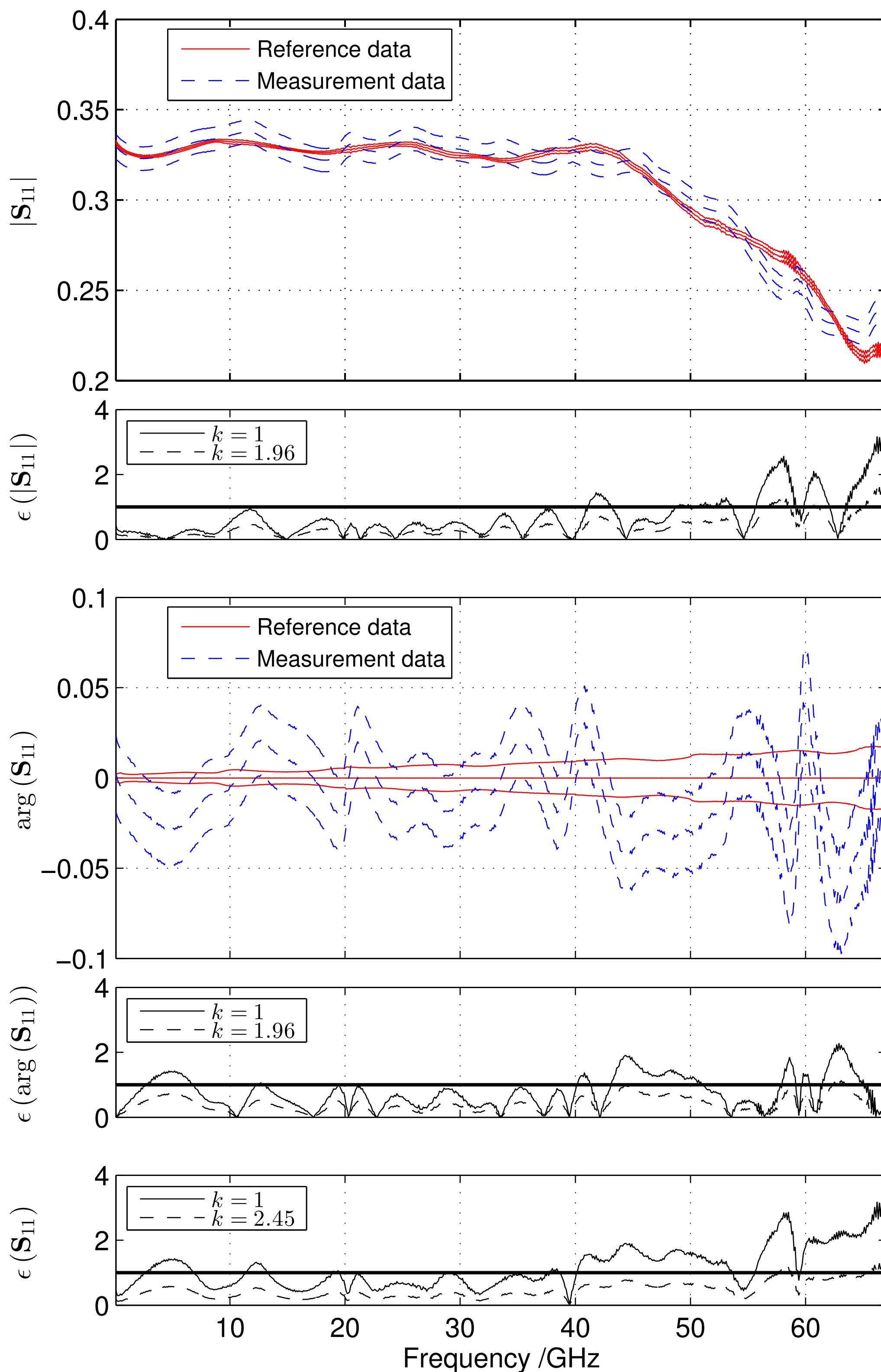

Figure E.4: Quantitative verification criteria applied to the verification measurement of a T-checker. Detailed explanation can be found in the text.

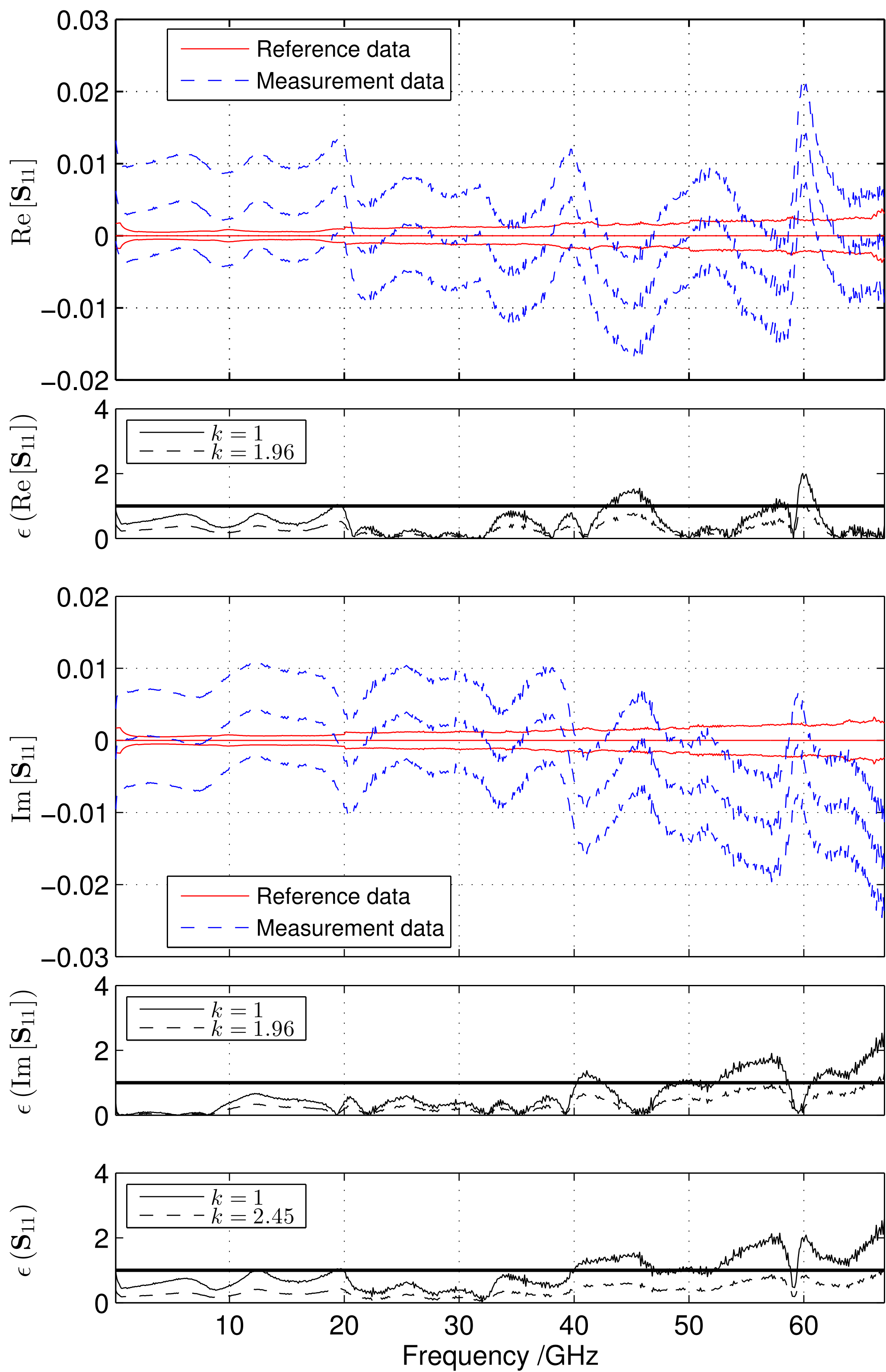

Figure E.5: Quantitative verification criteria applied to the verification measurement of a matched load. Detailed explanation can be found in the text.

F VNA measurement models

F.1 Introduction

The propagation of input measurement uncertainties to the final result is based on VNA measurement models. Such models are not unique, i.e. different levels of refinement are possible. A VNA measurement model incorporates the same error model used during the calibration of the VNA, see section 3, and adds the additional quantities discussed in 5.3, which are influencing the measurements.

Sections F.2, F.3 and F.4 discuss rigorous models, covering the entire VNA measurement process. Section F.5 introduces a simplified residual model, which is used by the Ripple Method. Section F.6 briefly discusses the influence quantities in the models with further references to the characterization of associated uncertainties in appendix G.

F.2 One-port measurement model

Figure F.1, shows the flow graph of a one-port measurement model based on the error model shown in figure D.1. The terms denoted by $\mathbf{E}_{\mathrm{ij}}$ are the error coefficients, which are determined during the VNA calibration. For the names associated with the error coefficients refer to table D.1. The additional terms are listed in table F.1 and further explained in F.6.

From the flow graph it is possible to derive the actual measurement equations, which represent both, the VNA calibration and the error corrected measurement of the DUT. Analytical evaluation of figure F.1 leads to an expression for the reflection coefficient indicated by the VNA $\mathbf{S}_{11}^{m} = b_1/a_1$:

$$\mathbf{S}_{11}^{m} = \mathbf{N}_{\mathrm{L}} + \mathbf{N}_{\mathrm{H}}\mathbf{L}\left(\mathbf{E}_{00}' + \mathbf{k}\mathbf{C}_{00}\mathbf{E}_{01}' + \frac{\mathbf{k}^2\mathbf{C}_{10}\mathbf{C}_{01}\mathbf{E}_{01}'\mathbf{S}_{11}}{1-\left(\mathbf{C}_{11}+\mathbf{k}\mathbf{C}_{01}\mathbf{C}_{10}\mathbf{E}_{11}'\right)\mathbf{S}_{11}}\right) \tag{F.1}$$

with

$$\begin{aligned}
\mathbf{E}_{00}' &= \mathbf{E}_{00} + \mathbf{D}_{00} \\
\mathbf{E}_{01}' &= \mathbf{E}_{01}\mathbf{D}_{01} \\
\mathbf{E}_{11}' &= \mathbf{E}_{11} + \mathbf{D}_{11} \\
\mathbf{k} &= \frac{1}{1-\mathbf{E}_{11}'\mathbf{C}_{00}}.
\end{aligned}$$

Equation (F.1) can be used to estimate the error coefficients in the VNA calibration process. Measuring three calibration standards leads again to a set of equations, which can be solved for the error coefficients.

Solving (F.1) for $\mathbf{S}_{11}$ leads to

$$\mathbf{S}_{11} = \frac{\frac{\mathbf{S}_{11}^{m}-\mathbf{N}_{\mathrm{L}}}{\mathbf{N}_{\mathrm{H}}\mathbf{L}} - \mathbf{E}_{00}' - \mathbf{k}\mathbf{C}_{00}\mathbf{E}_{01}'}{\left(\mathbf{C}_{11}+\mathbf{k}\mathbf{C}_{01}\mathbf{C}_{10}\mathbf{E}_{11}'\right)\left(\frac{\mathbf{S}_{11}^{m}-\mathbf{N}_{\mathrm{L}}}{\mathbf{N}_{\mathrm{H}}\mathbf{L}} - \mathbf{E}_{00}' - \mathbf{k}\mathbf{C}_{00}\mathbf{E}_{01}'\right) + \mathbf{k}^2\mathbf{C}_{10}\mathbf{C}_{01}\mathbf{E}_{01}'}. \tag{F.2}$$

Equation (F.2) can be used to determine an estimate of the reflection coefficient of the DUT by substituting the error coefficients determined in the calibration process.

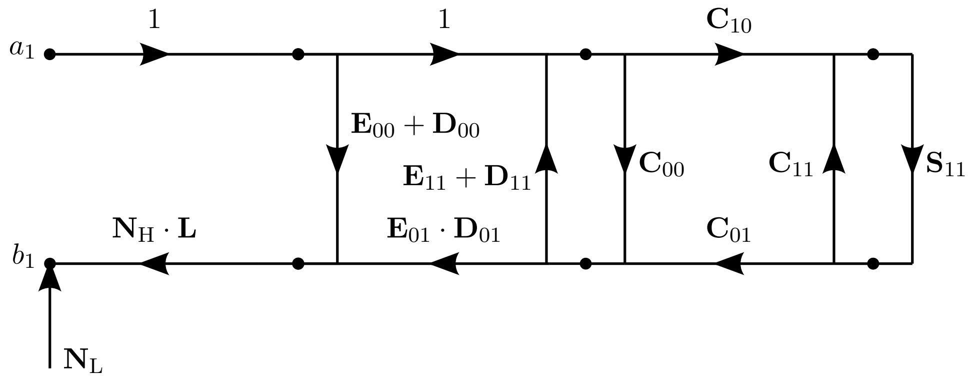

Figure F.1: Signal flow graph of one-port VNA measurement model. The model represents an extension of the one-port VNA error model with additional terms influencing the measurements.

Table F.1: List of additional influence quantities in the one-port measurement model shown in figure F.1.

Symbol	Description
$\mathbf{N}_\mathrm{L}$	Noise floor
$\mathbf{N}_\mathrm{H}$	Trace noise
$\mathbf{L}$	Non-linearity
$\mathbf{D}_{00}$	Drift of directivity
$\mathbf{D}_{01}$	Drift of reflection tracking
$\mathbf{D}_{11}$	Drift of source match
$\mathbf{C}_{00}$ $\mathbf{C}_{11}$	Reflection of cable and connector
$\mathbf{C}_{01}$ $\mathbf{C}_{10}$	Transmission of cable and connector

Equations (F.1) and (F.2) are extensions of (D.1) and (D.2) by including additional quantities influencing the measurements. Together they represent a measurement model of the complete one-port measurement process. This model can be used to propagate measurement uncertainties associated with the estimates of all quantities to the error-corrected S-parameters of the DUT. These uncertainties are discussed in detail in section 5 and explicit procedures for their quantification are given in appendix G.

F.3 Two-port measurement models

Figures F.2 and F.3 show flow graphs representing the two-port measurement models based on the error models shown in D.2. For the names associated with the error coefficients refer to tables D.2 and D.3. The additional terms are principally the same as for the one-port model, see table F.1, except that additional drift terms have to be considered for transmission tracking and load match in the 10-term model and for the switch term in the 7-term model. Obviously all influence quantities occur twice, once for each port, and the indices are chosen accordingly. Further details on these influence quantities are given in F.6.

From the flow graph it is possible to determine the actual measurement equations, representing both, VNA calibration and VNA error correction, in the same way as it is done for the one-port case in F.2. The equations become significantly more elaborate and are therefore not shown here. In practice the equations can be derived by using matrix flow graph reduction [16] and symbolic mathematical computation software.

The equations represent a measurement model that can be used to propagate uncertainties associated with estimates of all influence quantities in a two-port measurement to the error corrected S-parameter of the DUT.

F.4 N-port measurement model

The same concepts can be used for an N-port model as for the one-port and two-port models described in F.2 and F.3. An example of a generalized N-port version of a measurement model can be found in [59].

F.5 Measurement model based on residual error coefficients

The one-port measurement model based on residual error coefficients, in short a “residual measurement model”, is shown in figure F.4. It is equivalent to the one-port measurement model shown in figure F.1, but it assumes that the measurement of the DUT is taken with an error corrected VNA. Hence, the error coefficients $\mathbf{E}_{\mathrm{ij}}$ are replaced by deviations from the ideal values. These deviations are called residual error coefficients $\delta\mathbf{E}_{\mathrm{ij}}$, with estimates $\hat{\delta\mathbf{E}}_{00} = \hat{\delta\mathbf{E}}_{11} = \hat{\delta\mathbf{E}}_{01} = 0$. The indicated reflection coefficient $\mathbf{S}_{11}^{m}$ is replaced by the error corrected reflection coefficient $\mathbf{S}_{11}^{c}$. Because all other terms in the model have estimates of 0 or 1 too, it is obvious that $\hat{\mathbf{S}}_{11}^{c} = \hat{\mathbf{S}}_{11}$. The residual measurement model is an approximation, because in reality a VNA is not measuring error corrected S-parameters. Validity and applicability of this model for the purpose of uncertainty evaluation are based on assumptions [62].

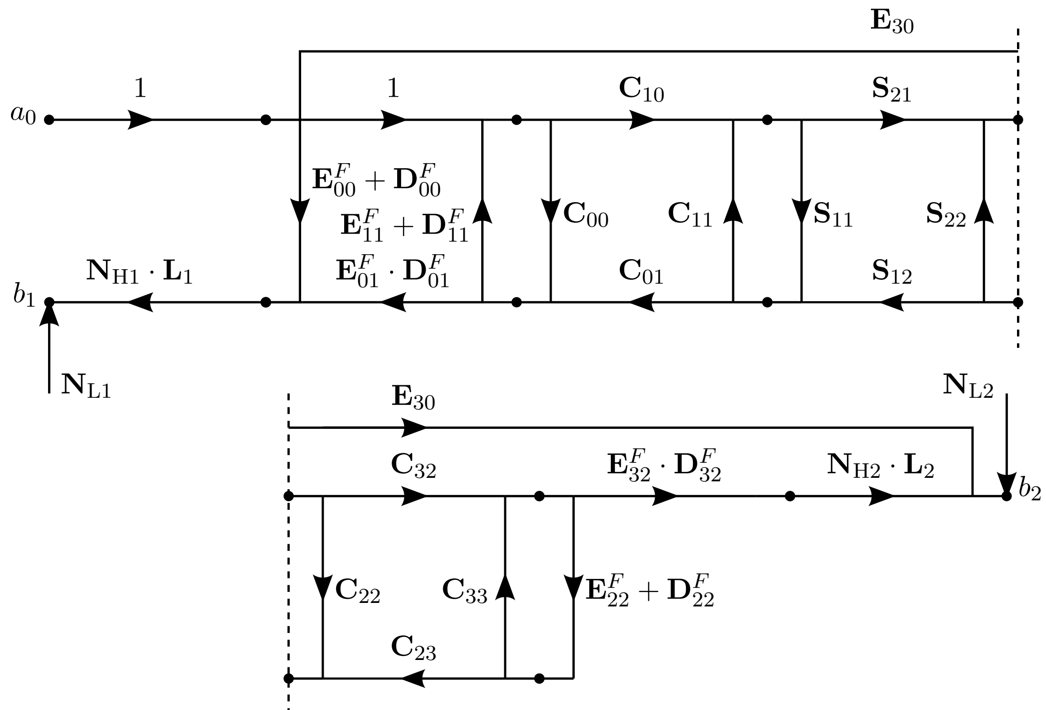

Figure F.2: Signal flow graph of two-port VNA measurement model. The model represents an extension of the ten-term forward VNA error model with additional terms influencing the measurements. Due to the limitations in page width the graph is separated in two parts, connected at the dashed lines. Accordingly, the measurement model for the reverse mode is identically based on the ten-term reverse VNA error model.

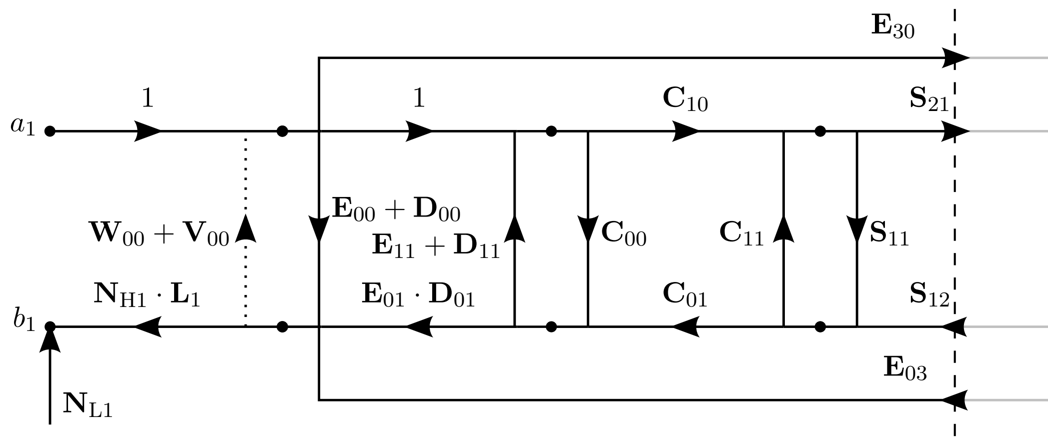

Figure F.3: Signal flow graph of two-port VNA measurement model (only the port 1 side is shown). Port 2 is symmetrical with the dashed line, except that both reflection tracking terms have to be considered at the port 2 side, see table D.3 and figure D.5. The model represents an extension of the seven-term VNA error model with additional terms influencing the measurements.

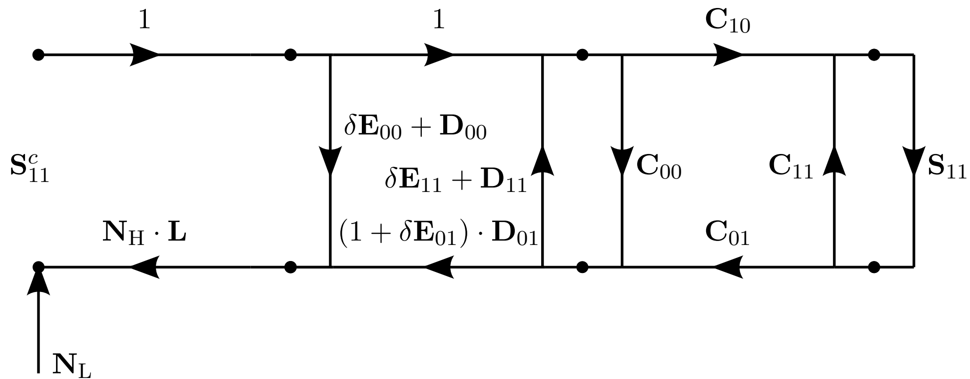

Figure F.4: Signal flow graph of residual one-port VNA measurement model. The model is equivalent to the one-port measurement model shown in figure F.1, except that the error coefficients E_{ij} are replaced by residual error coefficients $\delta\mathrm{E}_{\mathrm{ij}}$ and the indicated reflection coefficient S^{m}_{11} is replaced by the error corrected reflection coefficient S^{c}_{11}.

Using the same approach as for the one-port case, residual two-port measurement models can be formulated, e.g. the corresponding forward model would be based on figure F.2.

The residual measurement model has the advantage that it leads to relatively simple equations for the propagation of measurement uncertainties. The Ripple Method, which is discussed in appendix H, is based on the residual measurement model with some further simplifications. The resulting equations for linear uncertainty propagation are shown in H.4.

It is known, however, from experience that in transmission measurements the load match has an amplifying effect on the uncertainty, which is often not negligible. Such an effect is simply not in the scope of the residual measurement model and it is necessary to take additional measures to avoid an underestimation of the uncertainty, see H.4.2.1. Use of the full model, as done for the rigorous uncertainty evaluation, doesn't have that problem.

F.6 Uncertainty contributions

In the following the different terms of the particular models shown in figures F.1, F.2 and F.3 are briefly discussed and put into relation with the characterization of associated uncertainties in 5.3. The nomenclature refers to the model in figure F.3 but is easily transferable to the other models.

The terms denoted by $\mathbf{E}_{\mathrm{ij}}$ are the error coefficients. Estimates $\hat{\mathbf{E}}_{\mathrm{ij}}$ are determined during VNA calibration. The measurement model includes potential drift of these terms, denoted by $\mathbf{D}_{\mathrm{ij}}$ except for the cross talk ($\mathbf{E}_{30}$ and $\mathbf{E}_{03}$), which is generally very small. Best estimates $\hat{\mathbf{D}}_{\mathrm{ij}}$ are 0 (when additive) and 1 (when multiplicative) with associated uncertainties as determined in G.3. The term $\mathbf{W}_{00}$ denotes the switch term with associated drift $\mathbf{V}_{00}$ and $\hat{\mathbf{V}}_{00}=0$. $\mathbf{W}_{00}$ is shown with a dotted line, as it is only present when the source is active at port 2. For four-receiver VNAs, which have the capability to read out all receivers simultaneously, it can be determined directly for each measurement

and is not part of the normal calibration process.

The terms denoted by $\mathbf{C}_{\mathrm{ij}}$ represent effects due to the movement of test port cables and due to connector repeatability. The relation to the characterization in G.4 and G.5 can be established through a simple sub-model as shown in figure F.5. The terms $\mathbf{CA}_{\mathrm{T}}$ and $\mathbf{CA}_{\mathrm{R}}$ are related to cable movement and have best estimates of 1 and 0, respectively, with associated uncertainties as specified in G.4. The term $\mathbf{CO}_{\mathrm{R}}$ is related to connector repeatability and has a best estimate of 0 with an associated uncertainty as specified in G.5. Cascading the two 2-ports in figure F.5 leads to the following relations (shown here just for port 1):

$$\mathbf{C}_{00} = \mathbf{CA}_{\mathrm{R}} + \frac{\mathbf{CA}_{\mathrm{T}}^2\mathbf{CO}_{\mathrm{R}}}{1-\mathbf{CO}_{\mathrm{R}}\mathbf{CA}_{\mathrm{R}}}$$

$$\mathbf{C}_{11} = \mathbf{CO}_{\mathrm{R}} + \frac{\mathbf{CA}_{\mathrm{R}}}{1-\mathbf{CO}_{\mathrm{R}}\mathbf{CA}_{\mathrm{R}}}$$

$$\mathbf{C}_{10} = \mathbf{C}_{01} = \frac{\mathbf{CA}_{\mathrm{T}}}{1-\mathbf{CO}_{\mathrm{R}}\mathbf{CA}_{\mathrm{R}}}.$$

These expressions simplify considerably if used for linear uncertainty propagation with best estimates of unity and zero.

$$\mathbf{C}_{00} = \mathbf{C}_{11} = \mathbf{CA}_{\mathrm{R}} + \mathbf{CO}_{\mathrm{R}}$$

$$\mathbf{C}_{10} = \mathbf{C}_{01} = \mathbf{CA}_{\mathrm{T}}.$$

The term $\mathbf{N}_{\mathrm{Li}}$ denotes noise floor with $\hat{\mathbf{N}}_{\mathrm{Li}} = 0$. The terms $\mathbf{N}_{\mathrm{Hi}}$ and $\mathbf{L}_{\mathrm{i}}$ denote trace noise and non-linearity, respectively, with $\hat{\mathbf{N}}_{\mathrm{Hi}} = 1$ and $\hat{\mathbf{L}}_{\mathrm{i}} = 1$. The associated uncertainties can be determined using the procedures in G.1 and G.2, respectively.

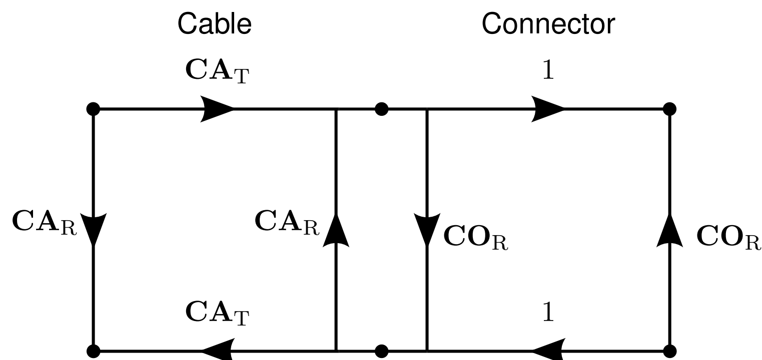

Figure F.5: Signal flow graph representing a simple measurement sub-model for cable movement and connector repeatability at port one.

G Characterization procedures of uncertainty contributions

The following step by step characterization procedures complement the discussion on uncertainty contributions in section 5. They are specifically chosen to be used with the measurement models in appendix F. The procedures below are examples, i.e. other ways of characterization are possible.

Fundamentally, procedures are shown for two types of influencing quantities, depending on how they act in the measurement model, additive quantities with an estimate of 0 and multiplicative quantities with an estimate of 1. Additive quantities are noise floor, drift related to directivity and match terms, cable and connector reflections. The associated uncertainties are characterized in Cartesian coordinates (real and imaginary components) in linear units. Multiplicative quantities are trace noise, non-linearity, drift related to the transmission error coefficients and cable transmission. The associated uncertainties are characterized in polar coordinates (magnitude and phase) in linear units.

G.1 Noise floor and trace noise

This procedure is applicable to a two port VNA. It is suitable to determine measurement uncertainties associated with the best estimates of the terms $\mathbf{N}_{\mathrm{Li}}$ (noise floor) and $\mathbf{N}_{\mathrm{Hi}}$ (trace noise) in the measurement models shown in appendix F. Best estimates of $\mathbf{N}_{\mathrm{Li}}$ and $\mathbf{N}_{\mathrm{Hi}}$ are $\hat{\mathbf{N}}_{\mathrm{Li}} = 0$ and $\hat{\mathbf{N}}_{\mathrm{Hi}} = 1$.

a) VNA settings: leave the VNA uncalibrated and set the test port power, IF bandwidth and averaging to the values that are being used for measurements. Set the sweep type to CW (continuous wave).

b) Connect two shorts or opens to port 1 and to port 2. Choose the standard, which shows a larger reflection coefficient. Wait a few minutes.

c) Collect at least a few hundred measurement data points of $\mathbf{S}_{11}^{m}$ and $\mathbf{S}_{22}^{m}$ (for the calculation of the trace noise) and $\mathbf{S}_{21}^{m}$ and $\mathbf{S}_{12}^{m}$ (for the calculation of the noise floor) for each frequency point.

d) Calculate the standard deviations of the real and imaginary components of $\mathbf{S}_{21}^{m}$. Take the larger of both: $\max(\mathrm{s}(\mathrm{Re}[\mathbf{S}_{21}^{m}]), \mathrm{s}(\mathrm{Im}[\mathbf{S}_{21}^{m}]))$ with $\mathrm{s}(\cdot)$ according to equation (C.7).

e) Define a reasonable envelope that encloses the calculated values over the whole frequency range. Typically, the whole frequency range is divided into frequency bands, each with a constant value that encloses the calculated values. The values can be taken as the standard uncertainties associated with the real and imaginary components of $\hat{\mathbf{N}}_{\mathrm{L2}}$.

f) Calculate the standard deviation of the normalized magnitude of $\mathbf{S}_{11}^{m}$: $\mathrm{s}(|\mathbf{S}_{11}^{m}/\mathbf{m}(\mathbf{S}_{11}^{m})|)$ with $\mathbf{m}(\cdot)$ and $\mathrm{s}(\cdot)$ according to equations (C.9) and (C.7), respectively.

g) Calculate the standard deviation of the normalized phase of $\mathbf{S}_{11}^{m}$: $\mathrm{s}(\arg[\mathbf{S}_{11}^{m}/\mathbf{m}(\mathbf{S}_{11}^{m})])$ with $\mathbf{m}(\cdot)$ and $\mathrm{s}(\cdot)$ according to equations (C.9) and (C.7), respectively.

h) For the values defined in step f) and g), define envelopes according to step e) and assign the values as uncertainties associated with magnitude and phase of $\hat{\mathbf{N}}_{\mathrm{H1}}$.

i) Repeat steps d) to h) for $\mathbf{S}_{12}^{m}$ and $\mathbf{S}_{22}^{m}$ to determine uncertainties associated with $\hat{\mathbf{N}}_{\mathrm{L1}}$ and $\hat{\mathbf{N}}_{\mathrm{H2}}$, respectively. Normally, this should give very similar results and the same uncertainties can be assigned to both ports by just taking the larger values for both.

Figures G.1, G.2, G.3, G.4, G.5 and G.6 are illustrating the above procedure.

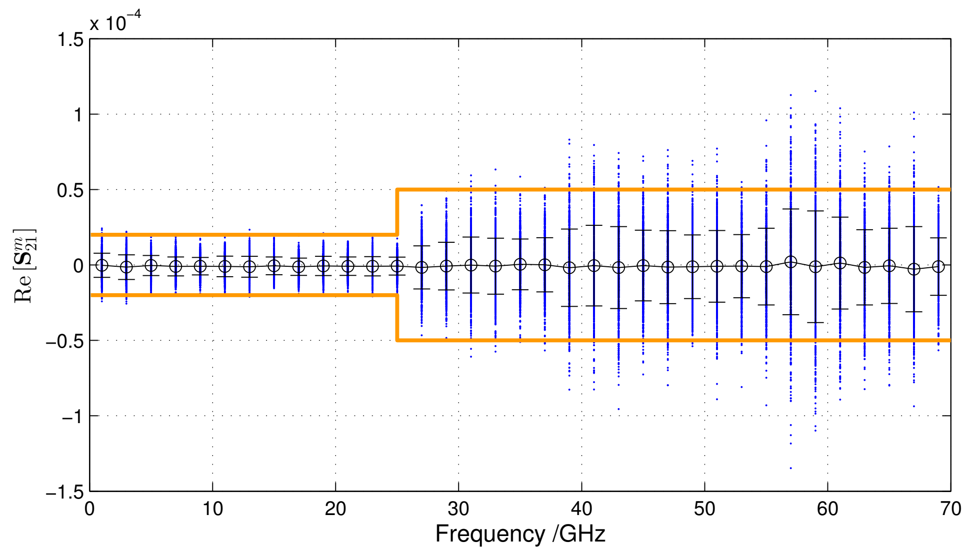

Figure G.1: Characterization of VNA noise floor according to the procedure in G.1. The blue data points are measurements of S^m_{21} according to step c) of the procedure. Only the real component of the S-parameter is shown. The imaginary component is not shown here, but gives very similar results. 801 measurements were made per frequency point. The black circles with bars indicate mean and standard deviation $\mathrm{s}(\mathrm{Re}\,[\mathbf{S}^m_{21}])$ of the measured sample at each frequency point, according to step d). The orange line indicates a possible envelope, according to step e). Note that the lowest frequency in this example is 1 GHz. At lower frequencies significantly larger noise floor is conceivable, see figure G.2.

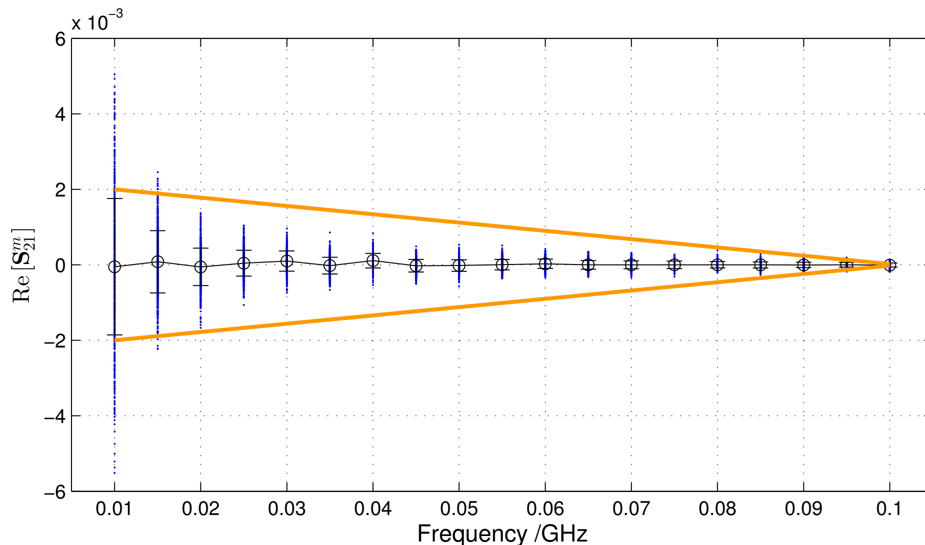

Figure G.2: The same as figure G.1, but for frequencies below 0.1 GHz. Note the significantly enlarged noise level towards low frequencies due to the reduced efficiency of couplers.

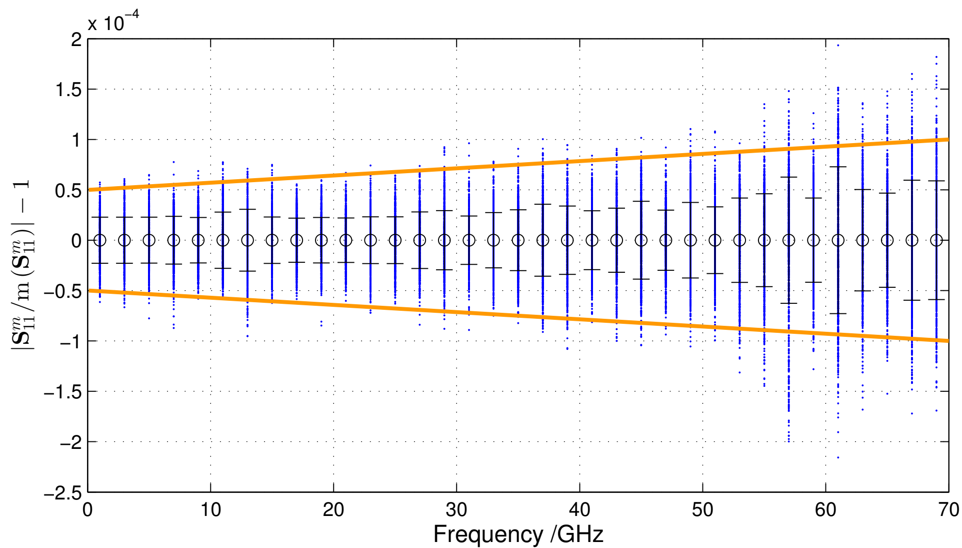

Figure G.3: Characterization of VNA trace noise magnitude according to the procedure in G.1. The blue data points are normalized measurements of S_{11}^m according to step c) of the procedure. 801 measurements were made per frequency point. The black circles with bars indicate mean and standard deviation of the displayed sample at each frequency point, according to step f). The orange line indicates a possible envelope, according to step h). Larger values of trace noise can occur for values at lower frequencies, see figure G.4.

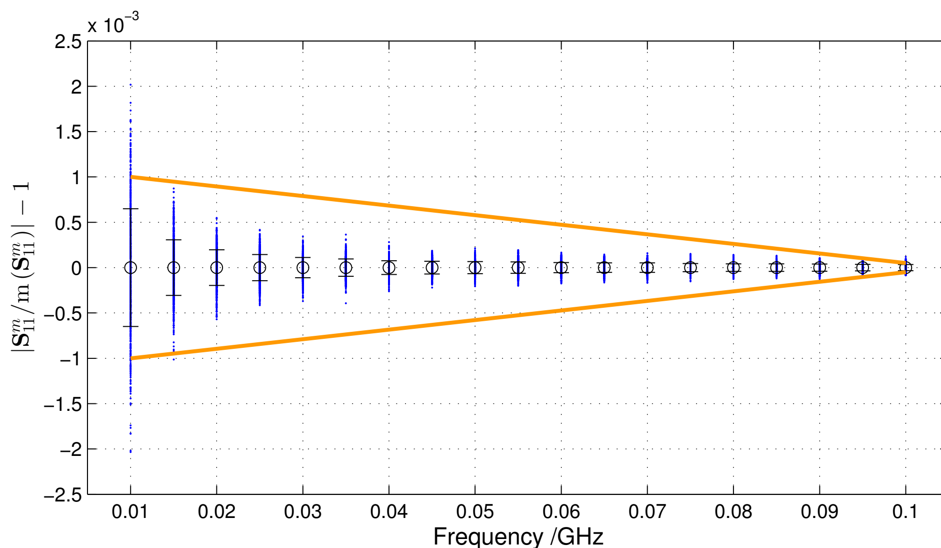

Figure G.4: The same as figure G.3, but for frequencies below 0.1 GHz. Note the significantly enlarged noise level towards low frequencies due to the reduced efficiency of couplers.

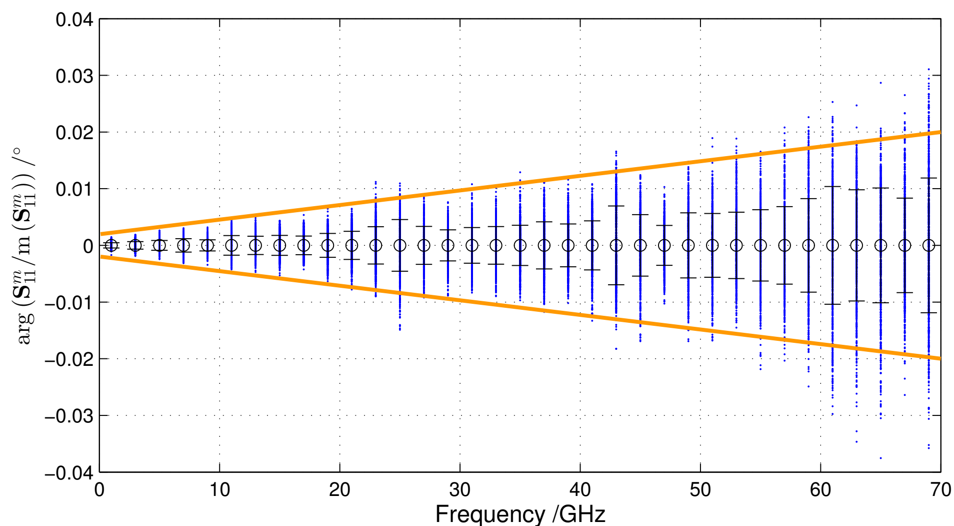

Figure G.5: Characterization of VNA trace noise phase according to the procedure in G.1. The blue data points are normalized measurements of S_{11}^m according to step c) of the procedure. 801 measurements were made per frequency point. The black circles with bars indicate mean and standard deviation of the displayed sample at each frequency point, according to step g). The orange line indicates a possible envelope, according to step h). Larger values of trace noise can occur for values at lower frequencies, see figure G.6.

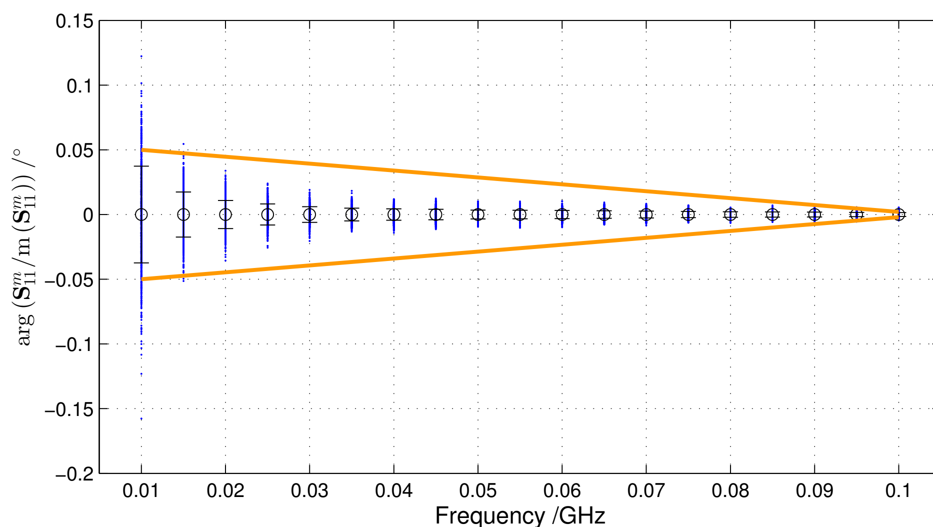

Figure G.6: The same as figure G.5, but for frequencies below 0.1 GHz. Note the significantly enlarged noise level towards low frequencies due to the reduced efficiency of couplers.

G.2 VNA non-linearity

This procedure is applicable to a two port VNA and uses an automatic step attenuation device. Manually operated step attenuation devices usually show worse repeatability. The procedure is suitable to determine uncertainties associated with the best estimate of the non-linearity term $\mathbf{L}_i$ in the measurement models given in appendix F. The best estimate of $\mathbf{L}_\mathrm{i}$ is $\hat{\mathbf{L}}_\mathrm{i} = 1$

a) Set the test port power of the VNA to the value that is being used for the measurements.

b) Set the IF bandwidth of the VNA to 10 Hz and the average factor to 1.

c) Perform a full two port calibration of the VNA. The SOLR calibration is preferred in order to avoid unnecessary cable movement.

d) Connect a characterized step attenuation device with a maximum attenuation of at least 60 dB. A device with 10 dB steps is sufficient for this type of assessment. The characterized incremental step width of the attenuation device is denoted by $A_{ref}(j)$ with $j = 1, 2, 3, ...$ indicating the attenuation step.

e) Measure all states of the step attenuation device over the whole frequency range and perform a VNA error correction to obtain estimates, $\hat{\mathbf{S}}_{21}(j)$ and $\hat{\mathbf{S}}_{12}(j)$, of the S-parameters of the attenuation device for each state $j = 0, 1, 2, 3, ...$ ($j = 0$ corresponds to the through state and represents the residual attenuation of the device).

f) Compute estimates of the incremental attenuations $\hat{A}_1(j) = |\hat{\mathbf{S}}_{21}(j)| - |\hat{\mathbf{S}}_{21}(0)|$ of the error corrected measurements. $|\hat{\mathbf{S}}_{21}(j)|$ and $|\hat{\mathbf{S}}_{21}(0)|$ need to be in logarithmic units. Repeat this process for $\mathbf{S}_{12}$ to calculate $\hat{A}_2(j)$.

g) Take the larger of the two differences between measured and characterized incremental attenuations: $d_j = \max(|\hat{A}_1(j) - A_{ref}(j)|, |\hat{A}_2(j) - A_{ref}(j)|)$.

h) Define a reasonable envelope that encloses the calculated differences d_j over the whole attenuation range. Since the frequency dependence is generally weak, this envelope might enclose any frequency dependence.

i) Transform d_j to linear units using $d_{j,lin} \simeq 0.12\, d_j$ and use $d_{j,lin}$ as uncertainties $\mathrm{u}(|\hat{\mathbf{L}}_\mathrm{i}|)$ and $\mathrm{u}(\arg(\hat{\mathbf{L}}_\mathrm{i}))$.

The procedure above is limited by the uncertainty associated with the attenuation steps. These uncertainties should be taken into account, if significant. The stated non-linearities can't be smaller than the uncertainty associated with the attenuation steps.

Figures G.7, G.8 and G.9 illustrate the procedure and provide additional information.

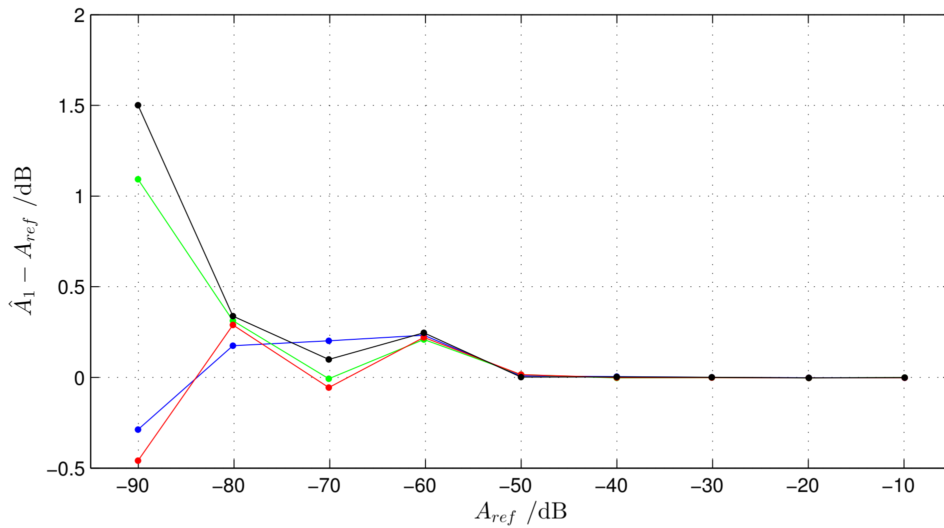

Figure G.7: Characterization of VNA non-linearity according to procedure G.2. The difference between a measurement and the reference value of incremental attenuation is shown for the entire attenuation range down to -90 dB at 1 GHz. This corresponds to step g) of the procedure, although only showing data for S_{21}. The different colors indicate four repetitions of the same measurement sequence. The large deviation from 0 and enhanced scatter below -50 dB are due to the influence of noise floor. Therefore, for the characterization of non-linearity only data above -60 dB should be considered, see figure G.8

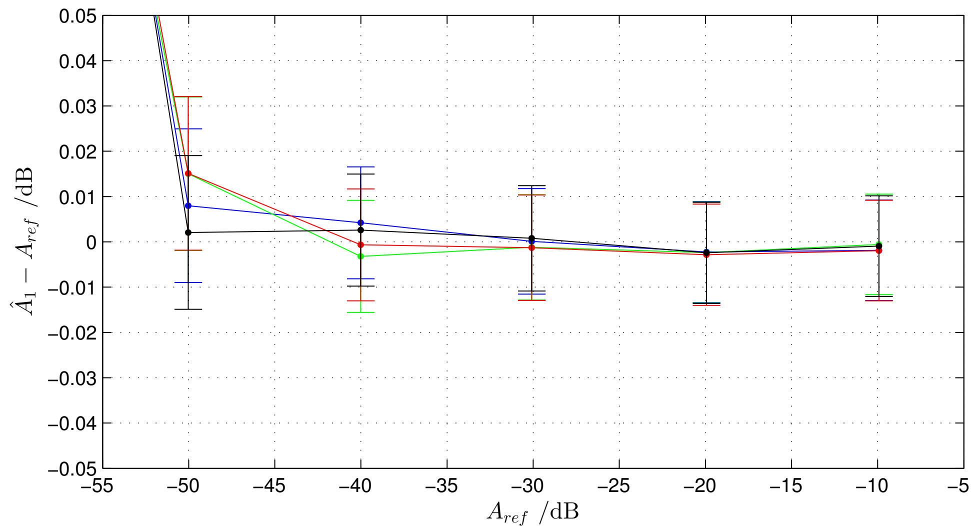

Figure G.8: The same as figure G.7. Only data above -60 dB should be used to characterize VNA non-linearity. Uncertainty intervals are shown as well. They need to be considered, when defining the envelope according to step h) of the procedure.

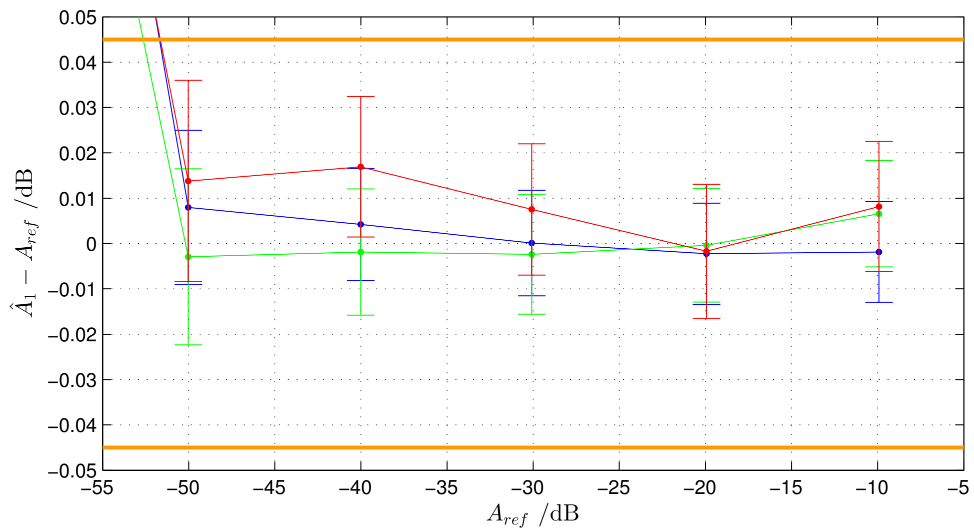

Figure G.9: The same as figure G.7. A single measurement sequence at three different frequencies, 1 GHz (blue), 10 GHz (green) and 18 GHz (red) is shown. The data indicates that the frequency dependence of non-linearity is weak. The orange line indicates a possible envelope, according to step h).

G.3 VNA drift

These procedures are valid for a two port VNA. They determine uncertainties associated with estimates of the drift of VNA error coefficients, as represented by the $\mathbf{D}_{\mathrm{ij}}$ and $\mathbf{V}_{\mathrm{ij}}$ terms in the VNA measurement models in appendix F. The characterization has to be performed under normal operating and environmental conditions, taking typical variations into account. It is necessary to repeat the characterization, if environmental conditions change.

Two methods are given. The first uses an electronic calibration unit (ECU), the second can be carried out without ECU. Recording of ambient temperature in parallel might be useful for the interpretation of the data.

Method with ECU:
This method can characterize the drift of each individual error coefficient.

a) Connect ECU to the VNA.

b) Measure the states of the ECU repeatedly over a period of 24 hours with an interval of 15 minutes. This necessitates computerized control of the ECU switching states (refer to VNA manual, ECU manual or contact manufacturer).

c) Use each measurement set to determine estimates of the error coefficients of the VNA as a function of time $\hat{\mathbf{E}}_{\mathrm{ij}}(t)$, starting at $t = 0$.

d) Determine the drift of the error coefficients related to directivity and match and the switch terms with respect to the first measurement at $t = 0$ with $\Delta\mathbf{E}_{\mathrm{ij}}(t) = \hat{\mathbf{E}}_{\mathrm{ij}}(t) - \hat{\mathbf{E}}_{\mathrm{ij}}(t = 0)$. Calculate the maximum deviation as $\max(|\operatorname{Re}[\Delta\mathbf{E}_{\mathrm{ij}}(t)]|, |\operatorname{Im}[\Delta\mathbf{E}_{\mathrm{ij}}(t)]|)$. Define a reasonable envelope that encloses the maximum deviation over the 24 hour time span. This could e.g. be a linear function of time and/or frequency. Take the values of this envelope as standard uncertainties associated with the estimates of both the real and imaginary components of the drift terms. It is important that these drift functions are defined rather generously to enclose possible variations in drift behavior.

e) Determine the drift of the error coefficients related to transmission with $\Delta\mathbf{E}_{\mathrm{ij}}(t) = \hat{\mathbf{E}}_{\mathrm{ij}}(t)/\hat{\mathbf{E}}_{\mathrm{ij}}(t = 0)$. Calculate the deviations in magnitude as $|\Delta\mathbf{E}_{\mathrm{ij}}(t)| - 1$ and in phase as $|\arg(\Delta\mathbf{E}_{\mathrm{ij}}(t))|$ Define a reasonable envelope that encloses the deviations over the 24 hour time span. This could e.g. be a linear function of time and/or frequency. Take the values of these envelopes as standard uncertainties associated with the estimates of magnitude and phase of the drift terms. It is important that these drift functions are defined rather generously to enclose possible variations in drift behavior.

Method using mechanical calibration standards:

a) Perform a two-port calibration of the VNA.

b) Establish a flush thru by connecting both test port cables.

c) Measure the full set of S-parameters repeatedly over a period of 24 hours with an interval of 15 minutes and perform VNA error corrections on each set to obtain estimates $\hat{\mathbf{S}}_{\mathrm{ij}}(t)$ starting at $t = 0$.

d) Determine the drift of $\mathbf{S}_{11}$ and $\mathbf{S}_{22}$ with respect to the first measurement at $t = 0$ with $\Delta\mathbf{S}_{\mathrm{ii}}(t) = \hat{\mathbf{S}}_{\mathrm{ii}}(t) - \hat{\mathbf{S}}_{\mathrm{ii}}(t = 0)$. Calculate the maximum deviation as $\max(|\,\mathrm{Re}[\Delta\mathbf{S}_{11}(t)]|, |\,\mathrm{Im}[\Delta\mathbf{S}_{11}(t)]|, |\,\mathrm{Re}[\Delta\mathbf{S}_{22}(t)]|, |\,\mathrm{Im}[\Delta\mathbf{S}_{22}(t)]|)$. Define a reasonable envelope that encloses the maximum deviation over the 24 hour time span. This could e.g. be a linear function of time and/or frequency. Take the values of this envelope as standard uncertainties associated with the estimates of both real and imaginary components of the drift terms related to the error coefficients directivity, match and switch terms. It is important that these drift functions are defined rather generously to enclose possible variations in drift behavior.

e) Determine the drift of $\mathbf{S}_{21}$ and $\mathbf{S}_{12}$ with respect to the first measurement at $t = 0$ with $\Delta\mathbf{S}_{\mathrm{ij}}(t) = \hat{\mathbf{S}}_{\mathrm{ij}}(t)/\hat{\mathbf{S}}_{\mathrm{ij}}(t = 0)$. Calculate the maximum deviations in magnitude and phase as $\max(|\Delta\mathbf{S}_{21}(t)|-1, |\Delta\mathbf{S}_{12}(t)|-1)$ and $\max(|\arg[\Delta\mathbf{S}_{21}(t)]|, |\arg[\Delta\mathbf{S}_{12}(t)]|)$ Define a reasonable envelope that encloses the maximum deviations over the 24 hour time span. This could e.g. be a linear function of time and/or frequency. Take the values of these envelopes as standard uncertainties associated with the estimates of magnitude and phase of the drift terms associated with the error coefficients related to transmission. It is important that these drift functions are defined rather generously to enclose possible variations in drift behavior.

Figures G.10, G.11 and G.12 illustrate the procedure without ECU. At very low frequency the enhanced noise floor due to inefficient couplers is visible again, in particular, in figures G.10 and G.11. This effect should already be taken into account in the characterization of the VNA noise floor, described in G.1, and can be ignored in the drift characterization.

Drift is affected by changes in the environment. After performing the VNA calibration, the operator connects the flush thru, starts the automated measurement sequence and then leaves the setup alone. The effect of this handling at the start of the procedure can be seen in figure G.12 when the phase of the transmission coefficient shows the largest deviation at the beginning of the sample of observations. To a lesser extent it can be also observed for the magnitude (figure G.11). Later in a quiet environment, the changes become more gradual.

It is important to understand that the procedure above characterizes drift related to the entire setup, consisting of VNA and test port cable. Using another test port cable might provide different results.

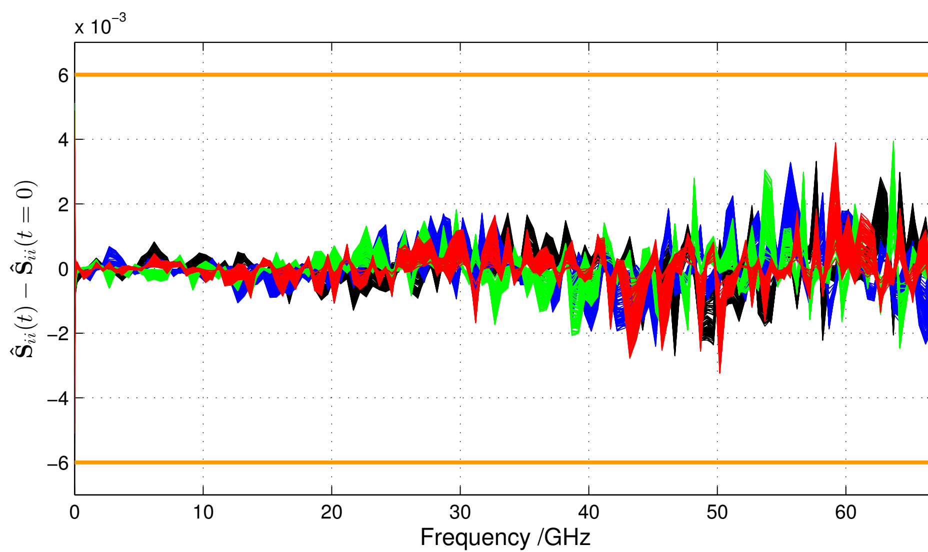

Figure G.10: Characterization of VNA drift with a flush thru measurement according to the second procedure in G.3. The traces are repeated measurements of $\mathrm{Re}\left[\hat{\mathrm{S}}_{11}\right]$ (black), $\mathrm{Im}\left[\hat{\mathrm{S}}_{11}\right]$ (blue), $\mathrm{Re}\left[\hat{\mathrm{S}}_{22}\right]$ (green), $\mathrm{Im}\left[\hat{\mathrm{S}}_{22}\right]$ normalized to the first measurements, according to step d) of the procedure. The measurements were done every 15 minutes for a duration of 24 hours. The orange line indicates a possible envelope, according to step d).

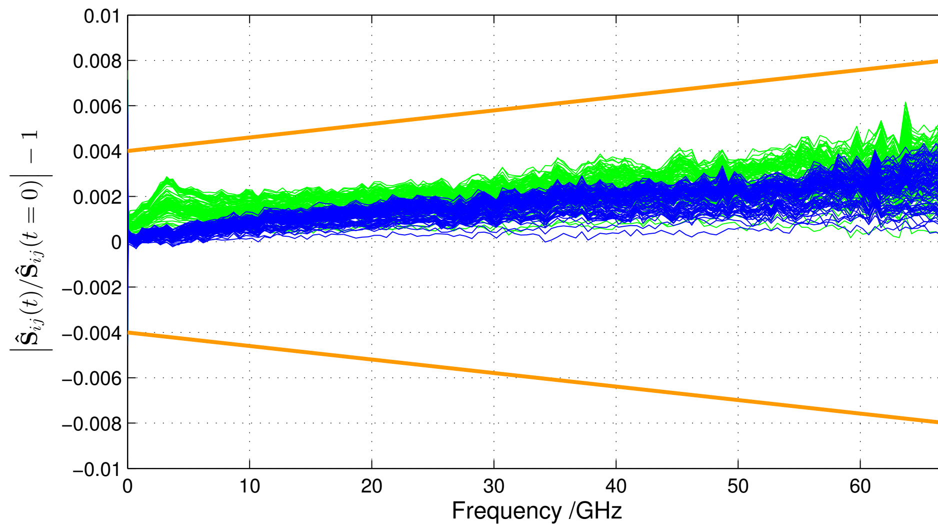

Figure G.11: Characterization of VNA drift with a flush thru measurement according to the second procedure in G.3. The traces are repeated measurements of $\left|\hat{S}_{21}\right|$ (green) and $\left|\hat{S}_{12}\right|$ (blue) normalized to the first measurements, according to step e) of the procedure. The measurements were done every 15 minutes for a duration of 24 hours. The orange line indicates a possible envelope, according to step e).

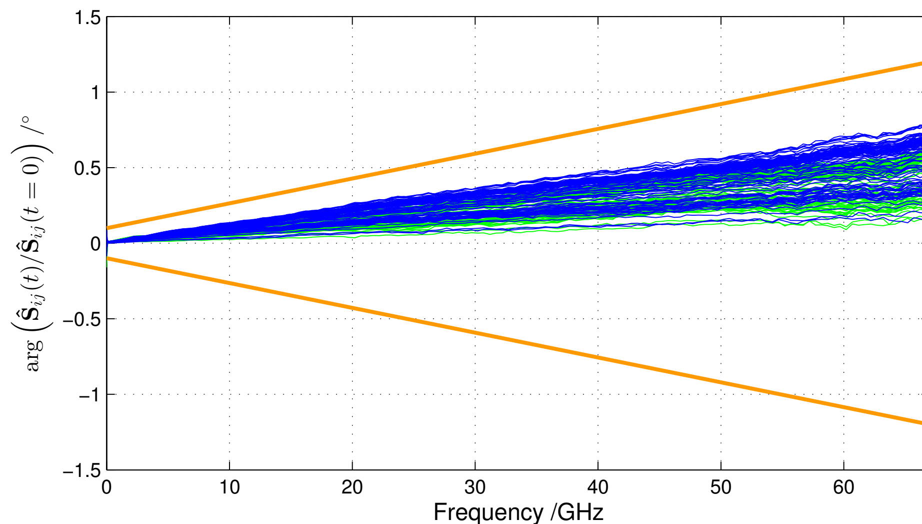

Figure G.12: Characterization of VNA drift with a flush thru measurement according to the second procedure in G.3. The traces are repeated measurements of $\arg\left(\hat{S}_{21}\right)$ (green) and $\arg\left(\hat{S}_{12}\right)$ (blue) normalized to the first measurements, according to step e) of the procedure. The orange line indicates a possible envelope. The measurements were done every 15 minutes for a duration of 24 hours.

G.4 Test port cable stability

This procedure aims at a relatively simple characterization of uncertainties associated with estimates of the terms $\mathbf{CA}_\mathrm{R}$ (cable reflection) and $\mathbf{CA}_\mathrm{T}$ (cable transmission) in figure F.5. Best estimates are $\hat{\mathbf{CA}}_\mathrm{R} = 0$ and $\hat{\mathbf{CA}}_\mathrm{T} = 1$. More sophisticated characterization procedures have been developed as well [63]. See also 8.5 for some practical hints on optimizing the setup of test port cables.

a) Perform a one-port calibration of the VNA at the VNA port.

b) Connect the test port cable to the VNA port. Wait for at least 30 minutes to achieve thermal equilibrium. To avoid the waiting time see figures G.15 and G.16 for an alternative setup.

c) Connect a short to the end of the test port cable.

d) Hold the cable in a straight line and take a first measurement ($n = 1$) of magnitude and phase.

e) Perform a gradual bend to a defined position. The defined position might be a 90 deg bend in the horizontal plane defined by the test port connectors of the VNA (8.5.1). If a subsequent measurement requires a cable bend leaving the horizontal plane, i.e. a vertical bend, this needs to be executed as well, because the behavior might be different due to the natural bending of the test port cable. In any case the characterization should enclose any movements that might occur in a subsequent measurement.

f) Take several measurements $n = 2, 3, ...$ of magnitude and phase during the gradual bend. Record the maximum deviation in magnitude and phase of the reflection coefficient with respect to measurement $n = 1$: $\Delta r = \max_n(||\hat{\mathbf{S}}_{11}(n)/\hat{\mathbf{S}}_{11}(n = 1)| - 1|)$ and $\Delta\phi = \max_n(\arg(\hat{\mathbf{S}}_{11}(n)/\hat{\mathbf{S}}_{11}(n = 1)))$. Define a generous envelope over frequency, enclosing the maximum deviations.

g) Use the envelope values determined in the previous step as uncertainties that are associated with the estimate of the term $\mathbf{CA}_\mathrm{T}$ in figure F.5 leading to $\mathrm{u}(|\hat{\mathbf{CA}}_\mathrm{T}|) = \Delta r/2$ and $\mathrm{u}(\arg(\hat{\mathbf{CA}}_\mathrm{T})) = \Delta\phi/2$. The division by 2 for magnitude and phase is applied, because the characterization with a short evaluates the stability of the cable for a signal that propagates back and forth in the cable. The uncertainty terms, however, are related to one-path effects.

h) For the term $\mathbf{CA}_\mathrm{R}$ in figure F.5 steps c) to g) have to be repeated with a matched load connected to the VNA cable instead of a short. In this case, the measured magnitude of $\mathbf{S}_{11}$ is small and hence the phase has minor significance. Thus, an evaluation in real and imaginary components is preferable, leading to $\Delta x = \max_n(\mathrm{Re}[\hat{\mathbf{S}}_{11}(n) - \hat{\mathbf{S}}_{11}(n = 1)])$ and $\Delta y = \max_n(\mathrm{Im}[\hat{\mathbf{S}}_{11}(n) - \hat{\mathbf{S}}_{11}(n = 1)])$. The uncertainties assigned to the real and imaginary parts of an estimate of $\mathbf{CA}_\mathrm{R}$ are $\mathrm{u}(\hat{\mathbf{CA}}_\mathrm{R}) = \mathrm{u}(\mathrm{Re}[\hat{\mathbf{CA}}_\mathrm{R}]) = \mathrm{u}(\mathrm{Im}[\hat{\mathbf{CA}}_\mathrm{R}]) = \max(\Delta x, \Delta y)$.

Figures G.13 and G.14 illustrate the characterization of the cable with respect to transmission stability. The corresponding measurement setups are shown in figures

G.15, for the start position of the cable, and G.16, for the end position of the cable (after gradual bend). The starting position is in this case not the straight cable. Instead the positional variation shown might be typical for two port measurements of a small-sized DUT. The characterization is viable as long as cable movements are kept within these limits. A clamping system, see 8.5.1, is helpful to keep control of cable positions.

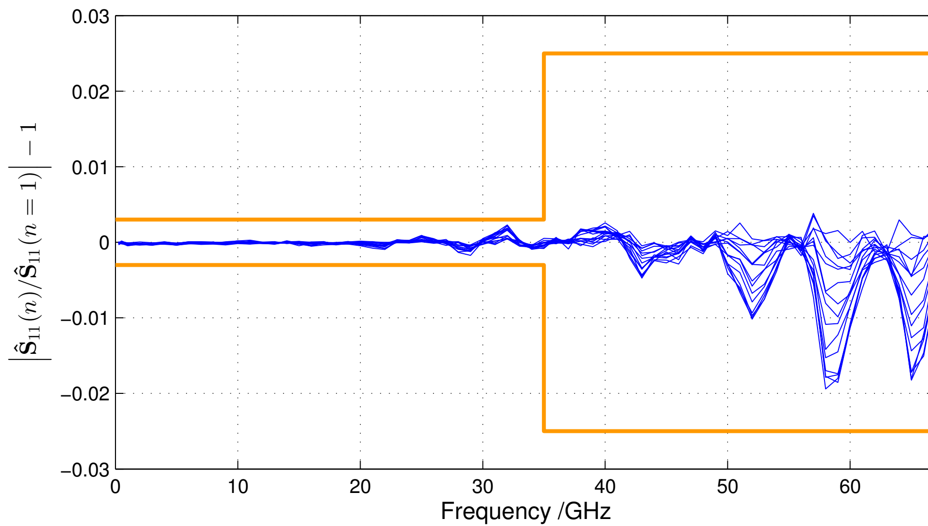

Figure G.13: Characterization of transmission magnitude stability of VNA test port cable according to the procedure in G.4. The traces are repeated normalized measurements, corresponding to step f) of the procedure, with the short connected to the end of the test port cable. The orange line indicates a possible envelope. The measurement setup is shown in figures G.15 (initial position of cable for measurement $n = 1$) and G.16 (final position after gradual bend of cable).

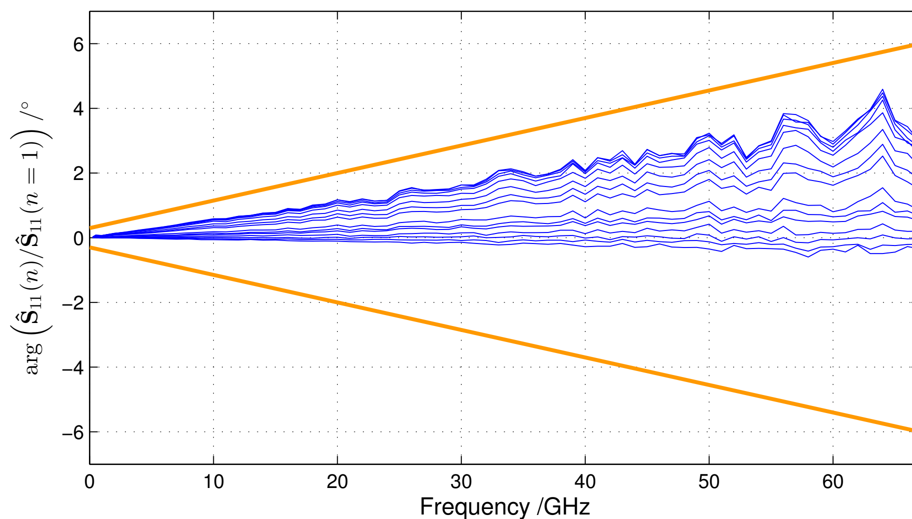

Figure G.14: The same as figure G.13 but now for the phase.

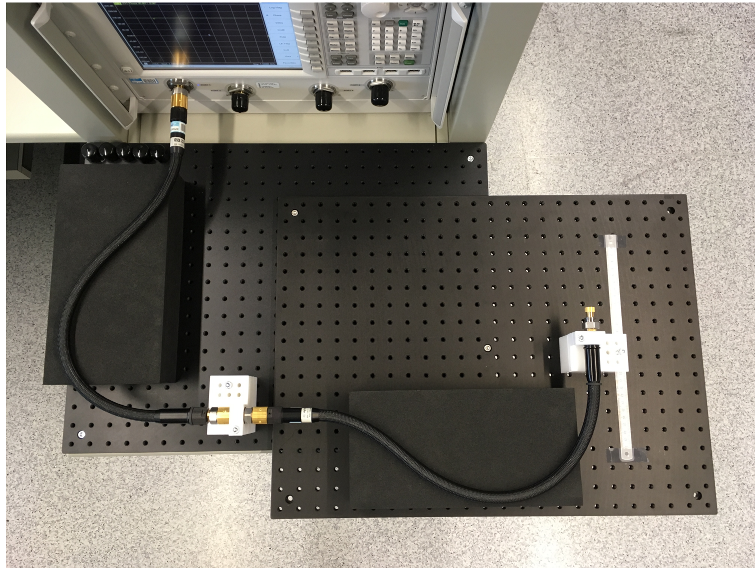

Figure G.15: Starting position (measurement $n = 1$) for the characterization of a VNA test port cable. In this setup the VNA has been calibrated at the end of the clamped test port cable on the left. The cable under test is the second cable, which is attached to the clamped test port. This way the cable under test is isolated from the warm VNA port and the waiting time of step b) is not necessary. In this setup it is important to keep the test port cable on the left fixed with clamps.

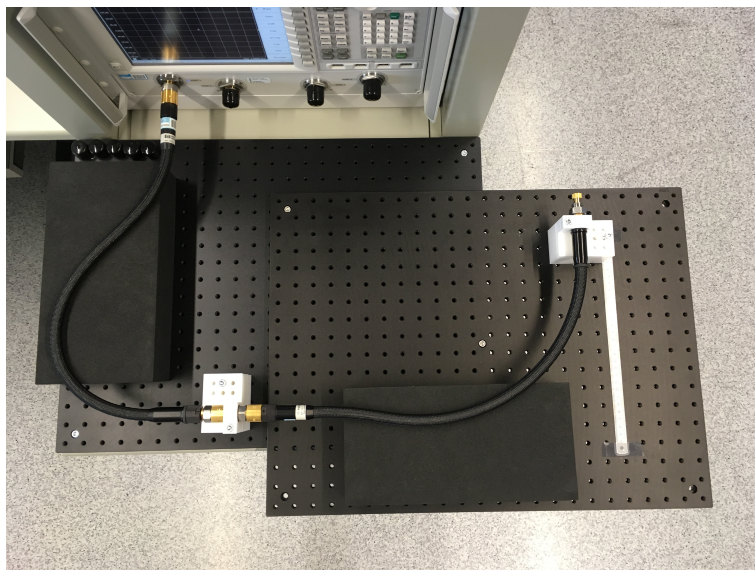

Figure G.16: The same as figure G.15, but showing the end position for the characterization of a VNA test port cable.

G.5 Connector repeatability

This procedure can be used for characterization of uncertainties associated with the estimate of the term $\mathbf{CO}_\mathrm{R}$ (connector reflection) in figure F.5. The estimate of $\mathbf{CO}_\mathrm{R}$ is $\hat{\mathbf{CO}}_\mathrm{R} = 0$. The procedure aims at characterizing the typical connector repeatability of a connector family. It therefore needs to be repeated for each connector family.

a) Perform a one-port calibration.

b) Connect a short and measure $\mathbf{S}_{11}^m$. Perform a VNA error correction to determine an estimate $\hat{\mathbf{S}}_{11}$

c) Repeat the previous step by re-connecting the short under different azimutal positions, at least 16 times to obtain a sample of estimates: $(\hat{\mathbf{S}}_{11}(1)\ \hat{\mathbf{S}}_{11}(2)\ \hat{\mathbf{S}}_{11}(3)\dots)$

d) Calculate the difference between maximum and minimum values of the sample in the real component of $\hat{\mathbf{S}}_{11}$: $\Delta x = \max_i(\mathrm{Re}[\hat{\mathbf{S}}_{11}(i)]) - \min_i(\mathrm{Re}[\hat{\mathbf{S}}_{11}(i)])$

e) Calculate the difference between maximum and minimum values of the measurement sample in the imaginary component of $\hat{\mathbf{S}}_{11}$: $\Delta y = \max_i(\mathrm{Im}[\hat{\mathbf{S}}_{11}(i)]) - \min_i(\mathrm{Im}[\hat{\mathbf{S}}_{11}(i)])$.

f) Take the larger of the two differences $\Delta z = \max(\Delta x, \Delta y)$

g) Define a reasonable envelope that encloses $\Delta z/2$ over the whole frequency range. Typically, this will be done by dividing the whole frequency range into frequency bands, each with a constant value that encloses the calculated values. This can be taken as the standard uncertainties associated with the real and imaginary components of $\hat{\mathbf{CO}}_R$.

NOTE — From a statistical point of view it seems more appropriate to take the standard deviation of the measurement sample as a measurement uncertainty, following the formalism in C.5. instead of the interval enclosing all values. Taking the interval that encloses all values is a more conservative approach, acknowledging the fact that this effect can strongly vary from one connector pair to another within the same connector family.

Figure G.17 shows example data for the evaluation of connector repeatability for the 1.85 mm connector family. The data has been collected according to the procedure above.

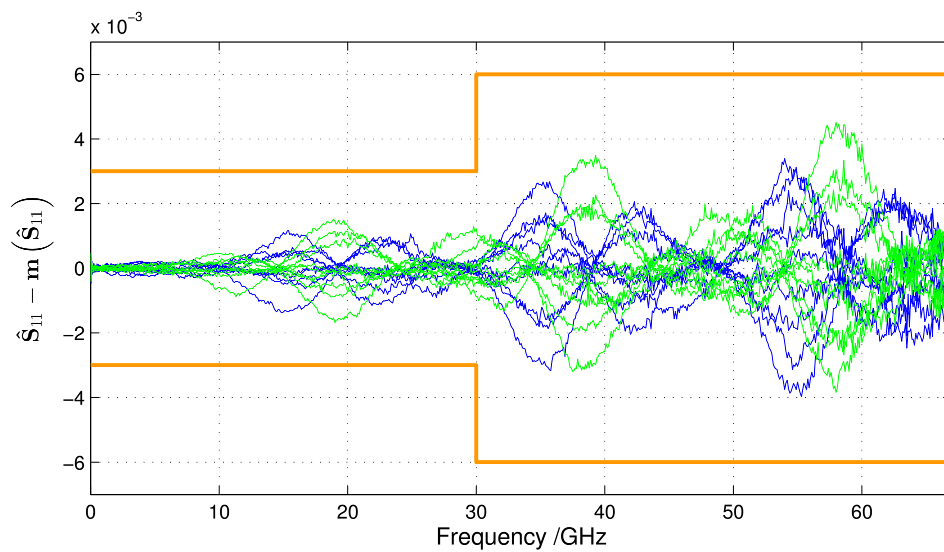

Figure G.17: Evaluation data for connector repeatability. $\hat{\mathrm{S}}_{11}$ has been determined for nine different connector orientations. Shown are $\mathrm{Re}\left[\hat{\mathbf{S}}_{11}\right]$ (blue) and $\mathrm{Im}\left[\hat{\mathbf{S}}_{11}\right]$ (green) normalized to the mean. The orange line indicates a possible envelope, according to step g) of the procedure.

H Ripple Method

H.1 Introduction

This section describes the implementation of the Ripple Method for the evaluation of measurement uncertainties in coaxial S-parameter measurements. The method, as described here, is recommended only up to 26.5 GHz, for coaxial line sizes of 3.5 mm and larger (e.g. Type-N), for reasons given in 1.2 and 7.2. The experimental part of the determination of the residual error coefficients is identical to that in the previous version of the guide. For the residual tracking term, which cannot be accessed experimentally, a formula is given that allows determination of the associated uncertainty from the characterization data of a data based calibration kit. Modifications are applied in the analysis of the ripple data by specifying minimal uncertainty limits for residual directivity and residual source match. The equations that propagate the uncertainties associated with the error coefficients to the DUT are modified in accordance with the suggestions in [32]. Additional uncertainty contributions are taken into account based on a more rigorous derivation of a measurement model for the error correction process.

H.2 Uncertainties

The uncertainties derived in this context do not need to be interpreted as uncertainties in the estimated magnitudes of the complex-valued quantities, as was the case in previous versions of the guide. Instead, they can be seen as equal sized uncertainties associated with the real and the imaginary components of the complex-valued estimate of the S-parameter, assuming there is no correlation between them, e.g. for $\mathbf{S}_{11}$: $\mathrm{u}(\hat{\mathbf{S}}_{11}) = \mathrm{u}(\mathrm{Re}[\hat{\mathbf{S}}_{11}]) = \mathrm{u}(\mathrm{Im}[\hat{\mathbf{S}}_{11}])$. This corresponds to a circular uncertainty region in the complex plane, following the suggestions in [64]. This uncertainty can be transformed to an uncertainty in magnitude and phase using standard uncertainty propagation techniques.

H.3 Practical Preparation

The Ripple Method requires at least one beadless air-dielectric line, for each type of connector. The nominal length of the air-dielectric line should be between 75 mm and 300 mm. Generally, the length of the air-dielectric line and the frequency range should be chosen such that several full cycles of the ripple pattern are visible in the procedures described in H.5.1 and H.5.2.

More discrimination, i.e. more ripples, will be obtained with a longer air-dielectric line. A 300 mm air-dielectric line will give ripples having a period of 0.5 GHz and a 100 mm air-dielectric line will result in ripples with a period of 1.5 GHz. The line length limits the lowest frequency at which a meaningful result can be obtained. E.g. in Type-N it should be possible to make reasonable estimates of the residual error coefficients at frequencies in the range of 0.5 GHz to 17.5 GHz with a frequency spacing of 250 MHz using a 300 mm air-dielectric line. Estimates between these discrete frequency points might be obtained through interpolation.

The physical dimensions of the air-dielectric line should be characterized and traceable to SI units. The relevant dimensions are the average outer diameter of the center

conductor and the average bore diameter of the outer conductor. In addition, it is important to verify that the difference in length between the center and outer conductors of each air-dielectric line is within specification [65]. This length measurement can usually be made using a pin-depth gauge, often found in some VNA calibration kits. The ratio of the diameters of the center and outer diameters can be used to determine the characteristic impedance of the air-dielectric line. A conversion between the geometrical dimensions and the electrical characteristic impedance, Z_0, for nominal 50 Ω lines, can be approximated by

$$Z_0 \simeq 59.939 \ln\left(\frac{d_o}{d_c}\right), \tag{H.1}$$

where d_o and d_c denote the outer and center conductor diameters of the air-dielectric line, respectively. Deviations in the geometrical dimensions can be used to estimate the deviation in the electrical characteristic impedance of the air-dielectric line, based on equation (H.1).

H.4 Measurement model

The Ripple Method is partly a “black box” method. The measurement model is based on the residual measurement model shown in F.5, basically assuming that the VNA is measuring error corrected S-parameters. Estimates of the residual error coefficients are determined experimentally and uncertainties only need to be propagated through the VNA error correction process. With a few additional simplifications it is possible to obtain reasonably simple equations for the uncertainties associated with estimates of the S-parameters of the DUT.

H.4.1 One-port equation

The one-port measurement model for reflection measurements is based on an evaluation of figure F.4 with $\delta\hat{\mathbf{E}}_{00} = \delta\hat{\mathbf{E}}_{01} = \delta\hat{\mathbf{E}}_{11} = 0$. For simplification it is necessary to keep the test port cable in a fixed position during measurement, see 8.5.1. Hence, uncertainty contributions from cable movement don't have to be considered. All random contributions, e.g. connector repeatability, are summarized in a single additive term $\mathbf{R}_{\mathrm{S}11}$. Linear uncertainty propagation leads to an expression for the uncertainty associated with an estimate of $\mathbf{S}_{11}$ of the DUT

$$\left[\mathrm{u}\left(\hat{\mathbf{S}}_{11}\right)\right]^2 = \left[\mathrm{u}\left(\delta\hat{\mathbf{E}}_{00}\right)\right]^2 + \left[\left|\hat{\mathbf{S}}_{11}^c\right| \mathrm{u}\left(\delta\hat{\mathbf{E}}_{01}\right)\right]^2 + \left[\left|\hat{\mathbf{S}}_{11}^c\right|^2 \mathrm{u}\left(\delta\hat{\mathbf{E}}_{11}\right)\right]^2 + \left[\left|\hat{\mathbf{S}}_{11}^c\right| \mathrm{u}\left(\hat{\mathbf{L}}\right)\right]^2 + \left[\mathrm{u}\left(\hat{\mathbf{R}}_{\mathrm{S}11}\right)\right]^2 . \tag{H.2}$$

$\mathbf{S}_{11}^c$ denotes the error corrected reflection coefficient. The residual error coefficients correspond to those listed in table D.1. The drift terms $\mathbf{D}_{\mathrm{ij}}$ are omitted in equation (H.2). They have to be considered as a part of the uncertainties associated with the estimates of the residual error coefficients. The term $\mathbf{L}$ denotes non-linearity.

H.4.2 Two-port equations

In analogy to the one-port case, the two-port measurement model is based on the two-port residual measurement model. For simplification, it is also necessary to fix the test port cable of port one, hence only cable movements at port two have to be considered. Using the same approach as the one-port case, the expressions for the uncertainties associated with estimates of the S-parameters of the DUT are:

$$\left[\mathrm{u}\left(\hat{\mathbf{S}}_{11}\right)\right]^2 = \left[\mathrm{u}\left(\delta\hat{\mathbf{E}}_{00}^F\right)\right]^2 + \left[\left|\hat{\mathbf{S}}_{11}^c\right| \mathrm{u}\left(\delta\hat{\mathbf{E}}_{01}^F\right)\right]^2 + \left[\left|\hat{\mathbf{S}}_{11}^c\right|^2 \mathrm{u}\left(\delta\hat{\mathbf{E}}_{11}^F\right)\right]^2 + \left[\left|\hat{\mathbf{S}}_{21}^c\hat{\mathbf{S}}_{12}^c\right| \mathrm{u}\left(\delta\hat{\mathbf{E}}_{22}^F\right)\right]^2 + \left[\left|\hat{\mathbf{S}}_{11}^c\right| \mathrm{u}\left(\hat{\mathbf{L}}\right)\right]^2 + \left[\left|\hat{\mathbf{S}}_{21}^c\hat{\mathbf{S}}_{12}^c\right| \mathrm{u}\left(\hat{\mathbf{C}}_{22}\right)\right]^2 + \left[\mathrm{u}\left(\hat{\mathbf{R}}_{\mathrm{S}11}\right)\right]^2 \tag{H.3a}$$

$$\left[\mathrm{u}\left(\hat{\mathbf{S}}_{21}\right)\right]^2 = \left[\left|\hat{\mathbf{S}}_{11}^c\hat{\mathbf{S}}_{21}^c\right| \mathrm{u}\left(\delta\hat{\mathbf{E}}_{11}^F\right)\right]^2 + \left[\left|\hat{\mathbf{S}}_{22}^c\hat{\mathbf{S}}_{21}^c\right| \mathrm{u}\left(\delta\hat{\mathbf{E}}_{22}^F\right)\right]^2 + \left[\left|\hat{\mathbf{S}}_{21}^c\right| \mathrm{u}\left(\delta\hat{\mathbf{E}}_{32}^F\right)\right]^2 + \left[\mathrm{u}\left(\delta\hat{\mathbf{E}}_{30}^F\right)\right]^2 + \left[\left|\hat{\mathbf{S}}_{21}^c\right| \mathrm{u}\left(\hat{\mathbf{L}}\right)\right]^2 + \left[\left|\hat{\mathbf{S}}_{21}^c\right| \mathrm{u}\left(\hat{\mathbf{C}}_{32}\right)\right]^2 + \left[\left|\hat{\mathbf{S}}_{21}^c\hat{\mathbf{S}}_{22}^c\right| \mathrm{u}\left(\hat{\mathbf{C}}_{22}\right)\right]^2 + \left[\mathrm{u}\left(\hat{\mathbf{R}}_{\mathrm{S}21}\right)\right]^2 \tag{H.3b}$$

$$\left[\mathrm{u}\left(\hat{\mathbf{S}}_{22}\right)\right]^2 = \left[\mathrm{u}\left(\delta\hat{\mathbf{E}}_{33}^R\right)\right]^2 + \left[\left|\hat{\mathbf{S}}_{22}^c\right| \mathrm{u}\left(\delta\hat{\mathbf{E}}_{32}^R\right)\right]^2 + \left[\left|\hat{\mathbf{S}}_{22}^c\right|^2 \mathrm{u}\left(\delta\hat{\mathbf{E}}_{22}^R\right)\right]^2 + \left[\left|\hat{\mathbf{S}}_{21}^c\hat{\mathbf{S}}_{12}^c\right| \mathrm{u}\left(\delta\hat{\mathbf{E}}_{11}^R\right)\right]^2 + \left[\left|\hat{\mathbf{S}}_{22}^c\right| \mathrm{u}\left(\hat{\mathbf{L}}\right)\right]^2 + \left[\left|\hat{\mathbf{S}}_{22}^c\right| \mathrm{u}\left(\hat{\mathbf{C}}_{32}\right)\right]^2 + \left[\left|\hat{\mathbf{S}}_{22}^c\right| \mathrm{u}\left(\hat{\mathbf{C}}_{23}\right)\right]^2 + \left[\left|\hat{\mathbf{S}}_{22}^c\right|^2 \mathrm{u}\left(\hat{\mathbf{C}}_{22}\right)\right]^2 + \left[\mathrm{u}\left(\hat{\mathbf{C}}_{33}\right)\right]^2 + \left[\mathrm{u}\left(\hat{\mathbf{R}}_{\mathrm{S}22}\right)\right]^2 \tag{H.3c}$$

$$\left[\mathrm{u}\left(\hat{\mathbf{S}}_{12}\right)\right]^2 = \left[\left|\hat{\mathbf{S}}_{22}^c\hat{\mathbf{S}}_{12}^c\right| \mathrm{u}\left(\delta\hat{\mathbf{E}}_{22}^R\right)\right]^2 + \left[\left|\hat{\mathbf{S}}_{11}^c\hat{\mathbf{S}}_{12}^c\right| \mathrm{u}\left(\delta\hat{\mathbf{E}}_{11}^R\right)\right]^2 + \left[\left|\hat{\mathbf{S}}_{12}^c\right| \mathrm{u}\left(\delta\hat{\mathbf{E}}_{01}^R\right)\right]^2 + \left[\mathrm{u}\left(\delta\hat{\mathbf{E}}_{03}^R\right)\right]^2 + \left[\left|\hat{\mathbf{S}}_{12}^c\right| \mathrm{u}\left(\hat{\mathbf{L}}\right)\right]^2 + \left[\left|\hat{\mathbf{S}}_{12}^c\right| \mathrm{u}\left(\hat{\mathbf{C}}_{23}\right)\right]^2 + \left[\left|\hat{\mathbf{S}}_{12}^c\hat{\mathbf{S}}_{22}^c\right| \mathrm{u}\left(\hat{\mathbf{C}}_{22}\right)\right]^2 + \left[\mathrm{u}\left(\hat{\mathbf{R}}_{\mathrm{S}12}\right)\right]^2. \tag{H.3d}$$

The terms $\mathbf{S}_{\mathrm{ij}}^c$ denote error corrected S-parameters. The residual error coefficients $\delta\mathbf{E}_{\mathrm{ij}}^F$ of the forward model and $\delta\mathbf{E}_{\mathrm{ij}}^R$ of the reverse model correspond to those listed in table D.2. Again, the drift terms are part of the uncertainties associated with the estimates of the residual error coefficients, as in the one-port case. The terms $\mathbf{C}_{\mathrm{ij}}$ denote cable movements on the port two side. The term $\mathbf{L}$ denotes non-linearity. The terms $\mathbf{R}_{\mathrm{Sij}}$ summarize all random effects.

H.4.2.1 Limitations of the residual measurement model

From practical experience it is known that uncertainties associated with transmission measurement can be underestimated with equations (H.3b) and (H.3d), if the raw load match of the VNA is significant. This is a shortcoming of the residual measurement

model, which doesn't consider the actual values of the error coefficients, see F.5. Therefore, instead of (H.3b) and (H.3d) the following equations are recommended [66]:

$$\begin{aligned}\left[\mathrm{u}\left(\hat{\mathbf{S}}_{21}\right)\right]^2 = &\left[\left|\hat{\mathbf{S}}^c_{11}\hat{\mathbf{S}}^c_{21}\right| \mathrm{u}\left(\delta\hat{\mathbf{E}}^F_{11}\right)\right]^2 + \left[\left|\hat{\mathbf{S}}^c_{22}\hat{\mathbf{S}}^c_{21}\right| \mathrm{u}\left(\delta\hat{\mathbf{E}}^F_{22}\right)\right]^2 + \left[\left|\hat{\mathbf{S}}^c_{21}\right| \mathrm{u}\left(\delta\hat{\mathbf{E}}^F_{32}\right)\right]^2 + \\ &\left[\mathrm{u}\left(\delta\hat{\mathbf{E}}^F_{30}\right)\right]^2 + \left[\left|\hat{\mathbf{S}}^c_{21}\right| \mathrm{u}\left(\hat{\mathbf{L}}\right)\right]^2 + \left[\left|\hat{\mathbf{S}}^c_{21}\right| \mathrm{u}\left(\hat{\mathbf{C}}_{32}\right)\right]^2 + \\ &\left[\left|\hat{\mathbf{S}}^c_{21}\hat{\mathbf{S}}^c_{22}\right| \mathrm{u}\left(\hat{\mathbf{C}}_{22}\right)\right]^2 + \left[\mathrm{u}\left(\hat{\mathbf{R}}_{\mathrm{S21}}\right)\right]^2 + \\ &\left|\hat{\mathbf{S}}^c_{21}\hat{\mathbf{E}}^F_{22}\left(1-\hat{\mathbf{S}}^c_{21}\hat{\mathbf{S}}^c_{12}\right)\right|^2 \left(\left[\mathrm{u}\left(\delta\hat{\mathbf{E}}^R_{33}\right)\right]^2 + \left[\mathrm{u}\left(\delta\hat{\mathbf{E}}^F_{11}\right)\right]^2\right)\end{aligned} \tag{H.4a}$$

$$\begin{aligned}\left[\mathrm{u}\left(\hat{\mathbf{S}}_{12}\right)\right]^2 = &\left[\left|\hat{\mathbf{S}}^c_{22}\hat{\mathbf{S}}^c_{12}\right| \mathrm{u}\left(\delta\hat{\mathbf{E}}^R_{22}\right)\right]^2 + \left[\left|\hat{\mathbf{S}}^c_{11}\hat{\mathbf{S}}^c_{12}\right| \mathrm{u}\left(\delta\hat{\mathbf{E}}^R_{11}\right)\right]^2 + \left[\left|\hat{\mathbf{S}}^c_{12}\right| \mathrm{u}\left(\delta\hat{\mathbf{E}}^R_{01}\right)\right]^2 + \\ &\left[\mathrm{u}\left(\delta\hat{\mathbf{E}}^R_{03}\right)\right]^2 + \left[\left|\hat{\mathbf{S}}^c_{12}\right| \mathrm{u}\left(\hat{\mathbf{L}}\right)\right]^2 + \left[\left|\hat{\mathbf{S}}^c_{12}\right| \mathrm{u}\left(\hat{\mathbf{C}}_{23}\right)\right]^2 + \\ &\left[\left|\hat{\mathbf{S}}^c_{12}\hat{\mathbf{S}}^c_{22}\right| \mathrm{u}\left(\hat{\mathbf{C}}_{22}\right)\right]^2 + \left[\mathrm{u}\left(\hat{\mathbf{R}}_{\mathrm{S12}}\right)\right]^2 + \\ &\left|\hat{\mathbf{S}}^c_{12}\hat{\mathbf{E}}^R_{11}\left(1-\hat{\mathbf{S}}^c_{21}\hat{\mathbf{S}}^c_{12}\right)\right|^2 \left(\left[\mathrm{u}\left(\delta\hat{\mathbf{E}}^F_{00}\right)\right]^2 + \left[\mathrm{u}\left(\delta\hat{\mathbf{E}}^R_{22}\right)\right]^2\right).\end{aligned} \tag{H.4b}$$

Equations (H.4a) and (H.4b) each have one additional term, containing estimates of the load matches, $\hat{\mathbf{E}}^F_{22}$ and $\hat{\mathbf{E}}^R_{11}$, of the respective ports.

H.5 Uncertainty contributions

The determination of the uncertainty terms in equations (H.2), (H.3) and (H.4) is described below for each contribution.

H.5.1 Directivity

The uncertainties $\mathrm{u}(\delta\hat{\mathbf{E}}_{00})$, $\mathrm{u}(\delta\hat{\mathbf{E}}^F_{00})$ and $\mathrm{u}(\delta\hat{\mathbf{E}}^R_{33})$ are determined experimentally by measuring the size of the residual directivity with the help of a ripple assessment. Typical values of residual directivity are in the range of 0.001 to 0.01 (i.e., from -60 dB to -40 dB) [67].

The procedure below is limited to one-port measurements and the determination of $\mathrm{u}(\delta\hat{\mathbf{E}}_{00})$. For two-port measurements the same procedure is performed at each port to determine $\mathrm{u}(\delta\hat{\mathbf{E}}^F_{00})$ and $\mathrm{u}(\delta\hat{\mathbf{E}}^R_{33})$.

H.5.1.1 Ripple magnitude

Connect the air-dielectric line to the VNA test port and terminate it with a suitable low-reflecting load. Make a measurement of $\mathbf{S}^c_{11}$ and display linear magnitude versus frequency. The display should show a significant undulation, called the 'ripple', superimposed on the reflection coefficient of the load itself. An example is shown in figure H.1.

The size of the residual directivity, $|\delta\mathbf{E}_{00}|$, is estimated from the peak-to-peak magnitude A_D of the ripple. A_D should be obtained from an adjacent peak and trough with

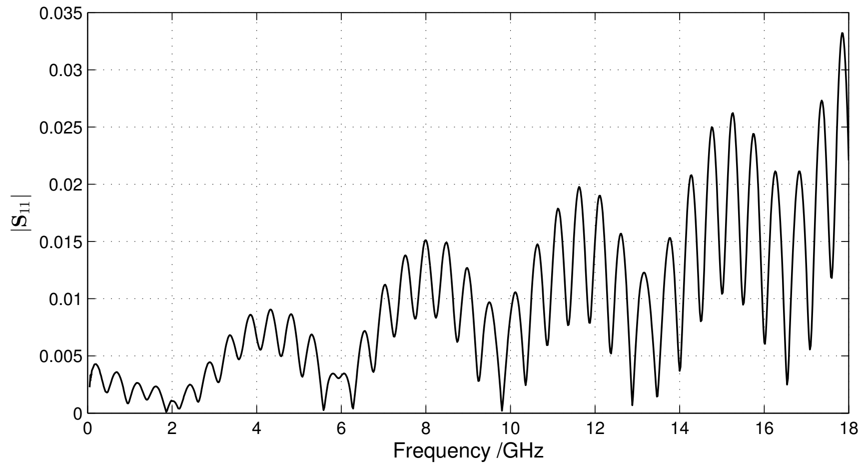

Figure H.1: The ripple pattern of a 30 cm beadless Type-N air-dielectric line terminated with a matched load.

adjustment made for any slope caused by the variation with frequency of the reflection coefficient of the terminating load, as illustrated in figure H.2. A_D corresponds to an estimate of twice the size of $|\delta\mathbf{E}_{00}|$.

NOTE — The load must have a reflection coefficient $\mathbf{\Gamma}_{\mathrm{L}}$ that is larger than the magnitude of the residual directivity, i.e. $|\mathbf{\Gamma}_{\mathrm{L}}| > |\delta\mathbf{E}_{00}|$. If this is not the case, the peak-to-peak ripple value A_D will be an estimate of $2\,|\mathbf{\Gamma}_{\mathrm{L}}|$, rather than $2\,|\delta\mathbf{E}_{00}|$. This would lead to an underestimation of the residual directivity.

H.5.1.2 Influence of connector

As pointed out previously, the reflections Γ_{CO} at the connector interfaces of the air-dielectric line interfere with the ripple caused by the residual directivity. This effect has to be considered in the uncertainty evaluation. The magnitude of the reflection can be

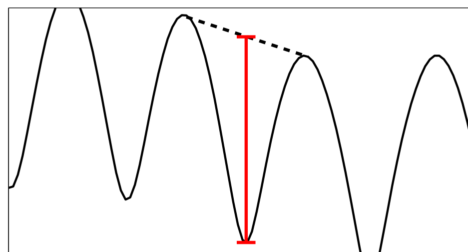

Figure H.2: A practical way to compensate for the slope when the peak-to-peak ripple value A_D is determined. A_D is indicated by the red solid line.

analytically approximated [68] by

$$|\mathbf{\Gamma}_{\mathrm{CO}}| \simeq kf\,(1 + 0.1 d_{\mathrm{pg}}) \tag{H.5}$$

with d_{pg} the maximal pin gap in μm and f the frequency in GHz. The factor k is dependent on the connector type, $k = 8 \cdot 10^{-5}$ for Type-N and $k = 7 \cdot 10^{-5}$ for 3.5 mm. d_{pg} is the absolute value of the sum of the recession of the center conductor at the test port and the maximum recession of the center conductor of the air-dielectric line. The uncertainty associated with $|\hat{\mathbf{\Gamma}}_{\mathrm{CO}}|$ can be approximated by

$$\mathrm{u}\left(\left|\hat{\mathbf{\Gamma}}_{\mathrm{CO}}\right|\right) \simeq 0.1kf \cdot \mathrm{u}\left(\hat{d}_{\mathrm{pg}}\right). \tag{H.6}$$

Example: The recession of the center conductor is -20 μm at the test port, -20 μm at the air-dielectric line and -10 μm at the matched load. This leads to a maximal pin gap of $\hat{d}_{\mathrm{pg}} = 50\,\mu$m. For a measurement in Type-N at 18 GHz this leads to $|\hat{\mathbf{\Gamma}}_{\mathrm{CO}}| \simeq 8.64 \cdot 10^{-3}$ when using equation (H.5). A single measurement of the pin depth is assumed to have an associated uncertainty of 4 μm. The addition of the three measurements leads to $\mathrm{u}(\hat{d}_{\mathrm{pg}}) = 12\,\mu$m, assuming that they are strongly correlated because the same connector gauge is used for all three measurements. This leads to $\mathrm{u}(|\hat{\mathbf{\Gamma}}_{\mathrm{CO}}|) \simeq 1.73 \cdot 10^{-3}$ when using equation (H.6).

NOTE — Equation (H.5) seems to favor a small maximal pin gap to keep the interfering reflections as small as possible. However, caution is advised. Equation (H.5) takes into account inductive coupling only. In case of a small pin gap capacitive coupling can become dominant leading to stability problems, see 8.5.2.2. The size of this effect can't be easily estimated analytically. It is therefore necessary to repeat the ripple evaluation under different connector orientations and record the variation in the ripple amplitude as described in H.5.1.4.

H.5.1.3 Characteristic impedance

The magnitude of the ripple is also influenced by the characteristic impedance of the air-dielectric line. A deviation from the ideal $50\,\Omega$ leads to a reflection coefficient

$$|\mathbf{\Gamma}_{\mathrm{AL}}| = \frac{Z_0 - 50\,\Omega}{Z_0 + 50\,\Omega} \tag{H.7}$$

with Z_0 as defined in equation (H.1). Furthermore, there is an uncertainty associated with the estimate of $|\Gamma_{\mathrm{AL}}|$, which can be approximated by

$$\mathrm{u}\left(\left|\hat{\mathbf{\Gamma}}_{\mathrm{AL}}\right|\right) = 0.6\sqrt{\left(\frac{\mathrm{u}\left(\hat{d}_o\right)}{\hat{d}_o}\right)^2 + \left(\frac{\mathrm{u}\left(\hat{d}_c\right)}{\hat{d}_c}\right)^2} \tag{H.8}$$

with d_o and d_c defined in H.3.

H.5.1.4 Repeatability

If more than one suitable air-dielectric line is available, the procedure should be repeated using the other available air-dielectric lines to check for the consistency of the value obtained for the residual directivity. The technique should also be repeated several times using the same air-dielectric line to estimate the variability in the value obtained for the residual directivity. Typically only a small number of repetitions will be

done. Because of the previously mentioned effects related to capacitive coupling, it is recommended to take a conservative approach and take the half width of the observed variations as $\mathrm{u}(\hat{\mathbf{R}}_{\mathrm{E00}})$.

H.5.1.5 Combined uncertainty associated with residual directivity

The uncertainty associated with an estimate of the residual directivity term can be written as

$$\left[\mathrm{u}\left(\delta\hat{\mathbf{E}}_{00}\right)\right]^2 = \left[\frac{A_D}{2\sqrt{2}}\right]^2 + \left[\frac{\left|\hat{\mathbf{\Gamma}}_{\mathrm{CO}}\right|}{\sqrt{2}}\right]^2 + \left[\mathrm{u}\left(\left|\hat{\mathbf{\Gamma}}_{\mathrm{CO}}\right|\right)\right]^2 + \left[\frac{\left|\hat{\mathbf{\Gamma}}_{\mathrm{AL}}\right|}{\sqrt{2}}\right]^2 + \left[\mathrm{u}\left(\left|\hat{\mathbf{\Gamma}}_{\mathrm{AL}}\right|\right)\right]^2 + \left[\mathrm{u}\left(\left|\hat{\mathbf{D}}_{00}\right|\right)\right]^2 + \left[\mathrm{u}\left(\hat{\mathbf{R}}_{\mathrm{E00}}\right)\right]^2. \quad \text{(H.9)}$$

The evaluations of the different terms in equation (H.9) are explained in H.5.1.1, H.5.1.2, H.5.1.3 and H.5.1.4, respectively. The uncertainty associated with an estimate of the drift $\mathrm{u}(|\hat{\mathbf{D}}_{00}|)$ is evaluated according to G.3. The divisor of $\sqrt{2}$ acknowledges the fact that the phase is unknown, see [50, 69].

H.5.2 Source match

The uncertainties $\mathrm{u}(\delta\hat{\mathbf{E}}_{11})$, $\mathrm{u}(\delta\hat{\mathbf{E}}_{11}^F)$ and $\mathrm{u}(\delta\hat{\mathbf{E}}_{22}^R)$ are determined according to the evaluation of uncertainties associated with the residual directivity, except that a high-reflecting short is used instead of a matched load as termination of the air-dielectric line. The residual source match is typically in the range 0.001 to 0.030 (i.e., from -60 dB to -30 dB) [67].

The procedure below is limited to one-port measurements and the determination of $\mathrm{u}(\delta\hat{\mathbf{E}}_{11})$. For two-port measurements the same procedure is performed at each port to determine $\mathrm{u}(\delta\hat{\mathbf{E}}_{11}^F)$ and $\mathrm{u}(\delta\hat{\mathbf{E}}_{22}^R)$.

H.5.2.1 Ripple magnitude

The VNA should display (again in linear magnitude format, after suitable scaling) an increase of line attenuation with frequency, superimposed by a ripple, the amplitude of which typically increases with frequency (though not necessarily monotonically). An example is shown in figure H.3. An estimate of the size of the residual source match, $|\delta\mathbf{E}_{11}|$, is obtained from the peak-to-peak ripple value A_S, following the same procedure used for the directivity.

The influences due to connectors and the characteristic impedance are the same as for the directivity and results from H.5.1.2 and H.5.1.3 can be used for the combined uncertainty.

A_S is also influenced by residual directivity, $\delta\mathbf{E}_{00}$, and residual reflection tracking, $\delta\mathbf{E}_{01}$, since the ripple of this measurement includes effects from all three error coefficients. The effect of residual directivity can be taken into account using the results of the evaluation in H.5.1.1. However, there is no suitable way to take the influence of residual reflection tracking into account.

A_S is also reduced by the losses of the air-dielectric line. The effect can be estimated from the decline of the average reflection coefficient in the ripple measurement and taken into account in the combined uncertainty by multiplying with a factor c_L.

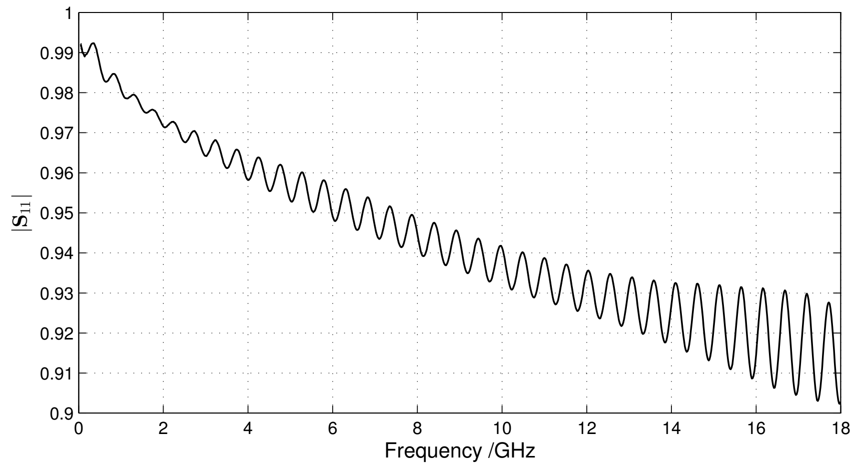

Figure H.3: Ripple pattern of a 30 cm beadless Type-N air-dielectric line terminated with a short.

Example: The attenuation of A_S due to losses can be estimated from the average reflection coefficient in figure H.3. At the maximum frequency the average reflection coefficient is approximately 0.915. Because the observed residual source match scales with $\mathbf{S}_{11}^2$ the observed A_S needs to be multiplied with a factor $c_L = 1/0.915^2 = 1.195$ at this frequency.

H.5.2.2 Combined uncertainty associated with source match

The uncertainty associated with the residual source match can be written as

$$\left[\mathrm{u}\left(\delta\hat{\mathbf{E}}_{11}\right)\right]^2 = \left[c_L\frac{A_S}{2\sqrt{2}}\right]^2 + \left[\frac{A_D}{2\sqrt{2}}\right]^2 + \left[\frac{\left|\hat{\mathbf{\Gamma}}_{\mathrm{CO}}\right|}{\sqrt{2}}\right]^2 + \left[\mathrm{u}\left(\left|\hat{\mathbf{\Gamma}}_{\mathrm{CO}}\right|\right)\right]^2 + \left[\frac{\left|\hat{\mathbf{\Gamma}}_{\mathrm{AL}}\right|}{\sqrt{2}}\right]^2 + \left[\mathrm{u}\left(\left|\hat{\mathbf{\Gamma}}_{\mathrm{AL}}\right|\right)\right]^2 + \left[\mathrm{u}\left(\left|\hat{\mathbf{D}}_{11}\right|\right)\right]^2 + \left[\mathrm{u}\left(\hat{\mathbf{R}}_{\mathrm{E11}}\right)\right]^2. \tag{H.10}$$

The first term in equation (H.10) is determined according to H.5.2.1 with A_S the peak-to-peak value in the ripple evaluation and c_L the amplification factor to compensate for losses in the air-dielectric line. The second term acknowledges the influence of the residual directivity with A_D determined in H.5.1.1. For the evaluation of the remaining terms the same procedures as described for the residual directivity (H.5.1.2, H.5.1.3 and H.5.1.4) can be applied. The uncertainty associated with the estimate of drift, $\mathrm{u}(|\hat{\mathbf{D}}_{11}|)$, is evaluated according to G.3. The divisor of $\sqrt{2}$ takes into account that the phase is unknown, see [50, 69].

H.5.3 Reflection tracking

The residual reflection tracking can be characterized using reference and measurement data of the short that has been used during VNA calibration. No additional measurement standard or extra measurement is needed. However, the short must be calibrated,

i.e. an estimate of the reflection coefficient $\mathbf{\Gamma}_s$ and its associated uncertainty should be known.

The one-port residual model, see F.5, is solved for the residual reflection tracking coefficient $\delta\mathbf{E}_{01}$ while ignoring the terms related to cable, connector ,non-linearity and noise. This leads to

$$\delta\mathbf{E}_{01} = \frac{\left(\mathbf{\Gamma}_s^c - \delta\mathbf{E}_{00}\right)\left(1 - \delta\mathbf{E}_{11}\mathbf{\Gamma}_s\right)}{\mathbf{\Gamma}_s} - 1, \tag{H.11}$$

with $\mathbf{\Gamma}_s^c$ denoting the error corrected reflection coefficient of the short.

The uncertainty associated with the estimate of $\delta\mathbf{E}_{01}$ is calculated from uncertainties associated with estimates of $\delta\mathbf{E}_{00}$, $\delta\mathbf{E}_{11}$ and $\mathbf{\Gamma}_s$, using linear uncertainty propagation through equation (H.11) with best estimates $\delta\mathbf{E}_{00} = \delta\mathbf{E}_{11} = 0$ and $\hat{\mathbf{\Gamma}}_s^c = \hat{\mathbf{\Gamma}}_s$. This leads to

$$\left[\mathrm{u}\left(\delta\hat{\mathbf{E}}_{01}\right)\right]^2 = \left[\frac{\mathrm{u}\left(\hat{\mathbf{\Gamma}}_s\right)}{\left|\hat{\mathbf{\Gamma}}_s\right|}\right]^2 + \left[\frac{\mathrm{u}\left(\delta\hat{\mathbf{E}}_{00}\right)}{\left|\hat{\mathbf{\Gamma}}_s\right|}\right]^2 + \left[\left|\hat{\mathbf{\Gamma}}_s\right| \mathrm{u}\left(\delta\hat{\mathbf{E}}_{11}\right)\right]^2 + \left[\mathrm{u}\left(\left|\hat{\mathbf{D}}_{01}\right|\right)\right]^2. \tag{H.12}$$

$\mathrm{u}(\delta\hat{\mathbf{E}}_{00})$ and $\mathrm{u}(\delta\hat{\mathbf{E}}_{11})$ are determined by the ripple assessment described in H.5.1 and H.5.2, respectively. The uncertainty associated with the estimate of the drift, $\mathrm{u}(|\hat{\mathbf{D}}_{01}|)$, is evaluated according to G.3.

Assuming that the characterization data of the short contains uncertainties associated with the real and imaginary component estimates, perhaps even including correlation, it can be simplified as

$$\mathrm{u}\left(\hat{\mathbf{\Gamma}}_s\right) = \max\left(\mathrm{u}\left(\mathrm{Re}\left[\hat{\mathbf{\Gamma}}_s\right]\right), \mathrm{u}\left(\mathrm{Im}\left[\hat{\mathbf{\Gamma}}_s\right]\right)\right). \tag{H.13}$$

The evaluation according to equation (H.12) is frequency dependent, because the characterization of the short is usually frequency dependent. For a simplified treatment enclosing uncertainty envelopes can be defined for different frequency ranges.

Equation (H.12) leads to a large overestimation of the uncertainty associated with the residual reflection tracking. The situation can be improved if measurement and reference data of the calibration open are also taken into account [70]. Derivation of the formalism is based again on equation (H.11). Combining the information about short and open leads to

$$\begin{aligned}\left[\mathrm{u}\left(\delta\hat{\mathbf{E}}_{01}\right)\right]^2 =& \frac{1}{4}\left[\frac{\mathrm{u}\left(\hat{\mathbf{\Gamma}}_s\right)}{\left|\hat{\mathbf{\Gamma}}_s\right|} + \frac{\mathrm{u}\left(\hat{\mathbf{\Gamma}}_o\right)}{\left|\hat{\mathbf{\Gamma}}_o\right|}\right]^2 + \frac{|x|^2}{4}\left(\left[\mathrm{u}\left(\delta\hat{\mathbf{E}}_{11}\right)\right]^2 + \left[\mathrm{u}\left(\delta\hat{\mathbf{E}}_{00}\right)\right]^2\right) + \\ & \left[\mathrm{u}\left(\left|\hat{\mathbf{D}}_{01}\right|\right)\right]^2,\end{aligned} \tag{H.14}$$

with x denoting

$$x = -\frac{\hat{\mathbf{\Gamma}}_o}{\hat{\mathbf{\Gamma}}_s} - 1.$$

The subscript o is referring to the calibration open. To apply equation (H.14) it is necessary that short and open have well matched electrical lengths to keep the factor x

small. In addition it is necessary that both standards, open and short, have been characterized with the same VNA in the same calibration. Both criteria are usually met if both standards are from the same SOL calibration kit, which has been characterized as a whole by one laboratory. If this is the case, equation (H.14) should be used instead of (H.12).

For two-port measurements, the procedure has to be performed separately at port one and at port two to determine $\mathrm{u}(\delta\hat{\mathbf{E}}_{01}^{F})$ and $\mathrm{u}(\delta\hat{\mathbf{E}}_{32}^{R})$, respectively.

H.5.4 Transmission tracking and load match

These contributions are only relevant for two-port measurements.

In the case of SOLT calibration the measurement of the flush thru is used to relate the one-port error coefficients with the transmission tracking and load match coefficients. This interrelation is used to estimate the uncertainties associated with residual transmission tracking and residual load match. The forward and reverse residual two-port models are evaluated, assuming an ideal thru connection. This leads to the following relationships for the residual transmission tracking

$$\left[\mathrm{u}\left(\delta\hat{\mathbf{E}}_{32}^{F}\right)\right]^2 = \left[\mathrm{u}\left(\hat{\mathbf{C}}_{32}\right)\right]^2 + \left[\mathrm{u}\left(\hat{\mathbf{L}}\right)\right]^2 + \left[\mathrm{u}\left(\hat{\mathbf{S}}_{21}^{t}\right)\right]^2 + \left[\mathrm{u}\left(\hat{\mathbf{D}}_{32}^{F}\right)\right]^2 \tag{H.15}$$

$$\left[\mathrm{u}\left(\delta\hat{\mathbf{E}}_{01}^{R}\right)\right]^2 = \left[\mathrm{u}\left(\hat{\mathbf{C}}_{23}\right)\right]^2 + \left[\mathrm{u}\left(\hat{\mathbf{L}}\right)\right]^2 + \left[\mathrm{u}\left(\hat{\mathbf{S}}_{12}^{t}\right)\right]^2 + \left[\mathrm{u}\left(\hat{\mathbf{D}}_{01}^{R}\right)\right]^2, \tag{H.16}$$

and for the residual load match

$$\left[\mathrm{u}\left(\delta\hat{\mathbf{E}}_{22}^{F}\right)\right]^2 = \left[\mathrm{u}\left(\delta\hat{\mathbf{E}}_{00}^{F}\right)\right]^2 + \left[\mathrm{u}\left(\hat{\mathbf{L}}\right)\right]^2 + \left[\mathrm{u}\left(\hat{\mathbf{C}}_{22}\right)\right]^2 + \left[\mathrm{u}\left(\hat{\mathbf{S}}_{11}^{t}\right)\right]^2 + \left[\mathrm{u}\left(\hat{\mathbf{D}}_{22}^{F}\right)\right]^2 \tag{H.17}$$

$$\left[\mathrm{u}\left(\delta\hat{\mathbf{E}}_{11}^{R}\right)\right]^2 = \left[\mathrm{u}\left(\delta\hat{\mathbf{E}}_{33}^{R}\right)\right]^2 + \left[\mathrm{u}\left(\hat{\mathbf{L}}\right)\right]^2 + \left[\mathrm{u}\left(\hat{\mathbf{C}}_{33}\right)\right]^2 + \left[\mathrm{u}\left(\hat{\mathbf{S}}_{22}^{t}\right)\right]^2 + \left[\mathrm{u}\left(\hat{\mathbf{D}}_{11}^{R}\right)\right]^2. \tag{H.18}$$

Uncertainties associated with estimates of $\delta\mathbf{E}_{00}^{F}$, $\delta\mathbf{E}_{33}^{R}$, $\mathbf{D}_{\mathrm{ij}}$, $\mathbf{D}_{\mathrm{ij}}^{R}$, $\mathbf{C}_{\mathrm{ij}}$ and $\mathbf{L}$ are determined as described in H.5.1, H.5.6, H.5.7 and H.5.8.

The terms $\mathrm{u}(\hat{\mathbf{S}}_{\mathrm{ij}}^{t})$ denote uncertainties associated with the estimates of the flush thru measurement during calibration. The size of the uncertainty is determined by the repeatability of the measurements. Several measurements of the flush thru have to be performed and statistically evaluated.

H.5.5 Isolation

This contribution only applies to two-port measurements. As discussed in 5.3.5 the effect might be of minor importance for coaxial measurements using a modern VNA. The effect might be masked by noise floor, which is already covered in H.5.9. If this is the case no separate uncertainty contribution needs to be specified. For all other cases refer to 5.3.5.

H.5.6 Drift

The uncertainties associated with the estimates of drifts of the error coefficients are determined by one of the procedures described in G.3. The uncertainty contributions

are added in quadrature to the corresponding uncertainties associated with the error coefficients, as determined in H.5.1, H.5.2, H.5.3 and H.5.4.

H.5.7 Test port cables

The measurement models (H.2) and (H.3) require the test port cables to be kept fixed on the port one side. Therefore there are only uncertainty contributions for two-port measurements. These contributions are determined by the procedure specified in G.4. The following relations apply.

$$\mathrm{u}\left(\hat{\mathbf{C}}_{32}\right) = \mathrm{u}\left(\hat{\mathbf{C}}_{23}\right) = \max\left(\mathrm{u}\left(\left|\hat{\mathbf{CA}}_T\right|\right), \mathrm{u}\left(\arg\left(\hat{\mathbf{CA}}_T\right)\right)\right)$$
$$\mathrm{u}\left(\hat{\mathbf{C}}_{22}\right) = \mathrm{u}\left(\hat{\mathbf{C}}_{33}\right) = \mathrm{u}\left(\hat{\mathbf{CA}}_R\right).$$

The procedures to assign uncertainties associated with the estimates of $|\mathbf{CA}_T|$, $\arg(\mathbf{CA}_T)$ and $\mathbf{CA}_R$ are given in G.4. For $\arg(\mathbf{CA}_T)$ the uncertainty needs to be expressed in radians.

H.5.8 Non-linearity

The uncertainty associated with the estimate of $\mathbf{L}$ is determined according to procedure G.2.

H.5.9 Repeatability

This uncertainty contribution includes all random effects related to the measurement of the DUT. It is generally dependent on the settings of the VNA, influencing noise floor and trace noise, and the connection between test port and DUT. It is possible to quote an uncertainty associated with the estimate of repeatability based on experience with DUTs of similar reflection and transmission coefficient and of similar type of construction. For this purpose pooled data can be analyzed according to the formalism and the advice given in C.5. Based on that approach, a value can be assigned to uncertainties associated with estimates of $\mathbf{R}_{\mathrm{Sij}}$. It is nevertheless always necessary to perform at least four measurements at different connector orientations to verify the quoted uncertainty, as pointed out in 8.8.

I Waveguide measurements

I.1 Introduction

The principles for evaluating VNA S-parameter measurements made in air-filled rectangular metallic waveguide are the same as for coaxial line. The measurements are affected by the same type of measurement errors, as discussed in section 5, and the same measurement models, as explained in appendix F, can be applied. With properly characterized calibration standards it is possible to use the Rigorous Method, see 7.1, to evaluate measurement uncertainties in the same way as it is done for coaxial measurements. The procedures to evaluate the basic uncertainty contributions, as presented in appendix G, might need some adjustments to accommodate setup and limitations specific to waveguide measurements.

This appendix gives a procedure for evaluating uncertainties following the principles of the Ripple Method described for the coaxial case in 7.2 and appendix H. The procedure is expected to be applicable to measurements made at frequencies up to 110 GHz, or thereabouts, where mismatches due to the dimensional tolerances of the waveguide apertures and flanges are likely to be relatively small. At frequencies above 110 GHz, where the dimensions of the waveguide become relatively small and alignment of the waveguide becomes more challenging, the procedure may need to be modified.

I.2 Equipment

I.2.1 VNA test ports

In order to make measurements in waveguide, the VNA needs to be configured so that it has waveguide test ports of the correct aperture size and flange type for the required measurements. Depending on the type of VNA, there are two ways to achieve this:

- Using coaxial cables and/or adapters to transform from coaxial tests ports found either on the front panel of the VNA or on external coaxial Extender Heads (e.g. as often used for 1 mm coaxial connector VNA test ports).
- Using external waveguide Extender Heads (also sometimes called Converters), which are typically available at frequencies from 40 GHz to 110 GHz (and above).

In both cases, it is very important that the waveguide test ports consist of good quality waveguide that is in good condition.

I.2.2 Calibration kits

At least one calibration kit is required for each waveguide size and flange type. It is important that the standards in the calibration kit can be defined in the VNA. This is often achieved using calibration kit definitions data (usually made available on digital media such as disks or memory sticks) supplied by the calibration kit manufacturer. Details of the types of calibration, and the components used for each type, are found in I.3.

I.2.3 Components

There are three types of components needed to evaluate the uncertainty in VNA measurements using the Ripple Method in waveguide. These are described below.

At least one well-matched precision waveguide line is needed for each waveguide size and flange type. These sections of waveguide are analogous with the beadless reference air-dielectric lines used for the Ripple Method in coaxial line, see H.3. The waveguide line is used for performing 'ripple' assessments of two post-calibration VNA residual error terms: directivity (analogous with H.5.1 for coaxial line) and source match (analogous with H.5.2 for coaxial line). The flange alignment and aperture dimensions of the waveguide line should be taken into account, as part of the uncertainty assessment. This is analogous with the allowance for connector interfaces and characteristic impedance of a beadless coaxial air-dielectric line as described in H.5.1.2 and H.5.1.3, respectively. For waveguide, the tolerances on the flange alignment mechanisms should be taken into account and these should be used to calculate the worst-case magnitude of the linear reflection coefficient (e.g. using [71, 72]). This is similar to the evaluation of $\mathbf{\Gamma}_{\mathrm{CO}}$ in H.5.1.2, for coaxial line. In addition, the dimensions of the height and width of the waveguide aperture should be measured mechanically and departures from nominal dimensions should be used to calculate the magnitude of the linear reflection coefficient, with uncertainty (e.g. using [71, 72]), analogous with $\mathbf{\Gamma}_{\mathrm{AL}}$ in H.5.1.3, for coaxial line. These values of reflection coefficient should be used as part of the uncertainty budget for the VNA's reflection measurements in the same way as used for coaxial measurements, analogous with equations (H.9) and (H.10).

Attenuation devices can be used to assess the non-linearity of the VNA test set (following the procedure given in 5.3.3). In the case where the VNA test set is (or the Extender Heads are) fitted with coaxial connectors, the non-linearity assessment can be performed in the usual way, using coaxial attenuation devices (including step attenuation devices). In which case, no waveguide attenuation devices are needed. For waveguide Extender Heads (that are not assessed using coaxial attenuation devices), it is important that the non-linearity of the Extender Heads is assessed and so it is usual to use waveguide attenuation devices for this purpose. These attenuation devices can either be fixed (or switched) attenuation devices, or variable attenuation devices that can be set to fixed values, e.g. Rotary Vane Attenuation devices or Waveguide Below Cut-Off (WBCO) attenuation devices. At millimeter-wave frequencies, another possible means of realizing fixed values of attenuation is through the use of a cross-connected section of a waveguide [73] (also known as highly reflective devices [74]). These devices may be available from some waveguide manufacturers.

It is recommended that at least one verification kit is used for each waveguide size and flange type, for the purposes of verification, see section 4. Manufacturers' verification kits usually contain:

- A well-matched precision waveguide line;
- A mismatched precision waveguide line. The mismatch is often produced by including a section of reduced-height waveguide within the device;
- Two fixed attenuation devices of typically 20 dB, and, 40 dB or 50 dB.

The well-matched precision waveguide line in the verification kit can also be used as the precision waveguide line used for the ‘ripple’ assessments. The two fixed attenuation devices can also be used as part of the set used for the non-linearity assessment, if the non-linearity assessment is being performed using waveguide attenuation devices.

I.3 Calibration

I.3.1 SSL calibration

A common one-port calibration technique is the flush-short / offset-short / well-matched load technique. This is sometimes called the SSL calibration technique (short-short-load).

The SSL calibration technique is analogous with the SOL (short-open-load) calibration technique that is used frequently in coaxial line. Sometimes, the SSL calibration is implemented using two offset-shorts (i.e. by using a second offset-short in place of the flush-short). This works well as long as the phases of the reflection coefficients produced by the offset-shorts do not coincide with each other at any frequency across the waveguide band.

SSL calibrations can be extended to two-port calibrations by applying a SSL calibration to each of the VNA’s two test ports followed by a Thru connection (made by joining the two waveguide tests ports together). This produces a SSLT calibration (short-short-load-thru).

I.3.2 TRL calibration

A common two-port calibration technique in waveguide is the thru-reflect-line (TRL) technique [48].

The TRL calibration technique is usually implemented using a length of precision waveguide line that is approximately a 1/4 wavelength long around the mid-band frequency of the waveguide. This line is called the line standard. The line standard will then produce an adequate phase change with respect to the thru standard across the full waveguide band. The reflect standard is usually produced using a flush-short, although other devices can be used (e.g. an offset-short).

Sometimes, at millimeter-wave frequencies (i.e. above 30 GHz), the LRL (line-reflect-line) technique [45] is used in place of the TRL technique (i.e. by using a second line in place of the thru). This works well if the phase difference between the two LRL line standards is approximately a 1/4 wavelength (i.e. 90°) around the mid-band frequency of the waveguide. This technique is useful as it can avoid the need to use very short lengths of line at high frequencies (where the wavelength is relatively short, so a 1/4 wavelength line can be very short and hence can be damaged easily).

Another method of avoiding the need to use short (1/4 wavelength) TRL line standards at millimeter-wave frequencies is to use 3/4 wavelength TRL lines. However, this requires the use of two separate 3/4 wavelength Line standards (in conjunction with the thru standard) in order to cover the full frequency range of the waveguide band. More details about using 3/4 wavelength line standards for TRL calibrations is given in [75].

I.4 Uncertainty Evaluation

The procedure for evaluating uncertainty in waveguide VNA measurements using the Ripple Method is very similar to the procedure in coaxial line, as explained in appendix H. Equations to determine the uncertainties associated with estimates of S-parameters of a DUT are as in the coaxial case (H.2) and (H.4).

I.4.1 Ripple Assessments

To evaluate the residual directivity, a 'ripple' assessment is performed using the precision waveguide line referred to in I.2.3, terminated with a low-reflecting load. The load should provide a reflection coefficient with linear magnitude typically in the range 0.1 to 0.2.

An example residual directivity 'ripple' trace obtained for X-band waveguide (8.2 GHz to 12.4 GHz) is shown in figure I.1. This is analogous to the ripple trace shown in figure H.1 for coaxial line.

To evaluate the residual source match, a 'ripple' assessment is performed using the precision waveguide line referred to in I.2.3, terminated with a short (or offset-short).

An example residual source match 'ripple' trace obtained for X-band waveguide is shown in figure I.2. This is analogous to the ripple trace shown in figure H.3 for coaxial line.

I.4.2 Other uncertainty components

The evaluation of the other components to the uncertainty in measurements of waveguide devices should follow the same techniques given for measurements of coaxial devices, as described in sub-sections of H.5.

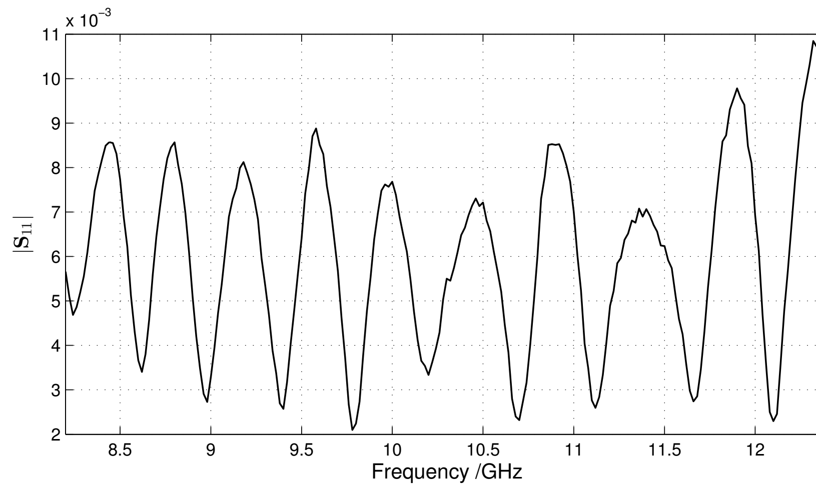

Figure I.1: Example of a residual directivity 'ripple' trace obtained from a VNA calibration in X-band waveguide (operating from 8.2 GHz to 12.4 GHz).

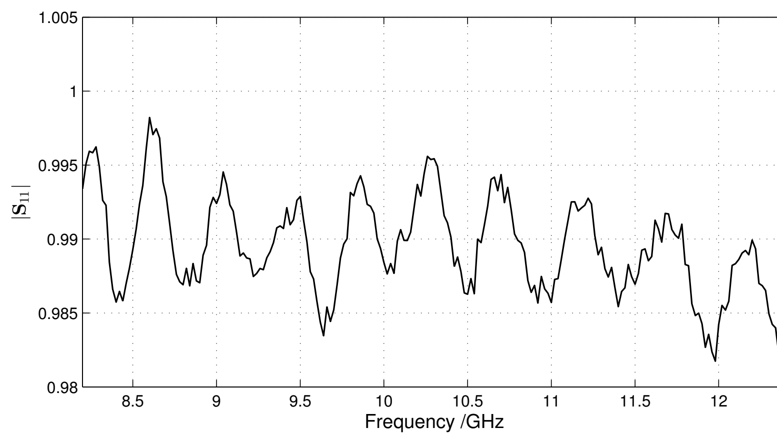

Figure I.2: Example of a residual source match 'ripple' trace obtained from a VNA calibration in X-band waveguide (operating from 8.2 GHz to 12.4 GHz).

J Examples

The following examples are based on measurements of one-port and two-port DUTs in the Type-N line system. The VNA has been calibrated with an SOLT scheme, using the definitions provided by the manufacturer of the calibration kit. The setup was such that test port one was kept fixed during all measurements. Therefore cable movements only occurred during two-port measurements and did not affect the results of the one-port DUTs. See as well 8.5.1 in that respect. The application of the Ripple Method requires one port to be kept fixed as explained in H.4.1 and H.4.2. The following DUTs have been measured: matched load, mismatch, short, adapter, 20 dB and 50 dB attenuation device. Uncertainties have been evaluated with rigorous uncertainty propagation through a measurement model, according to 7.1, and the Ripple Method, according to 7.2.

For the rigorous uncertainty propagation the software VNA Tools [19] has been used. The uncertainties assigned to the calibration standards are based on manufacturer specifications. The other uncertainty contributions were determined according to the procedures in appendix G. The measurement model is very similar to the 10-term model shown in appendix F. Details of the actual measurement model being used can be found in the documentation [19]. The uncertainty contributions are propagated to the DUT results using linear uncertainty propagation. The results below show measurement uncertainty intervals for single components of the complex quantities. However, the method also evaluates the correlation between S-parameters as well as the inter frequency correlations, but this is not shown.

For the Ripple Method a 30 cm long beadless air-dielectric line was used together with a matched load and a short. The center conductors showed a recession of -67.8 μm (still within IEEE specifications [65]) for the test port, -4.8 μm for the air-dielectric line and -2.5 μm for the matched load. The short had a slight protrusion of +2.8 μm. The separate sums of these values for the configurations with the matched load and with the short are needed to evaluate uncertainty contributions of directivity and source match according to equation (H.5). That calculation leads to $d_{pg} = 75.1\,\mu$m for the matched load and $d_{pg} = 69.8\,\mu$m for the short. The uncertainty associated with a single measurement of the pin depth is 3.8 μm. Adding three measurements and assuming full correlation leads to $\mathrm{u}(d_{pg}) = 11.4\,\mu$m, which is needed in equation (H.6). Figure J.1 illustrates four measurements of the ripple pattern taken with the matched load. Only the longitudinal position of the center conductor of the air-dielectric line was varied, using the whole available space. The two extreme positions were achieved by pushing the inner conductor onto the test port and onto the load before making the connection. The two other positions were achieved with the help of dielectric spacers. This illustrates the effect of the connector interfaces on the ripple pattern. The blue trace in figure J.1 has been used later in the examples to determine the uncertainty associated with residual directivity.

The uncertainties associated with the DUT are evaluated according to the procedure described in appendix H. The uncertainties quoted in the examples are all standard uncertainties ($k = 1$). The examples show results for $\mathbf{S}_{11}$ for the one-port devices and $\mathbf{S}_{22}$ and $\mathbf{S}_{12}$ for the two-port devices. The results are representative of $\mathbf{S}_{11}$ and $\mathbf{S}_{21}$ as

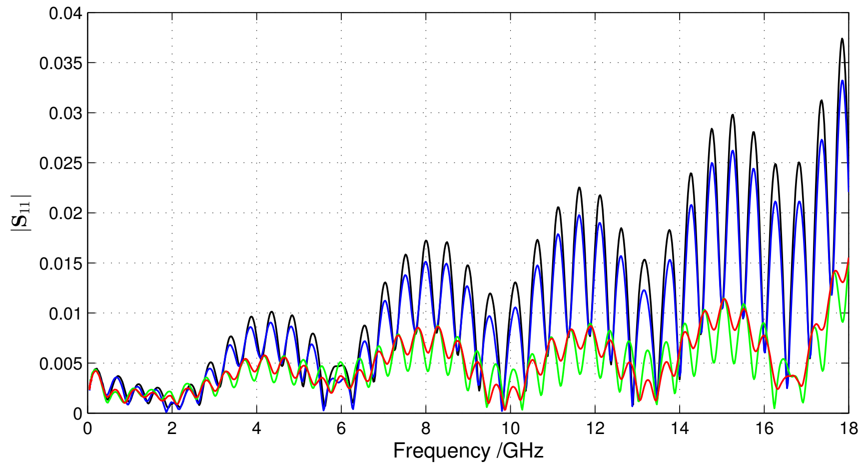

Figure J.1: Four different ripple patterns in the Type-N line system. All four traces were taken with a 30 cm beadless air-dielectric line terminated with a matched load. The differences are due to different longitudinal positions of the center conductor of the air-dielectric line. See also H.5.1.2

well. Results are expressed either in real and imaginary components, for low reflection coefficients, or magnitude and phase, for the other cases. The magnitude of the transmission coefficient is displayed in logarithmic units. The results are shown graphically over the whole frequency range. For three selected frequencies, uncertainty budgets are shown in tabular form. The uncertainty budget of the Ripple Method quotes a single uncertainty $\mathrm{u}(\mathbf{S}_{\mathrm{ij}}) = \mathrm{u}(\mathrm{Re}[\mathbf{S}_{\mathrm{ij}}]) = \mathrm{u}(\mathrm{Im}[\mathbf{S}_{\mathrm{ij}}])$, as explained in H.2. The uncertainties associated with magnitude and phase are derived using linear uncertainty propagation

$$\mathrm{u}(|\mathbf{S}_{\mathrm{ij}}|) = \mathrm{u}(\mathbf{S}_{\mathrm{ij}})$$
$$\mathrm{u}(\arg(\mathbf{S}_{\mathrm{ij}})) = \frac{\mathrm{u}(\mathbf{S}_{\mathrm{ij}})}{|\mathbf{S}_{\mathrm{ij}}|}.$$

The transformation between linear and logarithmic units is also done using linear uncertainty propagation

$$X_{\mathrm{log}} = 20\log_{10} X_{\mathrm{lin}} \longrightarrow \mathrm{u}(X_{\mathrm{log}}) = \frac{20}{\log_e 10}\frac{\mathrm{u}(X_{\mathrm{lin}})}{X_{\mathrm{lin}}} \simeq 8.686\frac{\mathrm{u}(X_{\mathrm{lin}})}{X_{\mathrm{lin}}}$$
$$X_{\mathrm{lin}} = 10^{\frac{X_{\mathrm{log}}}{20}} \longrightarrow \frac{\mathrm{u}(X_{\mathrm{lin}})}{X_{\mathrm{lin}}} = \frac{\log_e 10}{20}\mathrm{u}(X_{\mathrm{log}}) \simeq 0.1151\mathrm{u}(X_{\mathrm{log}})\,.$$

The numerical values of the uncertainty contributions in these examples should not be taken as generally representative. E.g. the uncertainty associated with the repeatability of the DUT measurements is very small in these examples. Such uncertainties can only be achieved with appropriate device settings, a well controlled measurement process and stable environmental conditions. It is necessary to individually characterize the uncertainty contributions for the specific measurement setups. This can also be

combined with experience and other sources of information, as e.g. manufacturer specifications, if available. For contributions that are not dominant, a conservatively large uncertainty value might be assigned without affecting the final combined uncertainty too much. This way it is possible to reduce the characterization effort.

J.1 One-port matched load

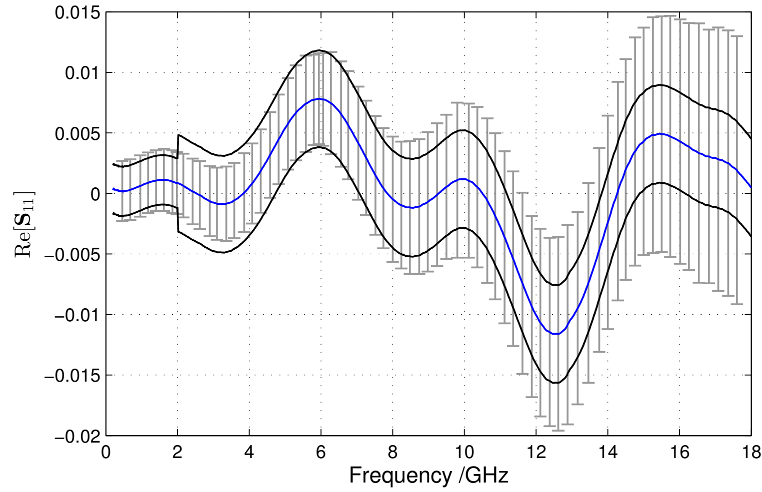

Figure J.2: Real component of the reflection coefficient of a matched load with associated standard uncertainties. The solid lines indicate the error corrected measurement data (center line) bounded by the interval of one standard uncertainty ($k = 1$) calculated with the rigorous method. The step in uncertainty at 2 GHz is due to the change from low band load to sliding load. The vertical bars indicate standard uncertainties evaluated with the Ripple Method.

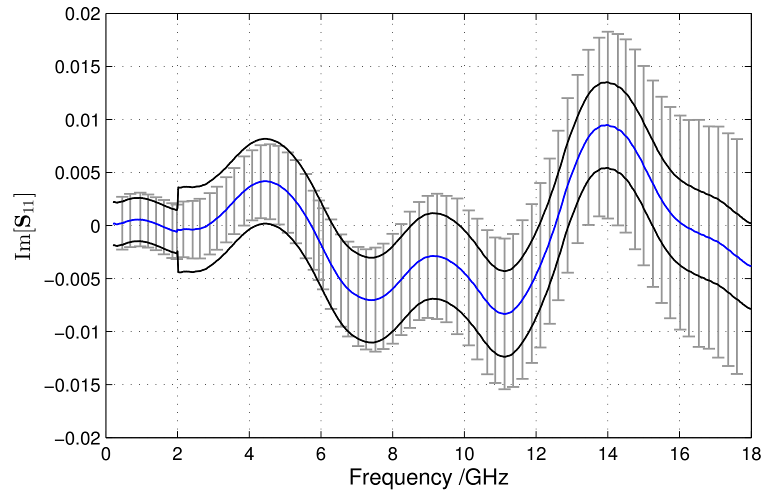

Figure J.3: The same as figure J.2 but for the imaginary component of the reflection coefficient.

Table J.1: Uncertainty budget of $\mathrm{Re}\,[\mathbf{S}_{11}]$ of a matched load at three different frequencies. The standard uncertainty is evaluated with the rigorous method.

Contribution	0.460 GHz	8.480 GHz	17.600 GHz
Cal Load	0.00200	0.00398	0.00398
Cal Open	0.00000	0.00004	0.00005
Cal Short	0.00000	0.00004	0.00005
Conn. Rep.	0.00045	0.00071	0.00071
VNA Drift	0.00002	0.00004	0.00004
VNA Linearity	0.00001	0.00003	0.00009
VNA Noise	0.00002	0.00001	0.00002
Combined	0.00205	0.00404	0.00404

Table J.2: The same as table J.1 but for $\mathrm{Im}\,[\mathbf{S}_{11}]$

Contribution	0.460 GHz	8.480 GHz	17.600 GHz
Cal Load	0.00200	0.00398	0.00398
Cal Open	0.00000	0.00004	0.00005
Cal Short	0.00000	0.00004	0.00005
Conn. Rep.	0.00045	0.00071	0.00071
VNA Drift	0.00002	0.00004	0.00004
VNA Linearity	0.00001	0.00003	0.00008
VNA Noise	0.00002	0.00001	0.00002
Combined	0.00205	0.00404	0.00404

Table J.3: Uncertainty budget of S_{11} of a matched load at three different frequencies. The standard uncertainty is evaluated with the Ripple Method. The terms in column 2 refer to equation (H.2) and the corresponding values in the subsequent columns have to be added accordingly for the combined standard uncertainty.

Name	Uncertainty contribution	0.460 GHz	8.480 GHz	17.600 GHz
Directivity	$\mathrm{u}(\delta\hat{\mathbf{E}}_{00})$	0.00228	0.00540	0.01103
Reflection tracking	$\lvert\hat{\mathbf{S}}^{c}_{11}\rvert\mathrm{u}(\delta\hat{\mathbf{E}}_{01})$	0.00001	0.00007	0.00009
Source match	$\lvert\hat{\mathbf{S}}^{c}_{11}\rvert^{2}\mathrm{u}(\delta\hat{\mathbf{E}}_{11})$	0.00001	0.00001	0.00001
Linearity	$\lvert\hat{\mathbf{S}}^{c}_{11}\rvert\mathrm{u}(\hat{\mathbf{L}})$	0.00001	0.00001	0.00001
Repeatability	$\mathrm{u}(\hat{\mathbf{R}}_{\mathrm{S}11})$	0.00100	0.00100	0.00100
Combined uncertainty	$\mathrm{u}(\hat{\mathbf{S}}_{11})$	0.00249	0.00549	0.01107

J.2 One-port mismatch

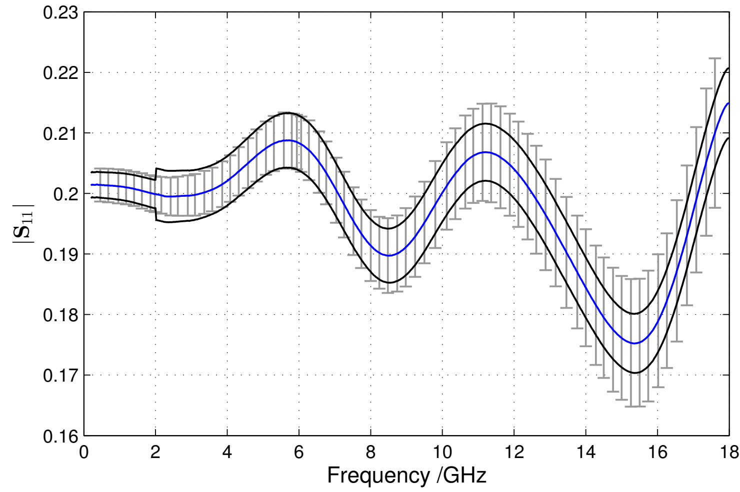

Figure J.4: Magnitude of the reflection coefficient of a mismatch with associated standard uncertainties. The solid lines indicate the error corrected measurement data (center line) bounded by the interval of one standard uncertainty ($k = 1$) calculated with the rigorous method. The step in uncertainty at 2 GHz is due to the change from low band load to sliding load. The vertical bars indicate standard uncertainties evaluated with the Ripple Method.

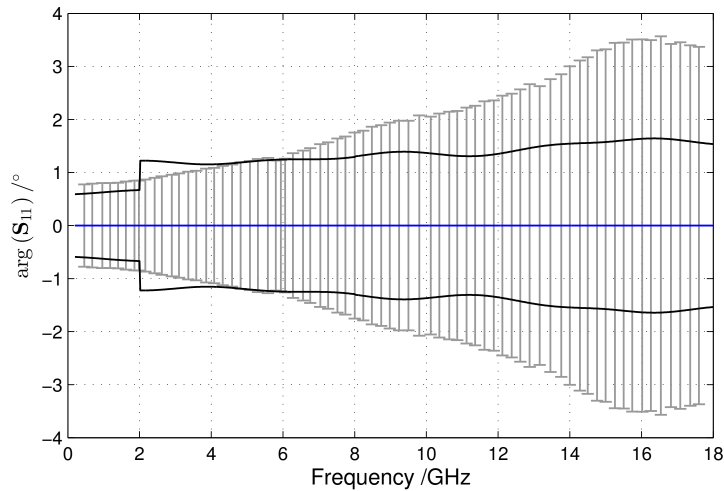

Figure J.5: The same as figure J.4 but for the phase of the reflection coefficient. For better visibility the error corrected measurement has been normalized to 0 and only the standard uncertainties are shown.

Table J.4: Uncertainty budget of $|\mathrm{S}_{11}|$ of a mismatch at three different frequencies. The standard uncertainty is evaluated with the rigorous method.

Contribution	0.460 GHz	8.480 GHz	17.600 GHz
Cal Load	0.00194	0.00393	0.00411
Cal Open	0.00041	0.00119	0.00310
Cal Short	0.00060	0.00162	0.00244
Conn. Rep.	0.00045	0.00071	0.00073
VNA Drift	0.00003	0.00003	0.00003
VNA Linearity	0.00016	0.00013	0.00017
VNA Noise	0.00003	0.00002	0.00003
Combined	0.00212	0.00446	0.00574

Table J.5: The same as table J.4 but for $\arg(\mathbf{S}_{11})$

Contribution	0.460 GHz	8.480 GHz	17.600 GHz
Cal Load	0.5493 deg	1.1839 deg	1.1198 deg
Cal Open	0.1148 deg	0.3568 deg	0.8434 deg
Cal Short	0.1679 deg	0.4868 deg	0.6656 deg
Conn. Rep.	0.1265 deg	0.2142 deg	0.1985 deg
VNA Drift	0.0081 deg	0.0064 deg	0.0064 deg
VNA Linearity	0.0394 deg	0.0332 deg	0.0396 deg
VNA Noise	0.0054 deg	0.0032 deg	0.0075 deg
Combined	0.6006 deg	1.3464 deg	1.5650 deg

Table J.6: Uncertainty budget of S_{11} of a mismatch at three different frequencies. The standard uncertainty is evaluated with the Ripple method. The terms in column 2 refer to equation (H.2) and the corresponding values in the subsequent columns have to be added accordingly for the combined standard uncertainty.

Name	Uncertainty contribution	0.460 GHz	8.480 GHz	17.600 GHz
Directivity	$\mathrm{u}(\delta\hat{\mathbf{E}}_{00})$	0.00228	0.00540	0.01103
Reflection tracking	$\lvert\hat{\mathbf{S}}_{11}^{c}\rvert\mathrm{u}(\delta\hat{\mathbf{E}}_{01})$	0.00103	0.00279	0.00541
Source match	$\lvert\hat{\mathbf{S}}_{11}^{c}\rvert^{2}\mathrm{u}(\delta\hat{\mathbf{E}}_{11})$	0.00042	0.00043	0.00081
Linearity	$\lvert\hat{\mathbf{S}}_{11}^{c}\rvert\mathrm{u}(\hat{\mathbf{L}})$	0.00027	0.00025	0.00028
Repeatability	$\mathrm{u}(\hat{\mathbf{R}}_{\mathrm{S11}})$	0.00100	0.00100	0.00100
Combined uncertainty	$\mathrm{u}(\hat{\mathbf{S}}_{11})$	0.00274	0.00618	0.01235

J.3 One-port short

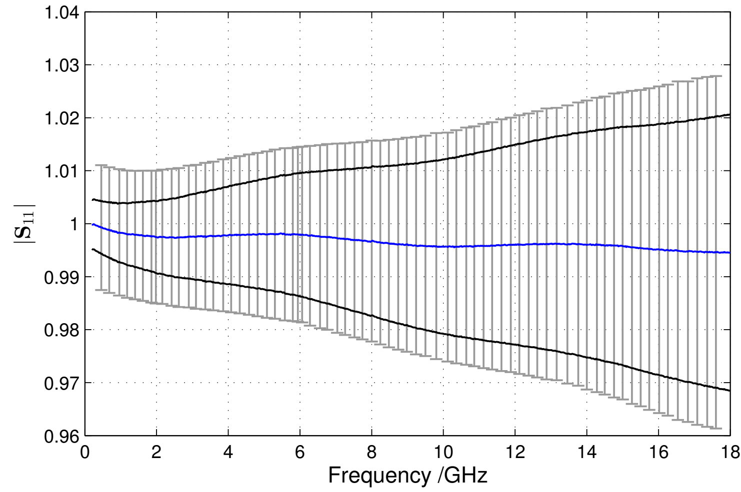

Figure J.6: Magnitude of the reflection coefficient of a short with associated standard uncertainties. The solid lines indicate the error corrected measurement data (center line) bounded by the interval of one standard uncertainty ($k = 1$) calculated with the rigorous method. The vertical bars indicate standard uncertainties evaluated with the Ripple Method.

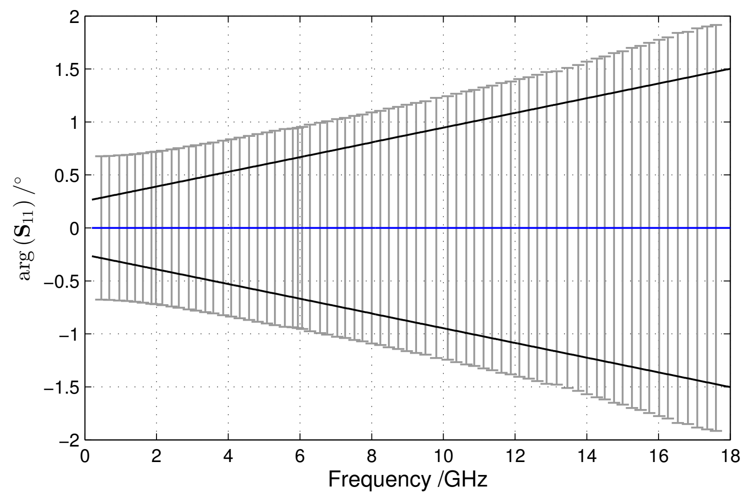

Figure J.7: The same as figure J.6 but for the phase of the reflection coefficient. For better visibility the error corrected measurement has been normalized to 0 and only the standard uncertainties are shown.

Table J.7: Uncertainty budget of $|S_{11}|$ of a short at three different frequencies. The standard uncertainty is evaluated with the rigorous method.

Contribution	0.460 GHz	8.480 GHz	17.600 GHz
Cal Load	0.00001	0.00002	0.00004
Cal Open	0.00001	0.00002	0.00006
Cal Short	0.00493	0.01460	0.02558
Conn. Rep.	0.00064	0.00100	0.00100
VNA Drift	0.00008	0.00008	0.00008
VNA Linearity	0.00036	0.00000	0.00000
VNA Noise	0.00012	0.00011	0.00014
Combined	0.00498	0.01463	0.02560

Table J.8: The same as table J.7 but for $\arg(\mathbf{S}_{11})$

Contribution	0.460 GHz	8.480 GHz	17.600 GHz
Cal Load	0.0003 deg	0.0006 deg	0.0019 deg
Cal Open	0.0002 deg	0.0006 deg	0.0031 deg
Cal Short	0.2821 deg	0.8392 deg	1.4731 deg
Conn. Rep.	0.0362 deg	0.0573 deg	0.0573 deg
VNA Drift	0.0042 deg	0.0041 deg	0.0040 deg
VNA Linearity	0.0187 deg	0.0000 deg	0.0000 deg
VNA Noise	0.0020 deg	0.0036 deg	0.0094 deg
Combined	0.2851 deg	0.8411 deg	1.4743 deg

Table J.9: Uncertainty budget of S_{11} of a short at three different frequencies. The standard uncertainty is evaluated with the Ripple method. The terms in column 2 refer to equation (H.2) and the corresponding values in the subsequent columns have to be added accordingly for the combined standard uncertainty.

Name	Uncertainty contribution	0.460 GHz	8.480 GHz	17.600 GHz
Directivity	$\mathrm{u}(\delta\hat{\mathbf{E}}_{00})$	0.00228	0.00540	0.01103
Reflection tracking	$\lvert\hat{\mathbf{S}}^{c}_{11}\rvert\mathrm{u}(\delta\hat{\mathbf{E}}_{01})$	0.00509	0.01465	0.02562
Source match	$\lvert\hat{\mathbf{S}}^{c}_{11}\rvert^{2}\mathrm{u}(\delta\hat{\mathbf{E}}_{11})$	0.01026	0.01172	0.01807
Linearity	$\lvert\hat{\mathbf{S}}^{c}_{11}\rvert\mathrm{u}(\hat{\mathbf{L}})$	0.00130	0.00130	0.00130
Repeatability	$\mathrm{u}(\hat{\mathbf{R}}_{S11})$	0.00100	0.00100	0.00100
Combined uncertainty	$\mathrm{u}(\hat{\mathbf{S}}_{11})$	0.01179	0.01959	0.03327

J.4 Two-port Adapter

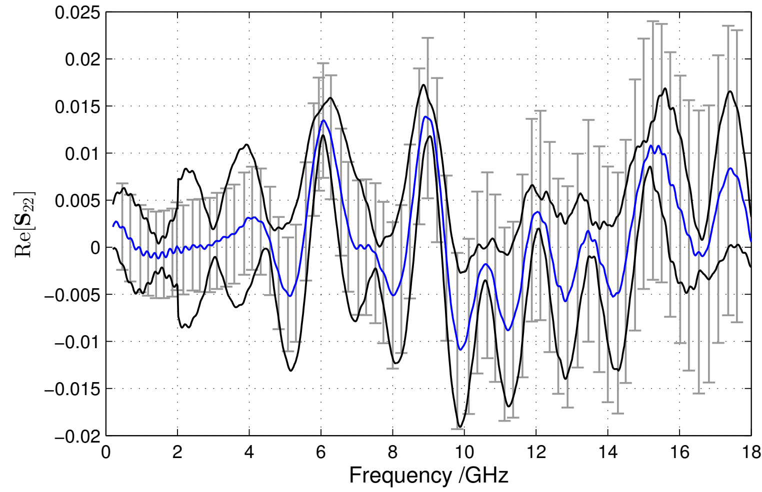

Figure J.8: Real component of the reflection coefficient of an adapter with associated standard uncertainties. The solid lines indicate the error corrected measurement data (center line) bounded by the interval of one standard uncertainty ($k = 1$) calculated with the rigorous method. The step in uncertainty at 2 GHz is due to the change from low band load to sliding load. The vertical bars indicate standard uncertainties evaluated with the Ripple Method.

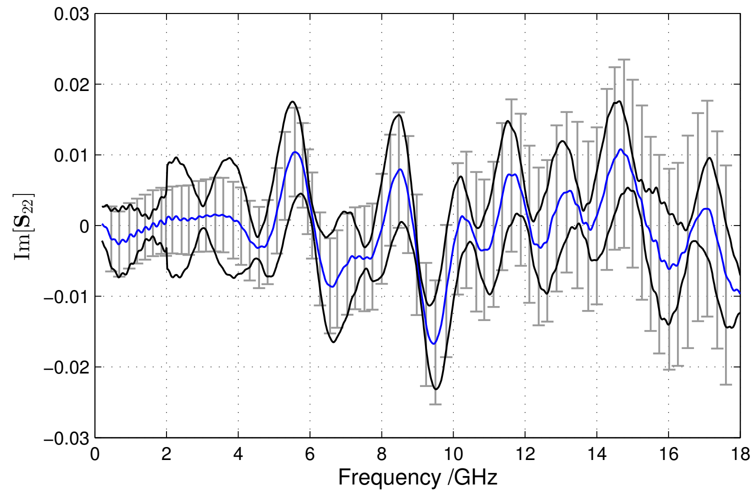

Figure J.9: The same as figure J.8 but for the imaginary component of the reflection coefficient.

Table J.10: Uncertainty budget of $\mathrm{Re}\left[\mathbf{S}_{22}\right]$ of an adapter at three different frequencies. The standard uncertainty is evaluated with the rigorous method.

Contribution	0.460 GHz	8.480 GHz	17.600 GHz
Cal Load	0.00326	0.00732	0.00684
Cal Open	0.00001	0.00006	0.00014
Cal Short	0.00001	0.00007	0.00014
Conn. Rep.	0.00082	0.00135	0.00129
Cable	0.00216	0.00231	0.00221
VNA Drift	0.00015	0.00016	0.00015
VNA Linearity	0.00002	0.00004	0.00013
VNA Noise	0.00003	0.00001	0.00003
Combined	0.00399	0.00779	0.00731

Table J.11: The same as table J.10 but for $\mathrm{Im}\left[\mathbf{S}_{22}\right]$

Contribution	0.460 GHz	8.480 GHz	17.600 GHz
Cal Load	0.00326	0.00732	0.00684
Cal Open	0.00001	0.00006	0.00014
Cal Short	0.00001	0.00007	0.00014
Conn. Rep.	0.00082	0.00135	0.00129
Cable	0.00216	0.00231	0.00221
VNA Drift	0.00015	0.00016	0.00015
VNA Linearity	0.00002	0.00005	0.00013
VNA Noise	0.00003	0.00001	0.00003
Combined	0.00399	0.00779	0.00731

Table J.12: Uncertainty budget of S_{22} of an adapter at three different frequencies. The standard uncertainty is evaluated with the Ripple Method. The terms in column 2 refer to equation (H.3) and the corresponding values in the subsequent columns have to be added accordingly for the combined standard uncertainty.

Name	Uncertainty contribution	0.460 GHz	8.480 GHz	17.600 GHz
Directivity	$\mathrm{u}(\delta\hat{\mathbf{E}}_{33}^{R})$	0.00228	0.00540	0.01103
Reflection tracking	$\lvert\hat{\mathbf{S}}_{22}^{c}\rvert\mathrm{u}(\delta\hat{\mathbf{E}}_{32}^{R})$	0.00002	0.00013	0.00027
Source match	$\lvert\hat{\mathbf{S}}_{22}^{c}\rvert^{2}\mathrm{u}(\delta\hat{\mathbf{E}}_{22}^{R})$	0.00001	0.00001	0.00001
Load match	$\lvert\hat{\mathbf{S}}_{21}^{c}\hat{\mathbf{S}}_{12}^{c}\rvert\mathrm{u}(\delta\hat{\mathbf{E}}_{11}^{R})$	0.00331	0.00572	0.01067
Linearity	$\lvert\hat{\mathbf{S}}_{22}^{c}\rvert\mathrm{u}(\hat{\mathbf{L}})$	0.00001	0.00002	0.00002
Cable transmission	$\lvert\hat{\mathbf{S}}_{22}^{c}\rvert\mathrm{u}(\hat{\mathbf{C}}_{32})$	0.00001	0.00005	0.00009
Cable transmission	$\lvert\hat{\mathbf{S}}_{22}^{c}\rvert\mathrm{u}(\hat{\mathbf{C}}_{23})$	0.00001	0.00005	0.00009
Cable reflection	$\lvert\hat{\mathbf{S}}_{22}^{c}\rvert^{2}\mathrm{u}(\hat{\mathbf{C}}_{22})$	0.00001	0.00001	0.00001
Cable reflection	$\mathrm{u}(\hat{\mathbf{C}}_{33})$	0.00200	0.00200	0.00200
Repeatability	$\mathrm{u}(\hat{\mathbf{R}}_{\mathrm{S22}})$	0.00100	0.00100	0.00100
Combined uncertainty	$\mathrm{u}(\hat{\mathbf{S}}_{22})$	0.00460	0.00817	0.01551

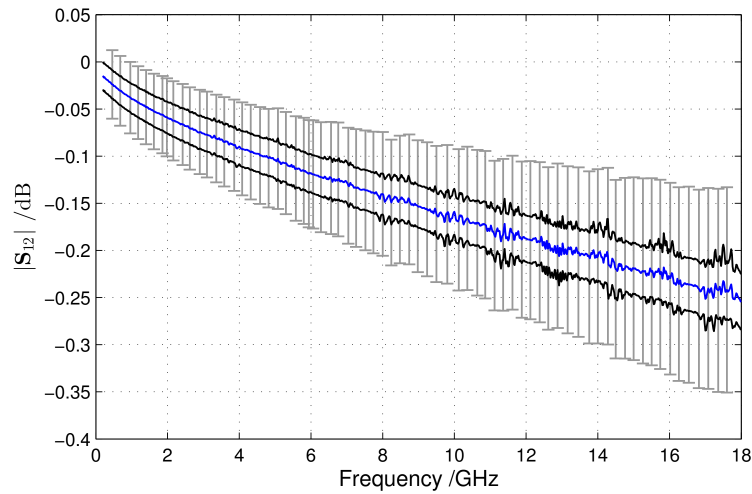

Figure J.10: Magnitude of the transmission coefficient of an adapter with associated standard uncertainties. The solid lines indicate the error corrected measurement data (center line) bounded by the interval of one standard uncertainty ($k = 1$) calculated with the rigorous method. The vertical bars indicate standard uncertainties evaluated with the Ripple Method.

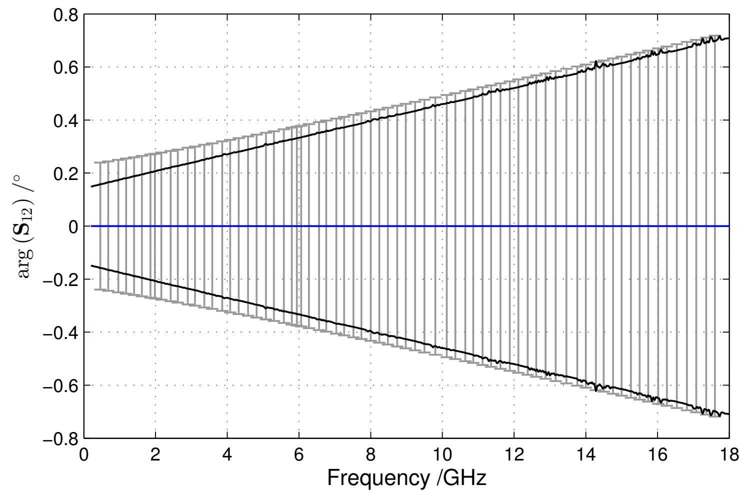

Figure J.11: The same as figure J.10 but for the phase of the transmission coefficient. For better visibility the error corrected measurement has been normalized to 0 and only the standard uncertainties are shown.

Table J.13: Uncertainty budget of $|S_{12}|$ of an adapter at three different frequencies. The standard uncertainty is evaluated with the rigorous method.

Contribution	0.460 GHz	8.480 GHz	17.600 GHz
Cal Load	0.0007 dB	0.0026 dB	0.0028 dB
Cal Open	0.0006 dB	0.0035 dB	0.0072 dB
Cal Short	0.0006 dB	0.0035 dB	0.0071 dB
Conn. Rep.	0.0002 dB	0.0005 dB	0.0006 dB
Cable	0.0145 dB	0.0208 dB	0.0280 dB
VNA Drift	0.0010 dB	0.0010 dB	0.0010 dB
VNA Linearity	0.0032 dB	0.0071 dB	0.0071 dB
VNA Noise	0.0010 dB	0.0010 dB	0.0010 dB
Combined	0.0150 dB	0.0227 dB	0.0307 dB

Table J.14: The same as table J.13 but for $\arg(\mathbf{S}_{12})$

Contribution	0.460 GHz	8.480 GHz	17.600 GHz
Cal Load	0.0046 deg	0.0174 deg	0.0184 deg
Cal Open	0.0041 deg	0.0231 deg	0.0473 deg
Cal Short	0.0041 deg	0.0232 deg	0.0468 deg
Conn. Rep.	0.0012 deg	0.0034 deg	0.0037 deg
Cable	0.1559 deg	0.4079 deg	0.6944 deg
VNA Drift	0.0061 deg	0.0061 deg	0.0061 deg
VNA Linearity	0.0190 deg	0.0425 deg	0.0424 deg
VNA Noise	0.0020 deg	0.0037 deg	0.0081 deg
Combined	0.1573 deg	0.4118 deg	0.6992 deg

Table J.15: Uncertainty budget of S_{12} of an adapter at three different frequencies. The standard uncertainty is evaluated with the Ripple Method. The terms in column 2 refer to equation (H.4) and the corresponding values in the subsequent columns have to be added accordingly for the combined standard uncertainty.

Name	Uncertainty contribution	0.460 GHz	8.480 GHz	17.600 GHz
Source match	$\lvert\hat{\mathbf{S}}^c_{22}\hat{\mathbf{S}}^c_{12}\rvert \mathrm{u}(\delta\hat{\mathbf{E}}^R_{22})$	0.0003 dB	0.0009 dB	0.0017 dB
Load match	$\lvert\hat{\mathbf{S}}^c_{11}\hat{\mathbf{S}}^c_{12}\rvert \mathrm{u}(\delta\hat{\mathbf{E}}^R_{11})$	0.0001 dB	0.0005 dB	0.0010 dB
Transmission tracking	$\lvert\hat{\mathbf{S}}^c_{12}\rvert \mathrm{u}(\delta\hat{\mathbf{E}}^R_{01})$	0.0232 dB	0.0466 dB	0.0762 dB
Isolation	$\mathrm{u}(\delta\hat{\mathbf{E}}^R_{03})$	0.0001 dB	0.0001 dB	0.0001 dB
Linearity	$\lvert\hat{\mathbf{S}}^c_{12}\rvert \mathrm{u}(\hat{\mathbf{L}})$	0.0113 dB	0.0113 dB	0.0113 dB
Cable transmission	$\lvert\hat{\mathbf{S}}^c_{12}\rvert \mathrm{u}(\hat{\mathbf{C}}_{23})$	0.0168 dB	0.0438 dB	0.0745 dB
Cable reflection	$\lvert\hat{\mathbf{S}}^c_{12}\hat{\mathbf{S}}^c_{22}\rvert \mathrm{u}(\hat{\mathbf{C}}_{22})$	0.0001 dB	0.0002 dB	0.0002 dB
Repeatability	$\mathrm{u}(\hat{\mathbf{R}}_{S12})$	0.0087 dB	0.0087 dB	0.0087 dB
Raw load match	$\lvert\hat{\mathbf{S}}^c_{12}\hat{\mathbf{E}}^R_{11}(1-\hat{\mathbf{S}}^c_{21}\hat{\mathbf{S}}^c_{12})\rvert \mathrm{u}(\delta\hat{\mathbf{E}}^F_{00})$	0.0006 dB	0.0024 dB	0.0054 dB
Raw load match	$\lvert\hat{\mathbf{S}}^c_{12}\hat{\mathbf{E}}^R_{11}(1-\hat{\mathbf{S}}^c_{21}\hat{\mathbf{S}}^c_{12})\rvert \mathrm{u}(\delta\hat{\mathbf{E}}^R_{22})$	0.0025 dB	0.0052 dB	0.0088 dB
Combined uncertainty	$\mathrm{u}(\hat{\mathbf{S}}_{12})$	0.0364 dB	0.0678 dB	0.1089 dB

J.5 Two-port 20 dB attenuation device

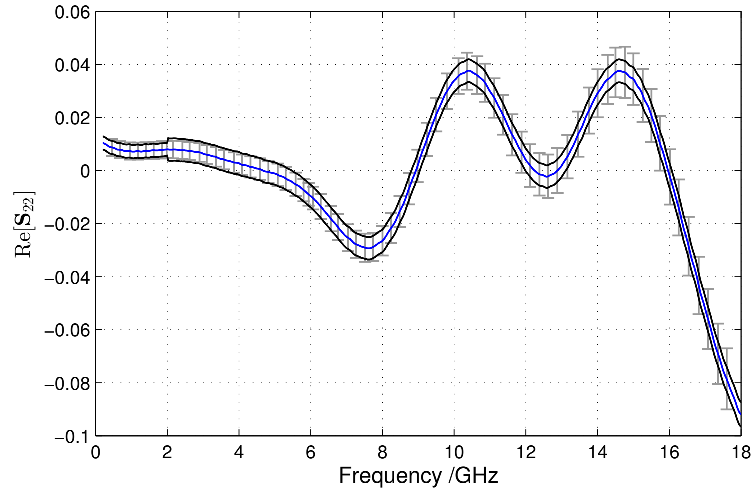

Figure J.12: Real component of the reflection coefficient of a 20 dB attenuation device with associated standard uncertainties. The solid lines indicate the error corrected measurement data (center line) bounded by the interval of one standard uncertainty ($k = 1$) calculated with the rigorous method. The step in uncertainty at 2 GHz is due to the change from low band load to sliding load. The vertical bars indicate standard uncertainties evaluated with the Ripple Method.

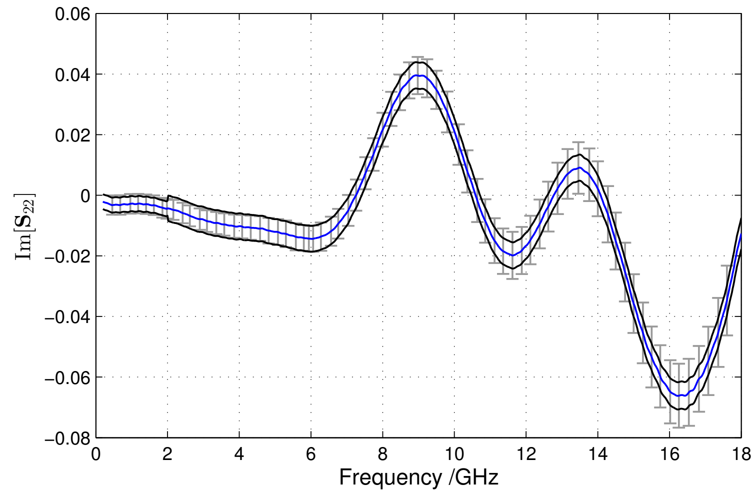

Figure J.13: The same as figure J.12 but for the imaginary component of the reflection coefficient.

Table J.16: Uncertainty budget of $\mathrm{Re}\,[\mathbf{S}_{22}]$ of a 20 dB attenuation device at three different frequencies. The standard uncertainty is evaluated with the rigorous method.

Contribution	0.460 GHz	8.480 GHz	17.600 GHz
Cal Load	0.00199	0.00400	0.00394
Cal Open	0.00003	0.00027	0.00114
Cal Short	0.00003	0.00029	0.00108
Conn. Rep.	0.00045	0.00071	0.00071
Cable	0.00141	0.00150	0.00172
VNA Drift	0.00009	0.00009	0.00010
VNA Linearity	0.00002	0.00002	0.00009
VNA Noise	0.00002	0.00001	0.00002
Combined	0.00248	0.00435	0.00463

Table J.17: The same as table J.16 but for $\mathrm{Im}\,[\mathbf{S}_{22}]$

Contribution	0.460 GHz	8.480 GHz	17.600 GHz
Cal Load	0.00199	0.00400	0.00394
Cal Open	0.00003	0.00027	0.00114
Cal Short	0.00003	0.00029	0.00108
Conn. Rep.	0.00045	0.00071	0.00071
Cable	0.00141	0.00145	0.00238
VNA Drift	0.00009	0.00009	0.00010
VNA Linearity	0.00002	0.00002	0.00008
VNA Noise	0.00002	0.00001	0.00002
Combined	0.00248	0.00433	0.00491

Table J.18: Uncertainty budget of S_{22} of a 20 dB attenuation device at three different frequencies. The standard uncertainty is evaluated with the Ripple Method. The terms in column 2 refer to equation (H.3) and the corresponding values in the subsequent columns have to be added accordingly for the combined standard uncertainty.

Name	Uncertainty contribution	0.460 GHz	8.480 GHz	17.600 GHz
Directivity	$\mathrm{u}(\delta\hat{\mathbf{E}}_{33}^{R})$	0.00228	0.00540	0.01103
Reflection tracking	$\lvert\hat{\mathbf{S}}_{22}^{c}\rvert\mathrm{u}(\delta\hat{\mathbf{E}}_{32}^{R})$	0.00005	0.00055	0.00222
Source match	$\lvert\hat{\mathbf{S}}_{22}^{c}\rvert^2\mathrm{u}(\delta\hat{\mathbf{E}}_{22}^{R})$	0.00001	0.00002	0.00014
Load match	$\lvert\hat{\mathbf{S}}_{21}^{c}\hat{\mathbf{S}}_{12}^{c}\rvert\mathrm{u}(\delta\hat{\mathbf{E}}_{11}^{R})$	0.00004	0.00006	0.00012
Linearity	$\lvert\hat{\mathbf{S}}_{22}^{c}\rvert\mathrm{u}(\hat{\mathbf{L}})$	0.00002	0.00005	0.00012
Cable transmission	$\lvert\hat{\mathbf{S}}_{22}^{c}\rvert\mathrm{u}(\hat{\mathbf{C}}_{32})$	0.00002	0.00019	0.00074
Cable transmission	$\lvert\hat{\mathbf{S}}_{22}^{c}\rvert\mathrm{u}(\hat{\mathbf{C}}_{23})$	0.00002	0.00019	0.00074
Cable reflection	$\lvert\hat{\mathbf{S}}_{22}^{c}\rvert^2\mathrm{u}(\hat{\mathbf{C}}_{22})$	0.00001	0.00001	0.00002
Cable reflection	$\mathrm{u}(\hat{\mathbf{C}}_{33})$	0.00200	0.00200	0.00200
Repeatability	$\mathrm{u}(\hat{\mathbf{R}}_{\mathrm{S}22})$	0.00100	0.00100	0.00100
Combined uncertainty	$\mathrm{u}(\hat{\mathbf{S}}_{22})$	0.00320	0.00587	0.01152

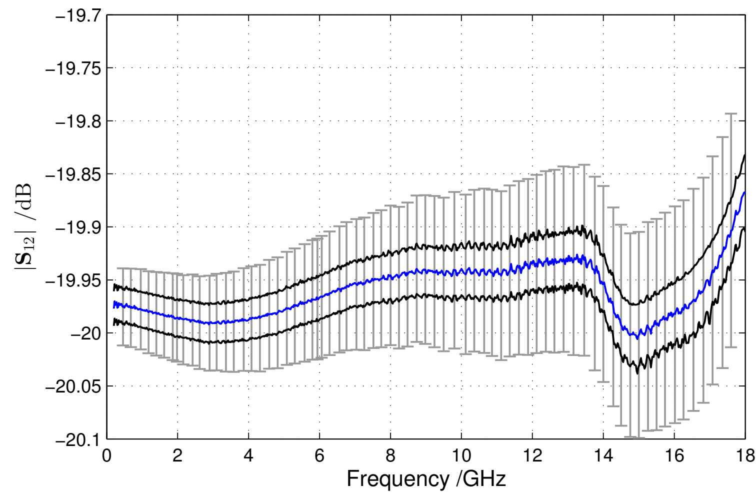

Figure J.14: Magnitude of the transmission coefficient of a 20 dB attenuation device with associated standard uncertainties. The solid lines indicate the error corrected measurement data (center line) bounded by the interval of one standard uncertainty ($k = 1$) calculated with the rigorous method. The vertical bars indicate standard uncertainties evaluated with the Ripple Method.

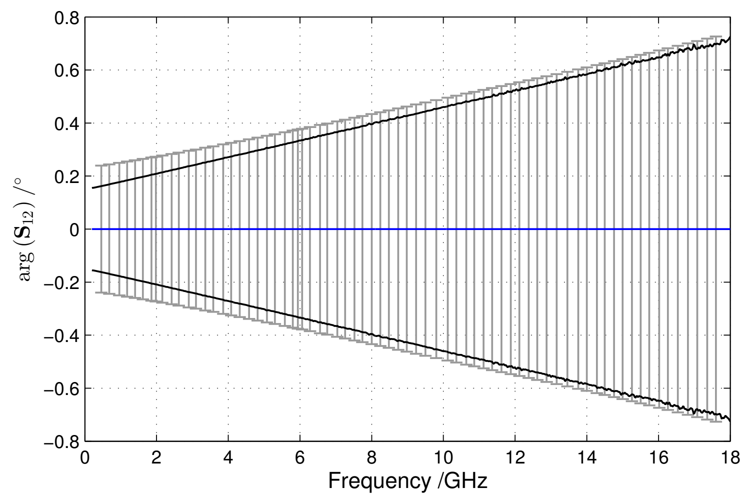

Figure J.15: The same as figure J.14 but for the phase of the transmission coefficient. For better visibility the error corrected measurement has been normalized to 0 and only the standard uncertainties are shown.

Table J.19: Uncertainty budget of $|S_{12}|$ of a 20 dB attenuation device at three different frequencies. The standard uncertainty is evaluated with the rigorous method.

Contribution	0.460 GHz	8.480 GHz	17.600 GHz
Cal Load	0.0006 dB	0.0010 dB	0.0044 dB
Cal Open	0.0006 dB	0.0041 dB	0.0063 dB
Cal Short	0.0006 dB	0.0039 dB	0.0058 dB
Conn. Rep.	0.0001 dB	0.0006 dB	0.0010 dB
Cable	0.0145 dB	0.0209 dB	0.0279 dB
VNA Drift	0.0018 dB	0.0018 dB	0.0018 dB
VNA Linearity	0.0071 dB	0.0071 dB	0.0071 dB
VNA Noise	0.0015 dB	0.0010 dB	0.0012 dB
Combined	0.0163 dB	0.0228 dB	0.0305 dB

Table J.20: The same as table J.19 but for $\arg(\mathbf{S}_{12})$

Contribution	0.460 GHz	8.480 GHz	17.600 GHz
Cal Load	0.0038 deg	0.0063 deg	0.0290 deg
Cal Open	0.0037 deg	0.0267 deg	0.0418 deg
Cal Short	0.0037 deg	0.0254 deg	0.0383 deg
Conn. Rep.	0.0009 deg	0.0038 deg	0.0067 deg
Cable	0.1559 deg	0.4085 deg	0.6929 deg
VNA Drift	0.0108 deg	0.0108 deg	0.0108 deg
VNA Linearity	0.0424 deg	0.0424 deg	0.0425 deg
VNA Noise	0.0077 deg	0.0045 deg	0.0091 deg
Combined	0.1622 deg	0.4126 deg	0.6973 deg

Table J.21: Uncertainty budget of S_{12} of a 20 dB attenuation device at three different frequencies. The standard uncertainty is evaluated with the Ripple Method. The terms in column 2 refer to equation (H.4) and the corresponding values in the subsequent columns have to be added accordingly for the combined standard uncertainty.

Name	Uncertainty contribution	0.460 GHz	8.480 GHz	17.600 GHz
Source match	$\lvert\hat{\mathbf{S}}^c_{22}\hat{\mathbf{S}}^c_{12}\rvert \mathrm{u}(\delta\hat{\mathbf{E}}^R_{22})$	0.0009 dB	0.0039 dB	0.0137 dB
Load match	$\lvert\hat{\mathbf{S}}^c_{11}\hat{\mathbf{S}}^c_{12}\rvert \mathrm{u}(\delta\hat{\mathbf{E}}^R_{11})$	0.0001 dB	0.0031 dB	0.0092 dB
Transmission tracking	$\lvert\hat{\mathbf{S}}^c_{12}\rvert \mathrm{u}(\delta\hat{\mathbf{E}}^R_{01})$	0.0232 dB	0.0466 dB	0.0762 dB
Isolation	$\mathrm{u}(\delta\hat{\mathbf{E}}^R_{03})$	0.0001 dB	0.0001 dB	0.0001 dB
Linearity	$\lvert\hat{\mathbf{S}}^c_{12}\rvert \mathrm{u}(\hat{\mathbf{L}})$	0.0113 dB	0.0113 dB	0.0113 dB
Cable transmission	$\lvert\hat{\mathbf{S}}^c_{12}\rvert \mathrm{u}(\hat{\mathbf{C}}_{23})$	0.0168 dB	0.0438 dB	0.0745 dB
Cable reflection	$\lvert\hat{\mathbf{S}}^c_{12}\hat{\mathbf{S}}^c_{22}\rvert \mathrm{u}(\hat{\mathbf{C}}_{22})$	0.0002 dB	0.0007 dB	0.0015 dB
Repeatability	$\mathrm{u}(\hat{\mathbf{R}}_{S12})$	0.0087 dB	0.0087 dB	0.0087 dB
Raw load match	$\lvert\hat{\mathbf{S}}^c_{12}\hat{\mathbf{E}}^R_{11}(1-\hat{\mathbf{S}}^c_{21}\hat{\mathbf{S}}^c_{12})\rvert \mathrm{u}(\delta\hat{\mathbf{E}}^F_{00})$	0.0004 dB	0.0013 dB	0.0031 dB
Raw load match	$\lvert\hat{\mathbf{S}}^c_{12}\hat{\mathbf{E}}^R_{11}(1-\hat{\mathbf{S}}^c_{21}\hat{\mathbf{S}}^c_{12})\rvert \mathrm{u}(\delta\hat{\mathbf{E}}^R_{22})$	0.0015 dB	0.0029 dB	0.0051 dB
Combined uncertainty	$\mathrm{u}(\hat{\mathbf{S}}_{12})$	0.0364 dB	0.0679 dB	0.1101 dB

J.6 Two-port 50 dB attenuation device

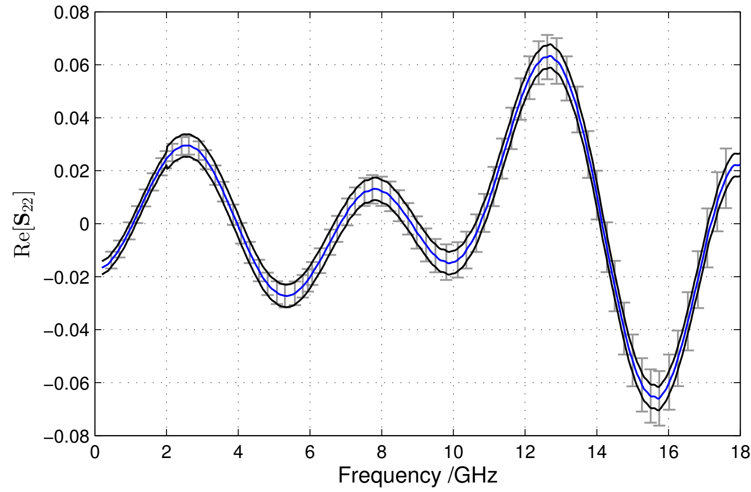

Figure J.16: Real component of the reflection coefficient of a 50 dB attenuation device with associated standard uncertainties. The solid lines indicate the error corrected measurement data (center line) bounded by the interval of one standard uncertainty ($k = 1$) calculated with the rigorous method. The step in uncertainty at 2 GHz is due to the change from low band load to sliding load. The vertical bars indicate standard uncertainties evaluated with the Ripple Method.

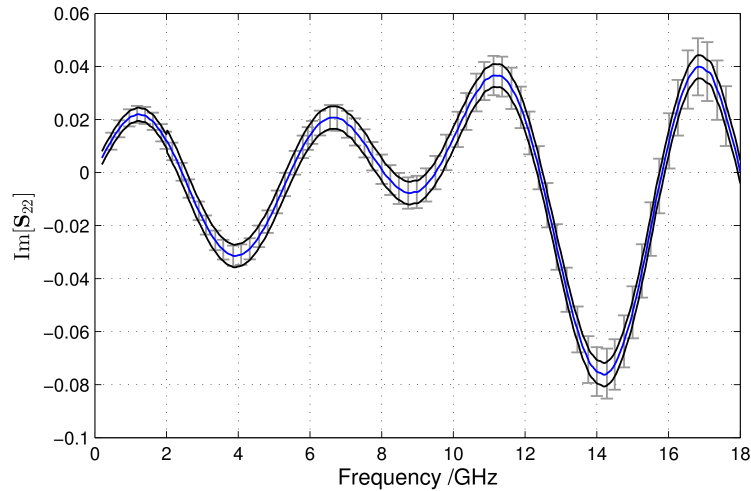

Figure J.17: The same as figure J.16 but for the imaginary component of the reflection coefficient.

Table J.22: Uncertainty budget of $\mathrm{Re}\,[\mathbf{S}_{22}]$ of a 50 dB attenuation device at three different frequencies. The standard uncertainty is evaluated with the rigorous method.

Contribution	0.460 GHz	8.480 GHz	17.600 GHz
Cal Load	0.00199	0.00398	0.00398
Cal Open	0.00005	0.00007	0.00035
Cal Short	0.00005	0.00007	0.00036
Conn. Rep.	0.00045	0.00071	0.00071
Cable	0.00142	0.00142	0.00151
VNA Drift	0.00010	0.00009	0.00009
VNA Linearity	0.00002	0.00003	0.00011
VNA Noise	0.00002	0.00001	0.00002
Combined	0.00249	0.00428	0.00435

Table J.23: The same as table J.22 but for $\mathrm{Im}\,[\mathbf{S}_{22}]$

Contribution	0.460 GHz	8.480 GHz	17.600 GHz
Cal Load	0.00199	0.00398	0.00398
Cal Open	0.00005	0.00007	0.00035
Cal Short	0.00005	0.00007	0.00036
Conn. Rep.	0.00045	0.00071	0.00071
Cable	0.00142	0.00142	0.00148
VNA Drift	0.00010	0.00009	0.00009
VNA Linearity	0.00002	0.00003	0.00010
VNA Noise	0.00002	0.00001	0.00002
Combined	0.00249	0.00428	0.00434

Table J.24: Uncertainty budget of S_{22} of a 50 dB attenuation device at three different frequencies. The standard uncertainty is evaluated with the Ripple Method. The terms in column 2 refer to equation (H.3) and the corresponding values in the subsequent columns have to be added accordingly for the combined standard uncertainty.

Name	Uncertainty contribution	0.460 GHz	8.480 GHz	17.600 GHz
Directivity	$\mathrm{u}(\delta\hat{\mathbf{E}}^{R}_{33})$	0.00228	0.00540	0.01103
Reflection tracking	$\lvert\hat{\mathbf{S}}^{c}_{22}\rvert\mathrm{u}(\delta\hat{\mathbf{E}}^{R}_{32})$	0.00010	0.00014	0.00071
Source match	$\lvert\hat{\mathbf{S}}^{c}_{22}\rvert^{2}\mathrm{u}(\delta\hat{\mathbf{E}}^{R}_{22})$	0.00001	0.00001	0.00002
Load match	$\lvert\hat{\mathbf{S}}^{c}_{21}\hat{\mathbf{S}}^{c}_{12}\rvert\mathrm{u}(\delta\hat{\mathbf{E}}^{R}_{11})$	0.00001	0.00001	0.00001
Linearity	$\lvert\hat{\mathbf{S}}^{c}_{22}\rvert\mathrm{u}(\hat{\mathbf{L}})$	0.00003	0.00002	0.00004
Cable transmission	$\lvert\hat{\mathbf{S}}^{c}_{22}\rvert\mathrm{u}(\hat{\mathbf{C}}_{32})$	0.00004	0.00005	0.00024
Cable transmission	$\lvert\hat{\mathbf{S}}^{c}_{22}\rvert\mathrm{u}(\hat{\mathbf{C}}_{23})$	0.00004	0.00005	0.00024
Cable reflection	$\lvert\hat{\mathbf{S}}^{c}_{22}\rvert^{2}\mathrm{u}(\hat{\mathbf{C}}_{22})$	0.00001	0.00001	0.00001
Cable reflection	$\mathrm{u}(\hat{\mathbf{C}}_{33})$	0.00200	0.00200	0.00200
Repeatability	$\mathrm{u}(\hat{\mathbf{R}}_{\mathrm{S22}})$	0.00100	0.00100	0.00100
Combined uncertainty	$\mathrm{u}(\hat{\mathbf{S}}_{22})$	0.00320	0.00584	0.01128

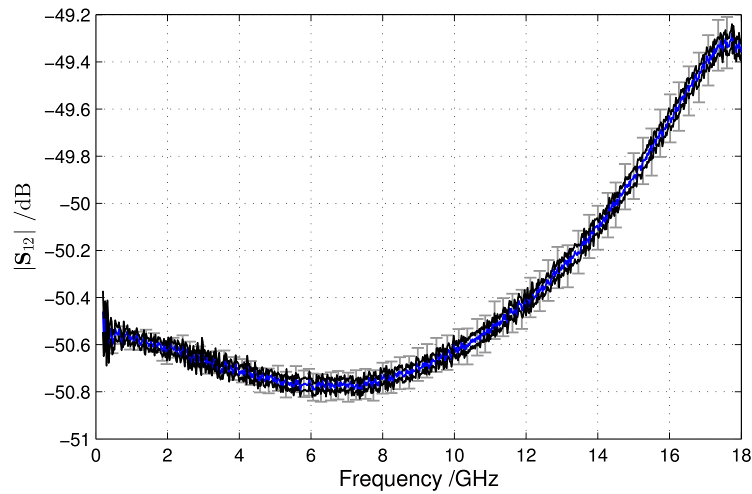

Figure J.18: Magnitude of the transmission coefficient of a 50 dB attenuation device with associated standard uncertainties. The solid lines indicate the error corrected measurement data (center line) bounded by the interval of one standard uncertainty ($k = 1$) calculated with the rigorous method. The vertical bars indicate standard uncertainties evaluated with the Ripple Method.

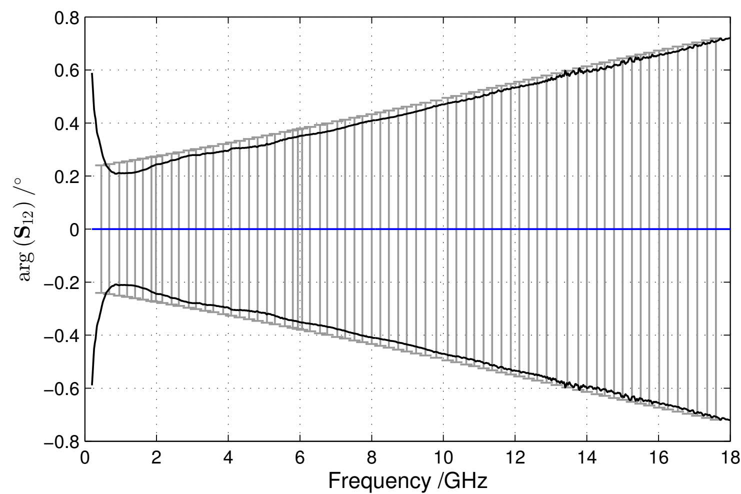

Figure J.19: The same as figure J.18 but for the phase of the transmission coefficient. For better visibility the error corrected measurement has been normalized to 0 and only the standard uncertainties are shown.

Table J.25: Uncertainty budget of $|S_{12}|$ of a 50 dB attenuation device at three different frequencies. The standard uncertainty is evaluated with the rigorous method.

Contribution	0.460 GHz	8.480 GHz	17.600 GHz
Cal Load	0.0005 dB	0.0014 dB	0.0021 dB
Cal Open	0.0002 dB	0.0012 dB	0.0065 dB
Cal Short	0.0002 dB	0.0012 dB	0.0066 dB
Conn. Rep.	0.0001 dB	0.0003 dB	0.0005 dB
Cable	0.0145 dB	0.0208 dB	0.0280 dB
VNA Drift	0.0028 dB	0.0028 dB	0.0028 dB
VNA Linearity	0.0071 dB	0.0071 dB	0.0071 dB
VNA Noise	0.0383 dB	0.0133 dB	0.0178 dB
Combined	0.0417 dB	0.0259 dB	0.0353 dB

Table J.26: The same as table J.25 but for $\arg(\mathbf{S}_{12})$

Contribution	0.460 GHz	8.480 GHz	17.600 GHz
Cal Load	0.0032 deg	0.0094 deg	0.0138 deg
Cal Open	0.0011 deg	0.0076 deg	0.0426 deg
Cal Short	0.0010 deg	0.0079 deg	0.0434 deg
Conn. Rep.	0.0009 deg	0.0018 deg	0.0031 deg
Cable	0.1559 deg	0.4078 deg	0.6940 deg
VNA Drift	0.0166 deg	0.0166 deg	0.0166 deg
VNA Linearity	0.0424 deg	0.0424 deg	0.0425 deg
VNA Noise	0.2525 deg	0.0872 deg	0.1176 deg
Combined	0.3003 deg	0.4198 deg	0.7081 deg

Table J.27: Uncertainty budget of S_{12} of a 50 dB attenuation device at three different frequencies. The standard uncertainty is evaluated with the Ripple Method. The terms in column 2 refer to equation (H.4) and the corresponding values in the subsequent columns have to be added accordingly for the combined uncertainty.

Name	Uncertainty contribution	0.460 GHz	8.480 GHz	17.600 GHz
Source match	$\lvert\hat{\mathbf{S}}^c_{22}\hat{\mathbf{S}}^c_{12}\rvert \mathrm{u}(\delta\hat{\mathbf{E}}^R_{22})$	0.0017 dB	0.0010 dB	0.0044 dB
Load match	$\lvert\hat{\mathbf{S}}^c_{11}\hat{\mathbf{S}}^c_{12}\rvert \mathrm{u}(\delta\hat{\mathbf{E}}^R_{11})$	0.0005 dB	0.0007 dB	0.0026 dB
Transmission tracking	$\lvert\hat{\mathbf{S}}^c_{12}\rvert \mathrm{u}(\delta\hat{\mathbf{E}}^R_{01})$	0.0232 dB	0.0466 dB	0.0762 dB
Isolation	$\mathrm{u}(\delta\hat{\mathbf{E}}^R_{03})$	0.0030 dB	0.0030 dB	0.0026 dB
Linearity	$\lvert\hat{\mathbf{S}}^c_{12}\rvert \mathrm{u}(\hat{\mathbf{L}})$	0.0113 dB	0.0113 dB	0.0113 dB
Cable transmission	$\lvert\hat{\mathbf{S}}^c_{12}\rvert \mathrm{u}(\hat{\mathbf{C}}_{23})$	0.0168 dB	0.0438 dB	0.0745 dB
Cable reflection	$\lvert\hat{\mathbf{S}}^c_{12}\hat{\mathbf{S}}^c_{22}\rvert \mathrm{u}(\hat{\mathbf{C}}_{22})$	0.0004 dB	0.0002 dB	0.0005 dB
Repeatability	$\mathrm{u}(\hat{\mathbf{R}}_{S12})$	0.0087 dB	0.0087 dB	0.0087 dB
Raw load match	$\lvert\hat{\mathbf{S}}^c_{12}\hat{\mathbf{E}}^R_{11}(1-\hat{\mathbf{S}}^c_{21}\hat{\mathbf{S}}^c_{12})\rvert \mathrm{u}(\delta\hat{\mathbf{E}}^F_{00})$	0.0004 dB	0.0013 dB	0.0031 dB
Raw load match	$\lvert\hat{\mathbf{S}}^c_{12}\hat{\mathbf{E}}^R_{11}(1-\hat{\mathbf{S}}^c_{21}\hat{\mathbf{S}}^c_{12})\rvert \mathrm{u}(\delta\hat{\mathbf{E}}^R_{22})$	0.0015 dB	0.0028 dB	0.0052 dB
Combined uncertainty	$\mathrm{u}(\hat{\mathbf{S}}_{12})$	0.0365 dB	0.0678 dB	0.1091 dB

EURAMET e.V.
Bundesallee 100
38116 Braunschweig
Germany

Phone: +49 531 592 1960
Fax: +49 531 592 1969
E-mail: secretariat@euramet.org

EURAMET e.V. is a non-profit association under German law.